APPENDIX C

Underwater Sound Assessment Report

Underwater Sound Assessment for Newfoundland Orphan Basin Exploration Drilling Program

Submitted to:

Ellen Tracy
Stantec

Authors:

Marie-Noel Matthews
Terry J. Deveau
Christopher Whitt
Bruce Martin

8 June 2018

P001417-001
Document 01592
Version 4.0

JASCO Applied Sciences (Canada) Ltd
Suite 202, 32 Troop Ave.
Dartmouth, NS B3B 1Z1 Canada
Tel: +1-902-405-3336
Fax: +1-902-405-3337
www.jasco.com

Suggested citation:

Matthews, M-N, T.J. Deveau, C. Whitt, and B. Martin. 2018. *Underwater Sound Assessment for Newfoundland Orphan Basin Exploration Drilling Program*. Document 01592, Version 4.0. Technical report by JASCO Applied Sciences for Stantec.

Disclaimer:

The results presented herein are relevant within the specific context described in this report. They could be misinterpreted if not considered in the light of all the information contained in this report. Accordingly, if information from this report is used in documents released to the public or to regulatory bodies, such documents must clearly cite the original report, which shall be made readily available to the recipients in integral and unedited form.

Contents

Figures

Tables

Executive Summary

The Newfoundland Orphan Basin Exploration Drilling Program, proposed by BP Canada Energy Group ULC (BP), includes exploration drilling activities in Exploration Licences (EL) 1145, 1146, 1148, and 1149 in Orphan Basin, located 270–470 km east of Newfoundland, Canada. This Program may involve drilling up to 20 exploration wells over the licences term (2017 to 2026). The Program will use either a semi-submersible platform or a drillship; both options will likely be maintained on station by dynamic positioning (DP). Other sound generating equipment will include a vertical seismic profiling (VSP) array and support vessels.

In this report, JASCO Applied Sciences (Canada) (JASCO) discusses the underwater sounds associated with the proposed Program activities by reviewing existing assessments of similar projects located offshore Newfoundland and Nova Scotia. Sound source spectra representative of the planned Program activities are estimated based on assessments published in previous studies. The acoustic environment is described and compared to the environmental parameters used in the underwater sound assessments for the Scotian Basin Exploration Drilling Project (hereafter the Scotian Basin Project; Zykov 2016) and the Nexen Energy ULC Flemish Pass Exploration Drilling Project (hereafter the Flemish Pass Project; Matthews et al. 2017). Transmission loss from the same two offshore projects are compared to that in EL 1145 and EL 1149 in June. Finally, ambient sound levels and various contributors to the soundscape in the area are derived from data measured at two Environmental Studies Research Fund (ESRF) recording stations, near EL 1145 and EL 1149. Anthropogenic contributors to the soundscape (including vessel traffic, previous seismic surveys, and oil and gas extraction activity) and naturally occurring ambient sound contributors (including wind, other environmental phenomena, as well as fin whales) are discussed.

The accurate assessment of sound propagating away from the planned Program activities will depend on the particulars of the equipment and activities. However, because of the similarities in operations and environmental parameters, underwater sound assessments for the Scotian Basin and the Flemish Pass exploration drilling projects help provide a preliminary assessment of likely sound propagation features in the Orphan Basin. Based on sound monthly-averaged speed profiles in EL 1145 and EL 1149, we expect distances to sound thresholds to be shorter from July to November than in June, and similar to the longer distances from December to May. The June sound speed profile in EL 1145 features a weak sound channel that results in longer distances than in EL 1149; we expected this difference in distances to persist throughout the year. Based on the analysis of transmission loss coefficient for drillship and semi-submersible platforms, longer distances to sound level isopleths than those modelled in Flemish Pass (in May) and the Scotian Basin (in both, August and February) are expected in EL 1145, while similar distances to those in Flemish Pass, and those in August in the Scotian Basin are expected in EL 1149. The transmission loss coefficients for the VSP operations indicate that distances to sound level isopleths in June in EL 1145 should be similar to those than in May in Flemish Pass, and longer than modelled in the Scotian Basin (in both, August and February). These distances from VSP operations in EL 1149 are expected to be shorter than in Flemish Pass and the Scotian Basin. The transmission loss coefficients for supply vessels were estimated in EL 1145 and EL 1149, but no comparable values were available from the Flemish Pass and Scotia Basin projects.

Based on the analysis of important contributors to the ambient soundscape in the region, sound levels associated with the Program activities are expected to dominate the soundscape within distances of 10–40 km from the platform, during the course of the activities. VSP operations are expected to contribute to the ambient sound levels to a lesser extend than seismic surveys because of their shorter operational timeframe and lower source levels. The relative contribution to the ambient soundscape will depend on the specifications of the Program activities, as well as the possible presence of other simultaneous contributors in the region.

1. Introduction

BP Canada Energy Group ULC (BP) is proposing to conduct an exploration drilling program on Exploration Licences (ELs) 1145, 1146, 1148, and 1149 in Orphan Basin (Figure 1), east of Newfoundland, Canada. The Newfoundland Orphan Basin Exploration Drilling Program, hereafter referred to as the Program, may involve drilling up to 20 exploration wells over the term of the ELs (ending in 2026). Initial well drilling operations are proposed to begin in 2020, pending regulatory approval.

The proposed mobile offshore drilling unit (MODU) could be either a semi-submersible platform or a drillship. Both platforms would likely be maintained on station by dynamic positioning (DP). Other planned sound generating activities include the use of a vertical seismic profiling (VSP) surveys for pre-drilling exploration and support vessels transiting between Newfoundland and the drill site during drilling operations.

In this report, JASCO Applied Sciences (Canada) (JASCO) discusses the underwater sounds likely to result from the proposed Program by reviewing existing underwater noise assessments of similar types of projects offshore Newfoundland and Nova Scotia. Specifically, this report:

- Discusses sound source parameters representative of the planned activities;
- Reviews modelled sound propagation and measurement studies to assess their pertinence to this Program based on similarity of environmental parameters;
- Quantifies transmission loss (TL) at two representative drilling sites and compares characteristics of modelled TL functions with those derived from existing model results for other offshore areas;
- Discusses the predicted Program sound levels relative to the expected ambient sound levels in the area; and
- Draws conclusions on likely implications to sound propagation for sound sources relevant to the Program activities.

Section 1.1 introduces past studies used for estimating ambient sound levels, comparing environmental parameters, and comparing TL functions. Background information on underwater sound, the factors influencing sound propagation, ambient sound, and anthropogenic sound is presented in Section 2. The methods and study-specific parameters are summarized in Section 3; more details on underwater acoustic metrics, source and sound propagation models, and data collection are provided in Appendix A–Appendix C. Representative sound sources, TL, and ambient sound levels are quantified, and the environmental parameters are compared to other studies in Section 4. Finally, the results are discussed in Section 4.

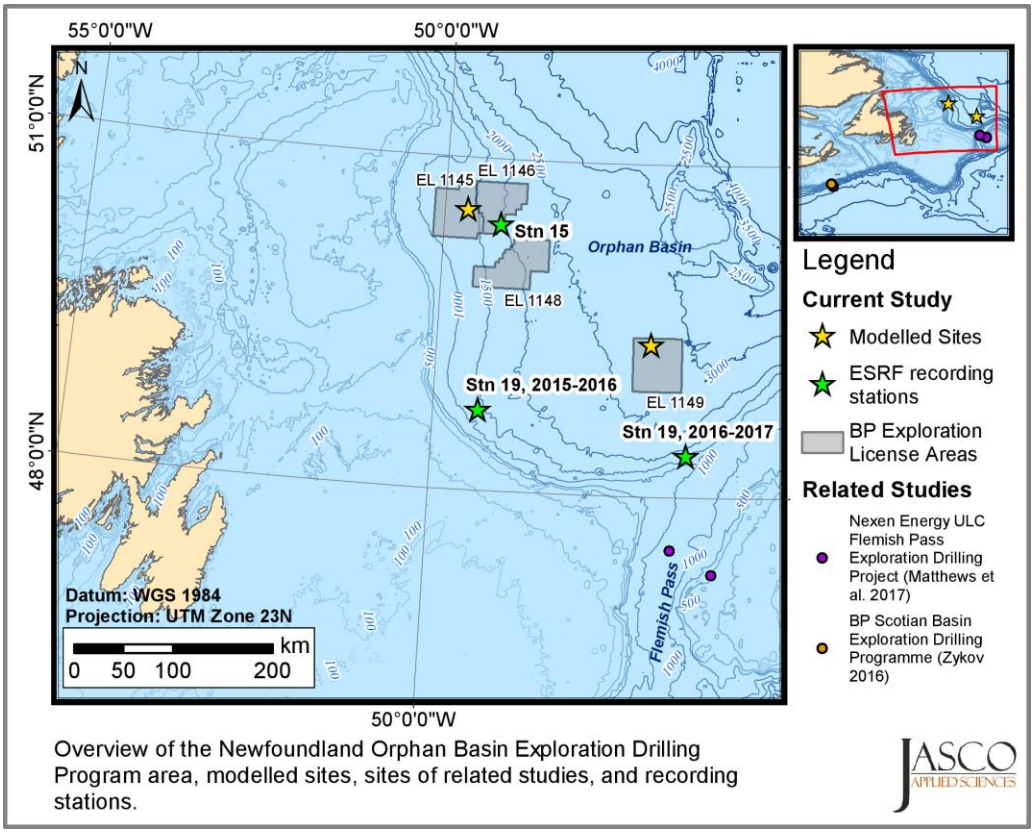

Figure 1. Overview of BP Exploration Licenses, the modelled sites, Environmental Studies Research Fund (ESRF) recording stations, and modelled sites of related studies.

1.1. Related Studies

Representative sound source levels as a function of frequency (i.e., source level spectra) for semi-submersible platforms, drillships, VSP arrays, and support vessels have been described in previous JASCO studies. Three recent studies were used in this analysis to derive the best representative sound level spectra for the Program (Zykov 2016, Matthews et al. 2017, Quijano et al. 2017).

Two of those studies, Zykov (2016) and Matthews et al. (2017), estimated distances to specific sound thresholds for each modelled operation. The environmental parameters used in these studies are compared to those characterizing the Program Area to assess the pertinence of the estimated distances for the current Program. TL functions derived from these published results are also compared to those modelled for the current Program.

The Environmental Studies Research Fund (ESRF) funded a two-year program aimed at describing the soundscape and the occurrence of marine mammals within the waters off the Canadian Atlantic coast (hereafter referred to as the ESRF Study). The ESRF Study area includes shallow and deep waters, and it extends from Dawson Canyon off Halifax, NS, to Nain Bank on the Labrador shelf. JASCO deployed 20 acoustic recorders along Canada's east coast for the ESRF Study. The recorders were active for most of 2015–2017. Data from recorder stations 15 and 19 were used in this study to provide the best available information on the existing soundscape in the Program Area (see Figure 1).

Station 15 was in 2000 m water depth, approximately between EL 1146 and EL 1148; Station 19 was ~150 km from the Program Area in ~1280 m water depth (Station 19, 2015–2016 in Figure 1) and later relocated to Sackville Spur at the north end of the Flemish Pass (Station 19, 2016–2017 in Figure 1) in ~1550 m water depth. To summarize the soundscape around the Program Area, we present the distribution of one-minute sound pressure levels (SPL) in Section 4.3.

2. Underwater Sound

2.1. Factors Affecting Sound propagation

Sound propagation in the ocean is a complex process that depends on many factors. Sound levels from an omnidirectional point source in the water column are reduced with range, a process known as geometric spreading. Before the sound emanating from the point source reaches the seabed or sea surface boundaries, sound waves propagate in a spherical pattern. In this case, the received levels at a recorder located a distance R from the source are $20\times\log(R)$ dB lower than the levels measured at a reference point (1 m from the source). This is known as spherical geometric spreading. Once the sound waves interact with the sea surface and seabed, the spreading becomes cylindrical, with a lower range-dependent decay of $10\times\log(R)$ dB. Spherical and cylindrical spreading factors provide rules of thumb for quickly estimating the expected levels from a given source; however, for more realistic scenarios, other factors must also be considered related to losses at the seabed and sea surface, frequency spectrum of the source, and environmental parameters (e.g., bathymetry, water sound speed profile, and seabed geoacoustics).

In general, sound levels at short ranges are higher in shallow waters than in deep waters. This is because in deep waters (and at ranges less than a water depth), sound levels are determined by acoustic arrivals from the source and perhaps from energy bouncing off the air-water interface, whereas for shallow environments at the same range, sound levels can increase due to contributions from multiple bounces off the seabed. The opposite situation can also be experienced at far ranges (i.e., several water depths for both deep and shallow waters): in shallow waters there are significant losses in acoustic energy due to multiple bounces off the seabed, whereas in deep waters there are fewer interactions of the acoustic wave with the seabed. These general trends must be applied with caution, however, because of the high complexity of the ocean waveguide.

Along with the environmental parameters (bathymetry, sound speed profile, and seabed geoacoustics), a sound's frequency content plays an important role in how it propagates in the ocean. For example, acoustic energy is attenuated by molecular absorption in seawater. The volumetric sound absorption is quantified by an attenuation coefficient, expressed in units of decibels per kilometre (dB/km). This absorption coefficient depends on the temperature, salinity, and pressure of the water, as well as the sound frequency. In general, the absorption coefficient increases with the square of the frequency (i.e., high frequencies are more affected). The absorption of acoustic wave energy has a noticeable effect (>0.05 dB/km) at frequencies above 1 kHz. For example, at 10 kHz the absorption loss over 10 km distance can exceed 10 dB, as computed according to the formulae of François and Garrison (1982b, b). Another mechanism of absorption in the water column is scattering, which results from the sound wave interacting with non-homogeneities (such as air bubbles) and with the rough boundaries at the air-sea and sea-seabed interfaces. Acoustic energy loss due to scattering is also frequency-dependent, with more noticeable effects when the scatterer is the same size or larger than the sound wavelength. Sounds at low frequencies, therefore, are less affected by scattering than sounds at high frequencies.

Although lower frequency sounds are less affected by absorption and scattering, there are other mechanisms that have the opposite effect (i.e., favour propagation of higher frequency sounds). For example, propagation through a surface duct only applies to frequencies above a certain cut-off. When sound has strong frequency components above this cut-off, acoustic energy is trapped in the surface channel. This trapped energy does not interact with the seabed, so it propagates to farther ranges. Low-frequency sounds, however, tend to interact with the seabed and are attenuated as they propagate through the seabed sediment.

2.1.1. Sea Surface and Ocean Floor

When sound propagates through the ocean, the sea surface and ocean floor act as boundaries that reflect, absorb, and scatter energy. In computational acoustics, the surface is referred to as a 'pressure-release' interface because it reflects sound with equal amplitude and opposite phase. The reflected direction is equal to the angle of incidence. Thus, if the surface is tilted by wave action, sound energy may be scattered, and the sound is attenuation at the sea surface. This loss resulting from surface roughness depends on the sound wavelength relative to the size of the surface waves; it becomes more important with increasing frequency.

The ocean floor is a different type of boundary and is generally modelled as viscous fluids where a portion of the sound energy is reflected and the remainder transmits into the sediment. The amounts of reflection and transmission depend on the angle of incidence, bottom roughness, and the physical properties of the material (e.g., density, grain size, and porosity). Lower density materials, such as clays and silts, allow more sound to penetrate. Hard materials, such as sand and gravel, reflect most of the incident sound. When there are layers of less dense sediment over more dense materials, such as bedrock, the sound can reflect off the lower layers and re-enter the water column. Soft materials like clays can also refract and trap sound, as well as absorb and attenuate it. Thus, seabed geoacoustics are an important environmental component for understanding and predicting acoustic propagation, especially in shallow waters where seabed interactions are frequent.

2.1.2. Bathymetry

At lower frequencies (less than a few kHz), acoustic propagation is highly dependent on water depth. In general, the deeper the water, the lower the propagation loss due to interaction with the seafloor. From an acoustic perspective, water depth should be considered in terms of the wavelength of the sound that is being transmitted. For example, when the water is more than several wavelengths in depth, it may be considered "deep" (Buckingham 2005). Shallow water, however, is often arbitrarily defined as that less than 200 m deep (Buckingham 1992) and includes most of the continental shelf regions of the world.

In shallow water, the acoustic energy transmitted from a source likely interacts many times with either or both the sea surface and the seabed, and energy is lost on each occasion. In contrast, in deeper waters, these interactions occur less frequently, and the overall acoustic energy levels persist. This is particularly true when the water is sufficiently deep to be defined by an underwater sound speed profile (Section 2.1.3) with a sound channel that prevents acoustic energy from interacting with the surface and seabed, resulting in extended propagation ranges.

2.1.3. Underwater Sound Speed Profile

As sound speed changes with depth, the sound refracts toward the depth with the lowest sound speed, which results in sound being trapped in a 'duct' and travelling very long distances with minimal attenuation. Conversely, in conditions where the sound speed decreases with depth, sound is refracted toward the seabed and may not reach an intended receiver.

The sound speed changes as a function of the temperature, salinity, and pressure (depth). Colder and fresher water has a lower sound speed and conversely warmer and saltier water has a higher sound speed. As the water depth increases the pressure increases the water density slightly, which increases the sound speed (Jensen et al. 2011). These effects combine with environmental forces, such as solar heating, wind mixing, and currents, to constantly affect the sound speed in the upper 500 m of the water column, which has daily variations around typical seasonal means (Figure 2). The ability of a minimum in the sound speed profile to 'trap' sound depends on the magnitude of the sound speed change at the minimum, the vertical height of the minimum and the sound's wavelength. Ducts must be several times larger than the wavelength for effective trapping of sound (Etter 1996). A corollary of this effect is that higher frequencies are refracted more readily by sound speed changes than lower frequencies that have longer wavelengths.

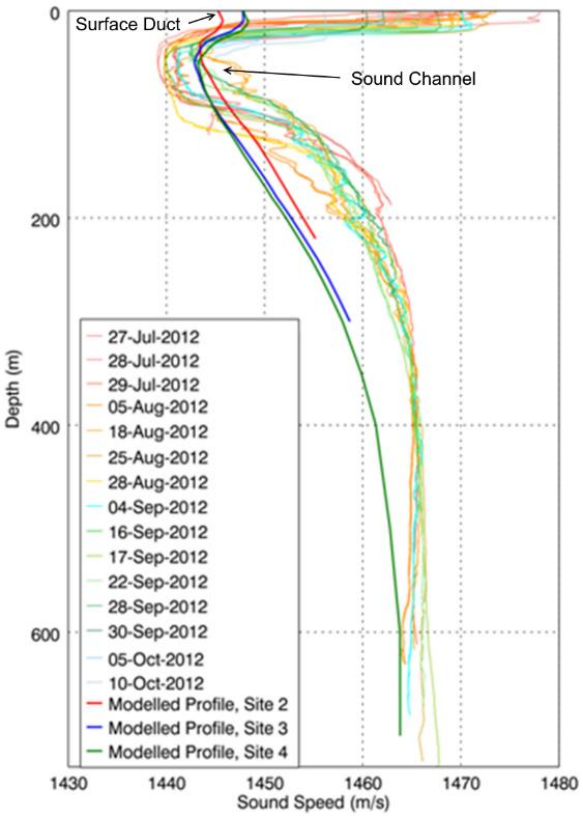

Figure 2. Example of seasonal sound speed profiles from climatology (Modelled Profiles) and actual sound speed profiles measured in situ in Baffin Bay. These profiles show daily variations and features, such as sound channels and surface duct.

2.2. Ambient Sound

The ambient, or background, sound levels that create the ocean soundscape are comprised of many natural and anthropogenic sources (Figure 3). The main environmental sources of sound are wind, precipitation, and sea ice. Wind-generated noise in the ocean is well-described (e.g., Wenz 1962, Ross 1976), and surf noise is known to be an important contributor to near-shore soundscapes (Deane 2000). Sea ice can produce loud sounds that are often the main contributor of acoustic energy in the local soundscape, particularly during ice formation and break up. Precipitation is a frequent noise source, with contributions typically concentrated at frequencies above 500 Hz. At low frequencies (<100 Hz), earthquakes and other geological events contribute to the soundscape.

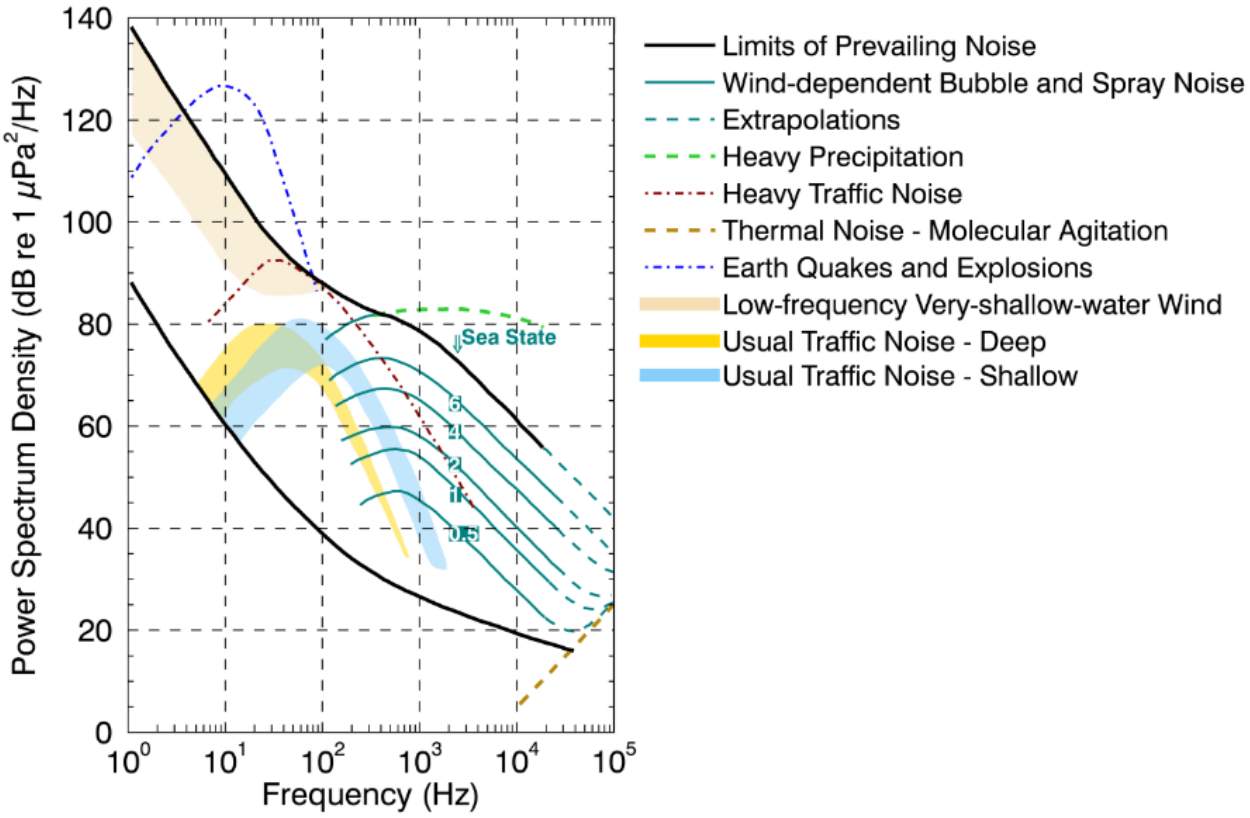

Figure 3. Wenz curves (NRC 2003), describing pressure spectral density levels of marine ambient noise from weather, wind, geologic activity, and commercial shipping, adapted from Wenz (1962).

2.3. Anthropogenic Contributors to the Soundscape

The relative contribution of any sound source to the ocean soundscape depends on factors such as:

- How loud the source is relative to other sounds (e.g., ambient sound);
- The source's frequency spectrum;
- The duration of the sound;
- The characteristics of sound propagation/transmission loss, determined by local environmental parameters (water depth, sound speed profile, and seabed type);
- The depth and distance between a sound source and the receiver or modelling/measurement location; and
- The overlap of the frequency content of the new sounds with the existing sounds in the environment.

Anthropogenic (human-generated) sounds are a by-product of vessel operations, such as engine sound radiating through vessel hulls and cavitating propulsion systems, or a product of active acoustic data collection with sonar, depth sounding, or seismic surveys. The contribution of anthropogenic sources to the ocean soundscape has increased steadily over the past several decades. From the 1950s to the 1990s, the increases were associated with increased commercial shipping (Ross 1976, Andrew et al. 2011). Since the 1990s, the increase has been attributed to oil and gas exploration (Hildebrand 2009). Seismic survey sounds have increased significantly following their expansion into deep water, and they can be detected across ocean basins (Nieukirk et al. 2004). Because seismic surveys are localized sources with only a discrete number occurring globally, their influence at any one location changes over time due to proximity and cyclic fluctuations in the number of surveys occurring (Miksis-Olds and Nichols 2016).

Seasonality influences the contribution of anthropogenic noise levels to the soundscape. For example, in the Program Area seismic survey activity and fishing occurs mostly in summer, whereas commercial shipping and oil and gas extraction sounds are present year-round. The activity in winter reduces due to higher average wind speeds and rough surface conditions, which also elevate the natural sound levels.

2.3.1. Vessel Traffic Activity

There are several major shipping lanes south of the study area. Vessel tracks fan out after leaving the Gulf of St. Lawrence, resulting in constant traffic on the Scotian Shelf and in areas south of Newfoundland. A few isolated areas of denser vessel traffic off the coast indicate the location of oil and natural gas extraction platforms and the associated transit of support vessels, as well as areas targeted by seismic surveys and potential fishing hotspots (Figure 4).

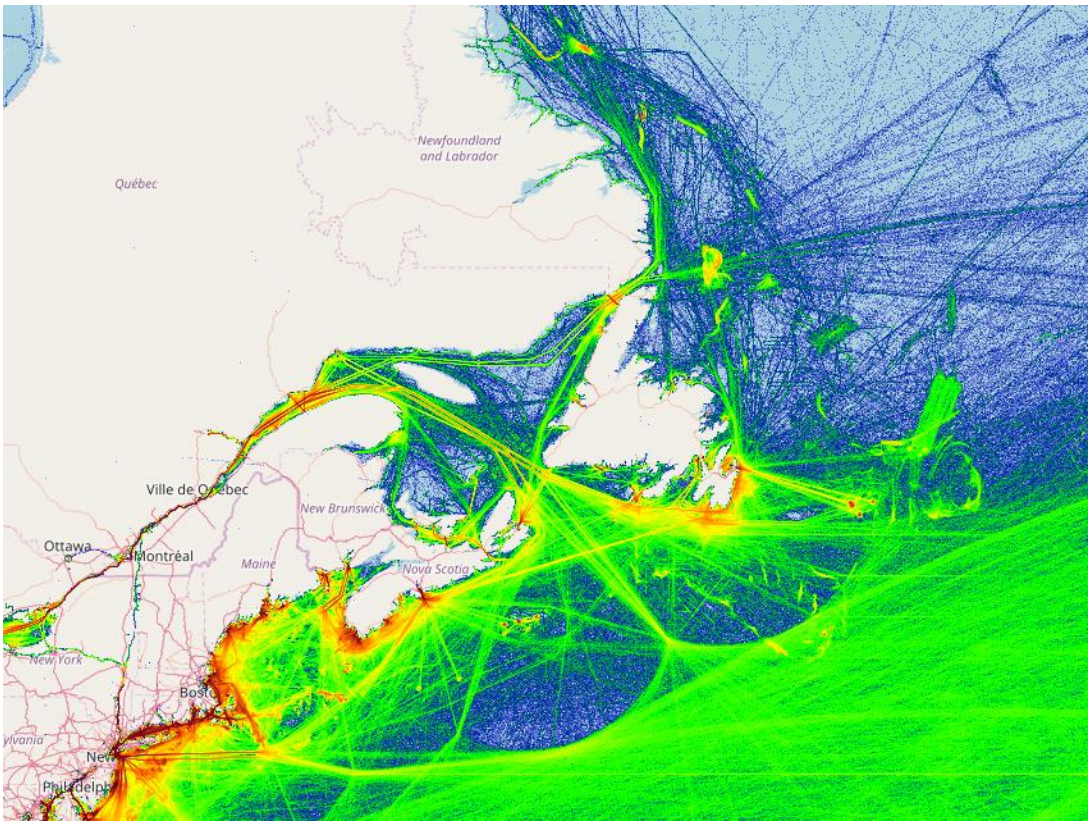

Figure 4. Shipping traffic off the US and Canadian east coast (source: marinetraffic.com; accessed 30 Aug 2017).

2.3.2. Seismic Surveys and Oil and Gas Extraction Activities

Seismic exploration has a long history on Canada's east coast. Increasing in the 1960s, success in both Nova Scotia and Newfoundland in the 1970s and 1980s resulted in an exploration peak in 1983. The next wave of seismic exploration began in 1995 and continued into the 2000s as 3-D work focused on the Scotian Shelf. In recent years TGS, Petroleum Geo-Services (PGS), Nalcor Energy, and to a lesser extent Shell and BP, have undertaken extensive surveys from Nova Scotia to Labrador.

The influence of such activities is present in the ambient sound levels derived from the ESRF Study data. Nearly 500 000 km were surveyed across areas under the jurisdiction of the Canada Newfoundland Labrador Offshore Petroleum Board (CNLOPB) during the 2015 season (Table 1). Figure 5 shows the extent of the surveys conducted by Multi Klient Invest AS, a joint venture between Nalcor, TGS, and PGS in 2015.

Table 1. Geoscientific programs with fieldwork authorized during 2015–2016 fiscal year in eastern Canadian waters (Source: CNLOPB 2016).

Operator	Program	Region	Distance surveyed (km)
Hibernia Management and Development Company Ltd.	4-D Seismic	Jeanne d'Arc Basin	90 818
Multi Klient Invest	2-D Seismic	Northern Labrador and Northeastern Newfoundland	9 951
Multi Klient Invest	3-D Seismic	Eastern Newfoundland	166 219
Multi Klient Invest	3-D Seismic	Eastern Newfoundland	211 734
Multi Klient Invest	2-D Seismic	Eastern and northeastern Newfoundland	2 483
Multi Klient Invest	2-D Seismic	Southern and southeastern Newfoundland	14 403

Oil and gas extraction activity is increasing on Canada's east coast. For example, exploratory drilling programs were performed Statoil from Nov 2014 to May 2016 in the Flemish Pass (see Section 4.3.1) and fall 2015 to summer 2016 by Shell offshore of Nova Scotia. Production platforms are in place in the White-Rose-Hibernia-Hebron developments on the Grand Banks as well as in the Sable and Panuke developments off Nova Scotia (all are visible in Figure 4). These activities affect the soundscape around them continuously (MacDonnell 2017, Quijano et al. 2017). The distance from the activity where the sounds exceed the ambient background are anywhere from 10–200 km depending on the receiver depth, sound propagation conditions, and the nature of the platform sound signature (Zykov 2016, MacDonnell 2017).

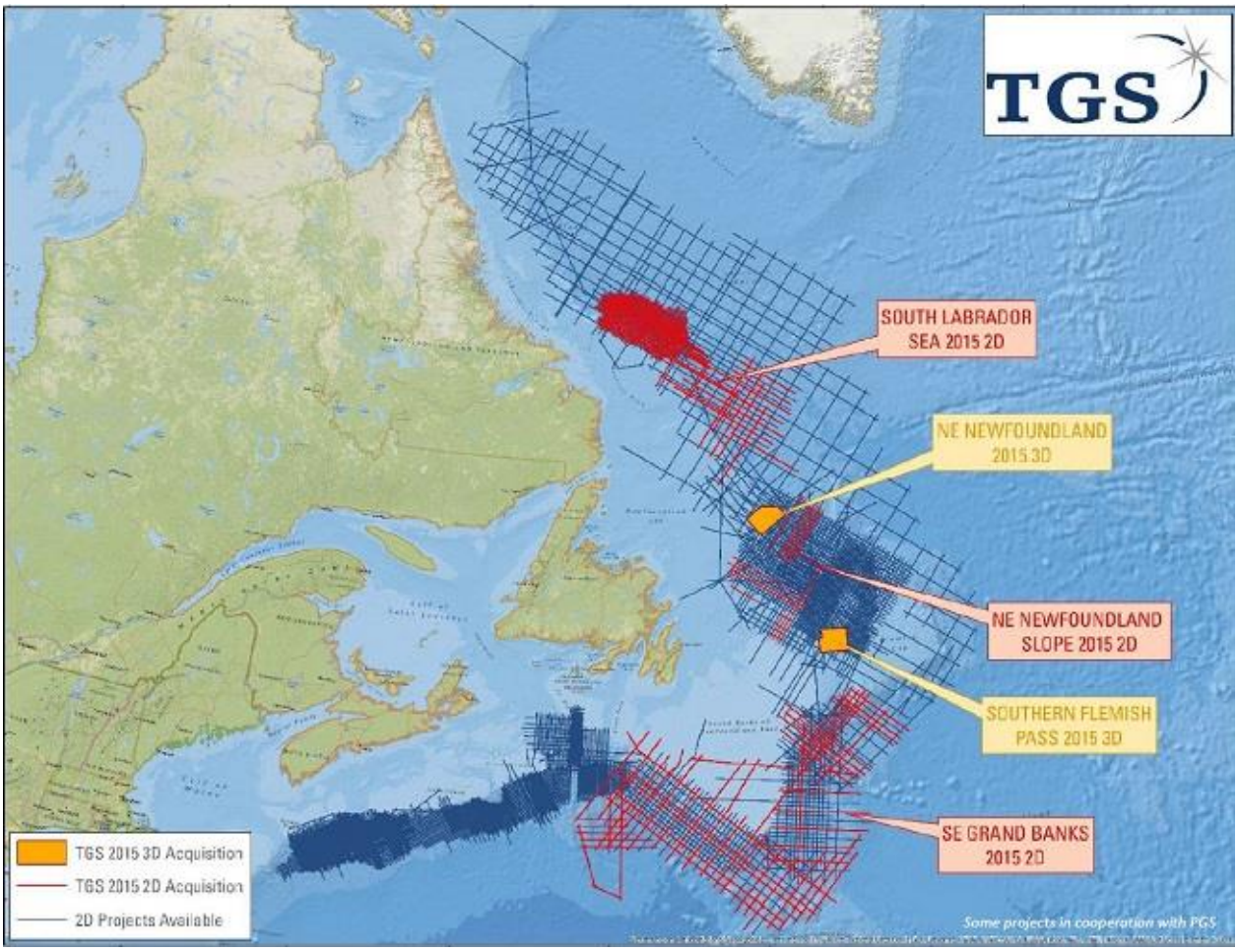

Figure 5. 2015 seismic surveys completed by TGS and PGS and previously available 2-D seismic data in eastern Canadian waters. (Source: Larsen and Ashby 2015).

3. Methods and Program-Specific Parameters

3.1. Sound Propagation

Underwater sound propagation loss, often referred to as transmission loss, was predicted with JASCO's Marine Operations Noise Model (MONM; Appendix B.2). The model was used to compute transmission loss in the Program-specific acoustic environment (detailed in Section 3.1.2), at the centre frequencies of 1/3-octave-bands from 10 to 1600 Hz.

In this study, broadband transmission loss (Appendix B.2.1) is reported for each sound source associated with the Program activity (i.e., semi-submersible platforms, drillship, VSP arrays, and supply vessels), and the estimated transmission loss functions are compare to functions derived from other modelling studies.

Transmission loss was modelled over 72 vertical planes, extending in depth and range, away from a source. Transmission loss contours were calculated based on the 3-D sound fields, sampled by taking the maximum value (i.e., minimum loss) over all modelled depths above the seafloor for each location in the modelled region. The predicted distances to specific levels were computed from these contours. Two distances relative to the source are reported for each transmission loss level: 1) R_{max}, the maximum range to the given level over all azimuths, and 2) $R_{95\%}$, the range to the given level after the 5% farthest points were excluded (see examples in Figure 6).

The $R_{95\%}$ is used because sound field footprints are often irregular in shape. In some cases, a sound level contour might have small protrusions or anomalous isolated fringes. This is demonstrated in the image in Figure 6(a). In cases such as this, where relatively few points are excluded in any given direction, R_{max} can misrepresent the area of the region exposed to such effects, and $R_{95\%}$ is considered more representative. In strongly asymmetric cases such as shown in Figure 6(b), on the other hand, $R_{95\%}$ neglects to account for significant protrusions in the footprint. In such cases R_{max} might better represent the region of effect in specific directions. Cases such as this are usually associated with bathymetric features affecting propagation. The difference between R_{max} and $R_{95\%}$ depends on the source directivity and the non-uniformity of the acoustic environment.

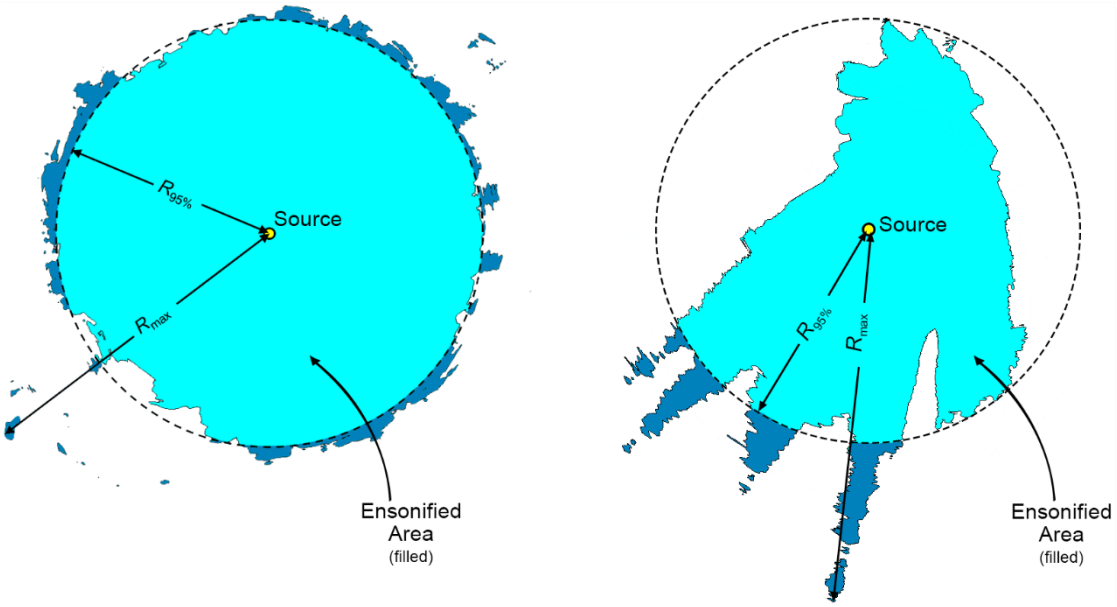

Figure 6. Sample areas ensonified to an arbitrary sound level with R_{max} and $R_{95\%}$ ranges shown for two different scenarios. (a) Largely symmetric sound level contour with small protrusions. (b) Strongly asymmetric sound level contour with long protrusions. Light blue indicates the ensonified areas bounded by $R_{95\%}$; darker blue indicates the areas outside this boundary which determine R_{max}.

3.1.1. Modelled Sites

Transmission loss was modelled at two sites in the Program Area: West Orphan Site in EL 1145 and East Orphan Site in EL 1149 (Table 2). The sites are shown in Figure 1. Table 3 provides the location and water depth for sites where comparable sources were modelled.

Table 2. Program modelled sites coordinates and water depth.

Site	Latitude	Longitude	UTM easting (m; zone 23N)	UTM northing (m; zone 23N)	Water depth (m)
West Orphan, in EL 1145	50°31'49" N	49°40'44" W	168 454	5 608 064	1 376
East Orphan, in EL 1149	49°22'26" N	47°02'08" W	352 231	5 471 024	2 774

Table 3. Related studies modelled sites coordinates and water depth.

Site	Latitude	Longitude	UTM easting (m)	UTM northing (m)	Water depth (m)
Zykov (2016)					
A	42° 50' 42.64" N	60° 17' 51.44" W	720 825 (zone 20N)	4 747 165 (zone 20N)	2 790
B	43° 02' 07.76" N	60° 26' 05.98" W	708 954 (zone 20N)	4 767 949 (zone 20N)	2 100
Matthews et al. (2017)					
A	47° 31' 01.23" N	46° 43' 09.20" W	370 563 (zone 23N)	5 264 052 (zone 23N)	1 137
B	47° 18' 13.21" N	46° 09' 18.53" W	412 678 (zone 23N)	5 239 558 (zone 23N)	378

3.1.2. Acoustic Environment in the Program Area

3.1.2.1. Bathymetry

Water depths throughout the Program Area were extracted from the SRTM15+ global bathymetry grid, a 15 arc-second grid (~300 × 460 m at the studied latitude) rendered for the entire globe (Rodríguez et al. 2005). The water depth in the Orphan Basin area varies from about 200 m on the continental shelf, west of the modelled sites to >4000 m toward the east (Figure 7).

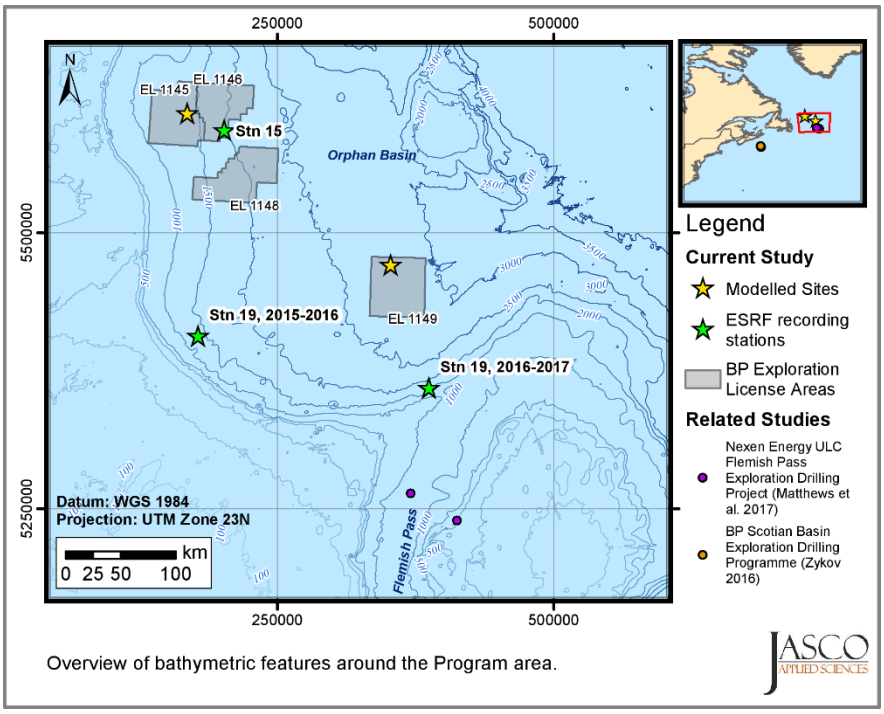

Figure 7. Orphan Basin bathymetry, derived from data from SRTM15+ global bathymetry grid (Rodríguez et al. 2005).

3.1.2.2. Geoacoustics

On the Grand Banks continental shelf, through the Flemish Pass and in southern Orphan Basin, the shallow sedimentary layers consist of thick grey muds (silt mixed with 10–30% sand and 20–40% clay) with varying amounts of debris and sand bed horizons (Huppertz 2007). The depth (~1100 m) and narrow banks of Flemish Pass trap sediment deposits from the continental shelf. Sediment thickness throughout the Program Area is >2500 m, reaching ~4000 m in Flemish Pass (Divins 2007, Géli et al. 2007).

For the purpose of predicting transmission loss at the two selected sites (presented in Section 3.1.1), generic geoacoustic profiles were constructed to represent two water depth regimes. A thick layer of silt/mud was assumed for both profiles. The average grain size of the silt was assumed to decrease with increasing water depth. Representative grain sizes and porosity were used in the grain-shearing model proposed by Buckingham (2005) to estimate the geoacoustic parameters required to model sound propagation. Tables 4 and 5 list the geoacoustic parameters derived for numeric modelling.

Table 4. *West Orphan (Site EL 1145, 1376 m)*: Geoacoustic parameters derived for the Program Area.

Depth below seafloor (m)	Material	Density (g/cm^3)	P-wave speed (m/s)	P-wave attenuation (dB/λ)	S-wave speed (m/s)	S-wave attenuation (dB/λ)
0–5		1.5–1.7	1525–1585	0.25–0.40	130	3.65

Depth below seafloor (m)	Material	Density (g/cm³)	P-wave speed (m/s)	P-wave attenuation (dB/λ)	S-wave speed (m/s)	S-wave attenuation (dB/λ)
5–50	Silt mixed with sand and clay	1.7–2.0	1585–1775	0.40–0.75		
50–500		2.0–2.1	1775–2100	0.75–1.40		
>500		2.1	2100	1.40		

Table 5. *East Orphan (Site EL 1149, 2774 m)*: Geoacoustic parameters derived for the Program Area.

Depth below seafloor (m)	Material	Density (g/cm³)	P-wave speed (m/s)	P-wave attenuation (dB/λ)	S-wave speed (m/s)	S-wave attenuation (dB/λ)
0–5	Silt mixed with sand and clay	1.5–1.7	1505–1555	0.20–0.30	85	3.65
5–50		1.7–2.0	1555–1700	0.30–0.50		
50–500		2.0–2.1	1700–1920	0.50–1.00		
>500		2.1	1920	1.00		

3.1.2.3. Underwater Sound Speed Profile

Sound speed profiles in the Program Area were derived from temperature and salinity profiles from the U.S. Naval Oceanographic Office's *Generalized Digital Environmental Model V 3.0* (GDEM; Teague et al. 1990, Carnes 2009). GDEM provides an ocean climatology of temperature and salinity for the world's oceans on a latitude-longitude grid with 0.25° resolution, with a temporal resolution of one month, based on global historical observations from the U.S. Navy's Master Oceanographic Observational Data Set (MOODS). The climatology profiles include 78 fixed depth points to a maximum depth of 6800 m (where the ocean is that deep). The GDEM temperature-salinity profiles were converted to sound speed profiles according to Coppens (1981).

Mean monthly sound speed profiles were derived from the GDEM profiles for the entire year at the two selected model sites (Figure 8). The left and middle figures only show the upper 200 m of the sound speed profiles, as this is where the monthly variability is exhibited; below this depth the sound speed exhibits the same uniform positive pressure-based gradient with increasing depth, essentially independent of seasonality. Figure 8, right, compares the profiles at both sites, for June, down to a water depth of 1500 m.

The upper portion of the sound speed profile in the Program Area varies between slightly upward-refracting and isovelocity (December to April) and downward refracting (August to November). A weak sound channel, with a sound speed minimum at ~50-75 m, develops in EL 1145 between May and July. In general, the sound emitted in the top 100 m of the water column will tend to refract toward the surface from December to April, toward the seafloor from August to November, but toward the sound speed minimum from May to July. There is little temporal variation in the profiles at depths greater than ~100 m. At these depths, the sound speed increases slightly with depth, mainly due to the increase in ambient pressure.

To assess transmission loss at sites EL 1145 and EL 1149, a single representative sound speed profile was selected at each location. This profile would be typical of the propagation conditions expected during the months that BP has indicated are preferred for drilling activity (May to October); the sound speed profile for June was selected.

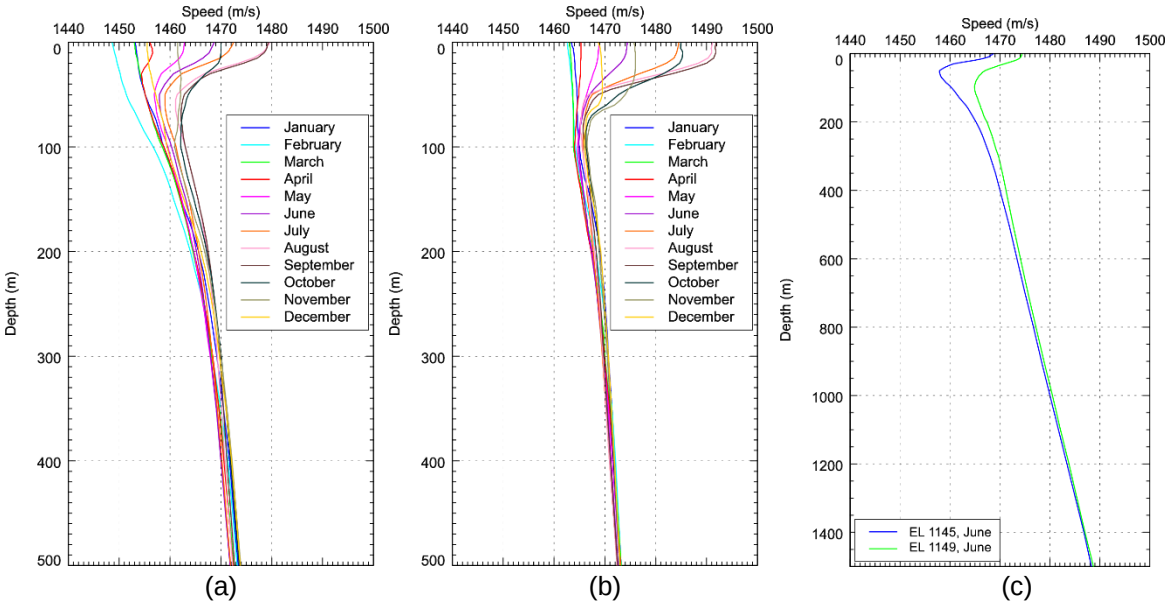

Figure 8. Mean monthly sound speed profiles for the a) West Orphan Site EL 1145, b) East Orphan Site EL 1149, c) both locations in June, derived from data obtained from *GDEM V 3.0* (Teague et al. 1990, Carnes 2009).

3.2. Ambient Sound Data Collection

For the ESRF Study, underwater sound was recorded with Autonomous Multichannel Acoustic Recorders (AMARs; Appendix C). AMARs were deployed at 20 locations (see Figures C-1 and 2) between Aug 2015 and Jul 2017 (see Tables C-1 and 2). Recordings at the two stations closest to the Program Area were used in the present study to derive ambient sound levels. Station 15 was in 2000 m water depth, approximately between EL 1146 and EL 1148, less than 50 km from any part of EL 1145, EL 1146, or EL 1148, and ~200 km from EL 1149. Station 19 was located ~150 km from the Program Area in ~1280 m water depth (Station 19a in Figure 1). The location of Station 19 was changed in 2016–2017 to Sackville Spur at the north end of the Flemish Pass (Station 19b in Figure 1), ~100 km south of EL 1149 and 300 km southeast of the other parts of the Program Area, in ~1550 m water depth. Both stations used the same mooring configuration (see Figure C-4) with an AMAR suspended about 25 m above the seafloor. A 42AC pistonphone calibrator (G.R.A.S. Sound & Vibration A/S; Figure C-8) was used to verify the sensitivity of systems.

Appendix C provides detailed information about deployment locations and mooring designs (Appendix C.1), the acoustic recorders (Appendix C.2), and recorder calibrations (Appendix C.3).

Acoustic data analysis methods are described in Appendix C.4, including methods to identify periods with seismic surveys and shipping were detectable in the soundscape.

4. Results

4.1. Sound Sources

4.1.1. Semisubmersible Platform, Drillship, and Support Vessel

The highest sound levels from MODU and vessels while in DP are generated by the propellers. Thus, source levels associated with drill rigs and support vessels are often estimated based on a platform's propulsion system (i.e., the number and type of thrusters, their diameter, revolution rate, and the number of blades). The source level spectra for these platforms can be estimated based on equations from Ross (1976) and Brown (1977) and the spectrum for sound generated by cavitation processes.

In this analysis, we considered the semi-submersible platforms West Hercules, West Aquarius, and West Sirius (from Seadrill) as relevant examples for the Program; Table 6 provides their propulsion system specifications. Although the thrusters type, blade speed, and number of blades for the West Hercules and West Aquarius were unavailable at the time of this study, their specifications would be similar to those for the sister platform, the West Sirius. The presented spectrum derived for the thrusters on these semi-submersible platforms (labelled *Seadrill SS* in Figure 9) has been previously reported by JASCO (Zykov 2016, Matthews et al. 2017, Quijano et al. 2017) and used in modelling studies to assess distances to marine mammal effect thresholds (Zykov 2016, Matthews et al. 2017).

The Stena Carron was used as a representative drillship for the Program. It has an identical DP system and similar thrusters to the Deep Ocean Clarion drillship, which was also analyzed by Zykov (2016). The representative spectra for the thrusters of the Deep Ocean Clarion is compared to those of the semi-submersible platforms in Figure 9 (labelled *Clarion*).

At the time of this study, the type of support vessel that might be used in the Program was unknown. A representative vessel was chosen from the previous study for BP, by Zykov (2016), off the Scotian shelf. The estimated source level spectra for the support vessel were based on the bow and aft thrusters of the Damen platform supply vessel 3300CD. This vessel design has been in service for 5–7 years. It has a similar power plant and thruster configuration to other platform supply vessels; Table 6 lists specifications.

Table 6. Propulsion system specifications of semi-submersible drilling units, a drillship, and a supply vessel. Specification for units considered in previous studies of similar operations (Zykov 2016, Matthews et al. 2017, Quijano et al. 2017).

Platform	Surrogate vessel	Propeller		Max. power (kW)	Number of thrusters	Thruster model	Number of blades	Acoustic source depth* (m)
		Diameter (m)	Nominal speed (rpm)					
Semi-submersible	West Hercules/ West Aquarius	3.5	NA	3500	8	Rolls Royce, specific model NA	NA	23
	West Sirius	3.5	177	3800	8	UUC355	4	18
Drillship	Deep Ocean Clarion (equivalent to Stena Carron)	4.1	157	5500	6	UUC455	4	10
Supply vessel	Damen platform supply vessel 3300CD, Aft thrusters	2.3	250	2000	2	NA (azimuthal)	4	5
	Damen platform supply vessel 3300CD, Bow thrusters	1.7	290	750	2	NA (tunnel)	4	5

* Based on the platform's draft and propeller diameter.
NA means the data were "Not Available" at the time of this study.

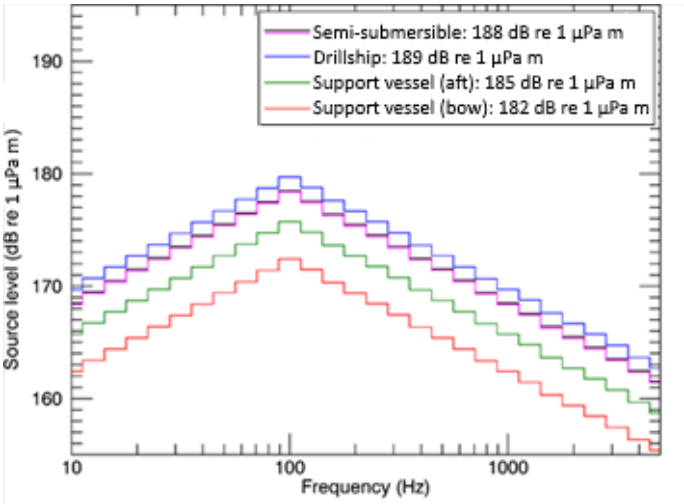

Figure 9. Estimated sound spectra for individual thrusters associated with semi-submersibles, drillship, and support vessels (Zykov 2016). Broadband SPL for individual thrusters are provided in the legend.

Equivalent source levels representative of the platforms in the far field (i.e., where multiple thrusters can be approximated as an equivalent single sound source) can be derived by summing over the total number of thrusters per platform (Zykov 2016). For the purpose of a simplified comparison between various platforms, broadband equivalent source levels are compared in Table 7.

When considered as a point source, the spectra and broadband source levels are identical for both platforms since the method accounts only for the broadband level value based on the specifications of the thrusters, i.e., 196.7 dB re 1 µPa. The drillship is equipped with UUC 455 thrusters, which are slightly louder than the UUC 355 thrusters on the semi-submersible platforms, but the number of thrusters differ (six on the drillship, and eight on the semi-submersible platforms). The differences in the depth of the thrusters will result in differences in received levels in the far field, however, because of various propagation effects.

Based on the analysis of the modelled acoustic fields of the presented platforms (Zykov 2016), accurate sound field assessment at distances less than 500 m must consider the actual locations of the thrusters on the platform.

Table 7. Equivalent source levels representative of the platforms in the far-field.

Platform	Surrogate vessel	Equivalent far-field broadband source level (dB re 1 µPa m)
Semi-submersible	West Hercules/ West Aquarius	196.7
	West Sirius	196.7
Drillship	Deep Ocean Clarion (equivalent to Stena Carron)	196.7
Supply vessel	Damen platform supply vessel 3300CD	188.6

4.1.2. VSP Source Array

The Program activities include the use of a Vertical Seismic Profiling (VSP) seismic array. Typically, these arrays include 3–6 seismic elements with volumes between 150 and 250 in^3. The Schlumberger's Hypercluster Air Gun Array is one such typical VSP array. It is a 6-element array with individual volumes of 250 in^3 (1500 in^3 total firing volume). This array layout consists of two triangular 3-element airgun clusters, separated by 1.7 m, with a central tow depth of 5 m (Figure 10, Table 8).

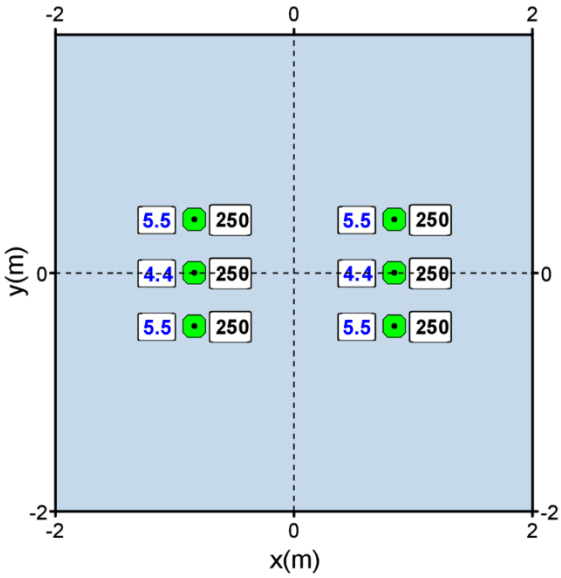

Figure 10. Layout of the Schlumberger's Hypercluster Air Gun Array (1500 in^3 total firing volume, 5 m depth). Black numbers are airgun firing volume in cubic inches. Blue numbers are the depth of the airgun below the sea surface.

Table 8. Relative airgun positions within the 1500 in^3 airgun array.

Gun	*x* (m)	*y* (m)	*z* (m)	Volume (in^3)
1	0	-0.85	4.4	250
2	-0.445	-0.85	5.5	250
3	0.445	-0.85	5.5	250
4	0	0.85	4.4	250
5	-0.445	0.85	5.5	250
6	0.445	0.85	5.5	250

The directional signature and power spectrum of the airgun array were predicted by Quijano et al. (2017) using JASCO's Airgun Array Source Model (AASM), which accounts for:

- Array layout;
- Volume, tow depth, and firing pressure of each airgun; and
- Interactions between different airguns in the array.

AASM includes both a low-frequency and a high-frequency module for predicting different components of the airgun array spectrum from 10 Hz to 2 kHz. In this model, the notional signatures (i.e., the pressure waveforms of the individual elements at a standard reference distance of 1 m) account for the interactions with the other airguns in the array. The signatures are summed with the appropriate phase delays to

obtain the far-field source signature of the entire array in all directions. More details on AASM are provided in Appendix B.1.

The maximum extent of the near field of an array (R_{nf}; where the array elements add incoherently) can be estimated as:

$$R_{nf} < \frac{l^2}{4\lambda} \quad (1)$$

where λ is the sound wavelength and l is the longest dimension of the array (Lurton 2002, §5.2.4). For example, an airgun array length of l = 16 m yields a near-field range of 85 m at 2 kHz and 17 m at 100 Hz. Beyond this R_{nf} range, the array is assumed to radiate like a directional point source and is usually treated as such for propagation modelling.

The horizontal overpressure signatures and corresponding power spectrum levels for the representative VSP array, at a depth of 5 m (to the vertical centre of the gun clusters), are shown in Figure 11 and Table 9 for the broadside (perpendicular to the tow direction) and endfire (parallel to the tow direction) directions. The signatures consist of a strong primary peak related to the initial firing of the airguns, followed by a series of pulses associated with bubble oscillations. Most energy is produced at frequencies below 400 Hz (Figure 11b). The spectrum contains peaks and nulls resulting from interference among airguns in the array, where the frequencies at which they occur depend on the volumes of the airguns and their locations within the array. The horizontal 1/3-octave-band directivities are shown in Figure 12.

For this array, energy is concentrated at frequencies below 400 Hz, with broadband SEL of 222.6 dB re 1 µPa²·s m (broadside) and 222.4 dB re 1 µPa²·s m (endfire). Levels calculated in the 1–2 kHz band are 43–53 dB lower than at lower frequencies. Levels at higher frequencies are expected to decrease by about 30 dB per decade.

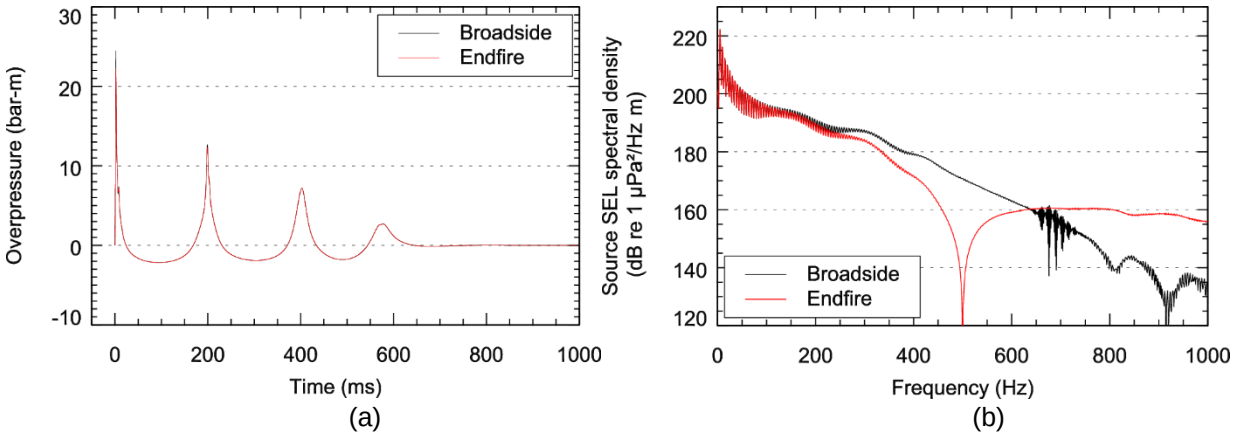

Figure 11. Predicted (a) overpressure signature and (b) power spectrum in the broadside and endfire (horizontal) directions for the representative 1500 in³ VSP array. Surface ghosts (effects of pulse reflection at the water surface) are not included in these signatures as they are accounted for by the propagation model (Quijano et al. 2017).

Table 9. Horizontal source level specifications (10–2000 Hz) for the representative 1500 in³ VSP array at 5 m depth, computed with AASM in the broadside and endfire directions. Surface ghost effects are not included as they are accounted for by the propagation model (Quijano et al. 2017).

Direction	Zero-to-peak sound pressure level (PK; dB re 1 µPa m)	SEL (dB re 1 µPa²·s m)		
		0.01–2 kHz	0.01–1 kHz	1–2 kHz
Broadside	247.8	222.6	222.6	169.5
Endfire	247.0	222.4	222.4	179.2

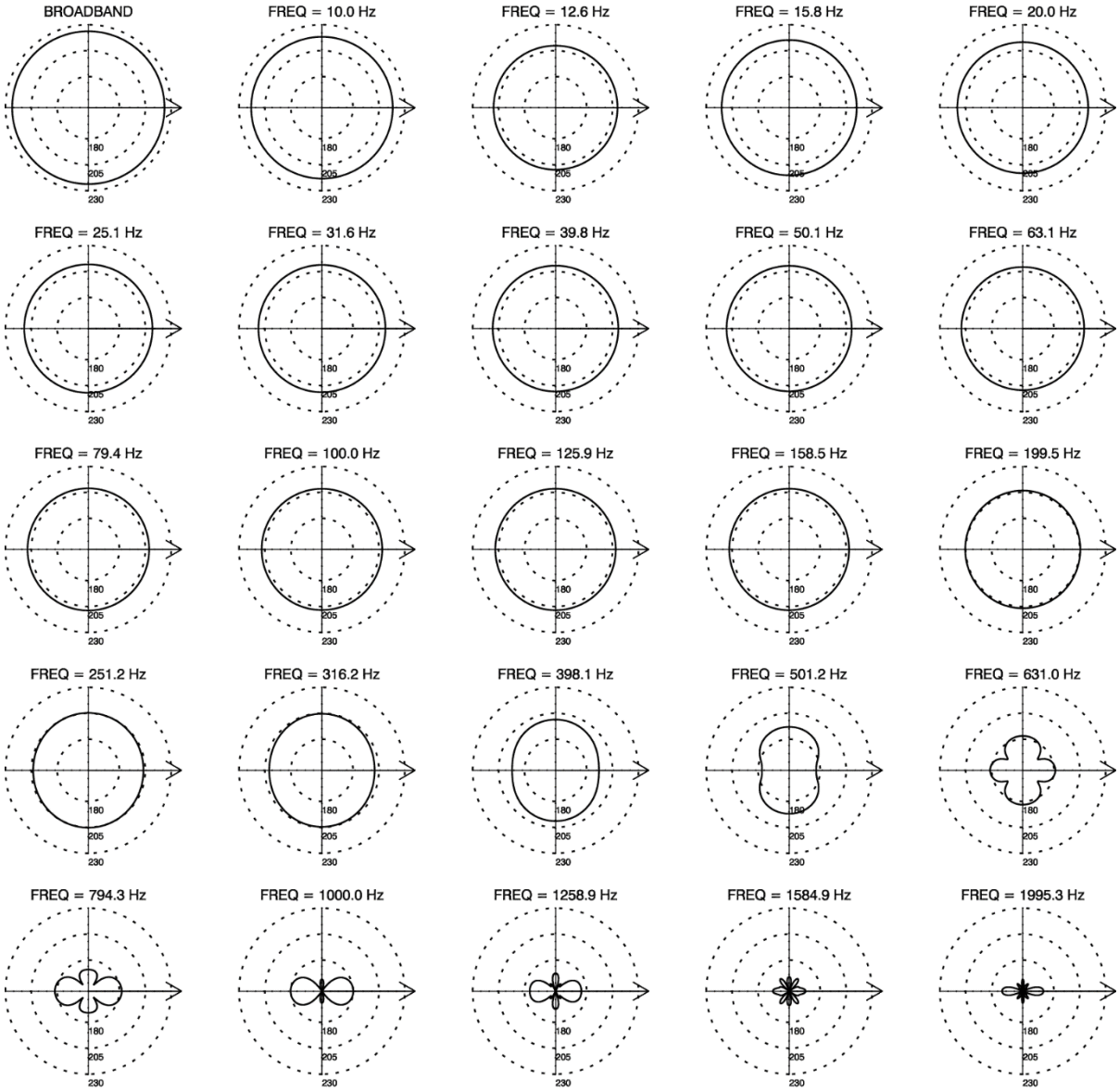

Figure 12. Horizontal directivity of the representative 1500 in^3 VSP array. Source levels (dB re 1 µPa^2·s m) in 1/3-octave-bands. The 1/3-octave-band centre frequencies are indicated above each plot.

Larger arrays have also been considered for VSP activities. For example, the array considered in the underwater sound assessment for the Scotian Basin Project (Zykov 2016) was the Schlumberger Dual Magnum 2400 in^3 airgun array at 4.5 m depth (to the vertical centre of the element clusters). This airgun array consists of four triangular clusters with in-line separations of 2 m; the two external clusters are assemblies of three 250 in^3 elements, and the two internal clusters are assemblies of three 150 in^3 elements. AASM modelling of this 2400 in^3 array yielded broadband SEL of 224.7 dB re 1 µPa^2·s m (broadside) and 224.1 dB re 1 µPa^2·s m (endfire), with most of the energy in the frequency band 10 to 200 Hz.

4.2. Sound Propagation

4.2.1. Comparing Acoustic Environments

The sound levels measured at some distance from a source depend mainly on the source-receiver distance, propagation effects of the physical environment, and the sound frequency. Sound propagation is influenced by the bathymetry at and around the sound source, the geoacoustic properties of the seafloor, the variation in sound speed in the water as a function of depth, and the spectral characteristics of the sound source. This section compares the environmental parameters expected within the Program Area (detailed in Section 3.1.2, Figures 7–8, and Tables 4–5) to those for the Scotian Basin Project (Zykov 2016) and the Flemish Pass Project (Matthews et al. 2017).

4.2.1.1. Bathymetry

Modelled sites for the Scotian Basin Project (Zykov 2016) were located off the continental shelf, near the bottom of the slope. The modelled area is characterized by the continental shelf to the northwest of the modelled sites, and relatively flat, deep water (>2000 m) to the southwest, south, and northeast. Sound levels that reach the continental shelf is rapidly attenuated between the 200 m and 50 m isobaths; sound levels propagating parallel and away from the shelf can persist for long distances (>100 km).

The bathymetry in Flemish Pass is characterized by a deep channel (~1200 m depth) bounded by the continental shelf (≤200 m depths) to the west, and the Flemish Cap (≤200 m depth) to the east. As for the sound off the Scotia Shelf, sound levels that reaches shallow water is rapidly attenuated, while sound levels propagating along deeper water persist for longer distances (Matthews et al. 2017).

Sound from the planned Program activities in EL 1145, EL 1146, and EL 1148 (Figure 7) is expected to be bounded by the continental shelf, west of the site. The bathymetric features around EL 1149 (such as the continental shelf, Flemish Pass, and Flemish Cap, more than 150 km away) are expected to have minimal influence on sound propagation in the area.

4.2.1.2. Geoacoustic Properties

In general, the differences between geoacoustic properties for the Program Area and the related studies (Zykov 2016, Matthews et al. 2017) are not expected to be a major factor influencing differences in sound propagation at the various sites. The profiles developed for representing the geoacoustic properties in the Program Area (Section 3.1.2.2) were based on the same references and model as those developed for the Flemish Pass Project (Matthews et al. 2017). The water depth being greater in Orphan Basin, the profiles are representative of smaller average grain size than for the shallow site used in the Flemish Pass Project. The Buckingham grain-shearing model was also used to derived a generic geoacoustic profile for the Scotian Basin Project (Zykov 2016). The expected think clay layer in this area, of the continental slope, results in similar geoacoustic properties than in Orphan Basin.

4.2.1.3. Underwater Sound Speed Profile

For comparison purposes, the top portion of the mean monthly sound speed profiles for the Scotian Basin Project (Zykov 2016) and the Flemish Pass Project (Matthews et al. 2017) are presented in Figure 13, along with the Program Area monthly profiles (near EL 1145).

The sound speed profile from the Scotian Basin Program (Figure 13b) results in more complex propagation effects than expected for in Program Area. In winter, there is a strong sound speed minimum in the top 200 m of the water column that supports long range propagation. Below 200 m, there is a second sound speed minimum that tends to confine sound closer to the seabed where it is attenuated through spreading and absorption. In spring and summer, there is a weaker sub-surface sound channel with a sound speed minimum near 50 m, and a stronger deep sound channel with its minimum below

500 m. In August, the maximum extent of the SPL thresholds of 160 dB re 1 µPa off the Scotia shelf was modelled to 8.44 km for the VSP array at Site B, and extent of the SPL thresholds of 120 dB re 1 µPa in modelled to 61.0 km for the semi-submersible platform (with support vessel) at Site B. In February, the distance for the VSP array at Site B is shorter (3.57 km), while the distance for the semi-submersible platform (with support vessel) at Site B is longer (>150 km).

The seasonal variation in the profiles derived for the Flemish Pass Project (Figure 13c) is more similar to the seasonal variation in the Program Area than in the Scotian Basin. The monthly profiles from January to May are the least downward refracting; sound is expected to propagate to longer distances during this period. For the Flemish Pass Project, May was selected for modelling since this profile is the least downward refracting during the months that are traditionally most operationally active (May to October). In May, the maximum extent of the SPL threshold of 160 dB re 1 µPa in Flemish Pass was modelled to 6.35 km for the VSP array at the deep site, and the extent of the SPL threshold of 120 dB re 1 µPa was modelled to 47.6 km for the drilling platform at the deep site.

In the Program Area, we expect smaller seasonal variations in propagation conditions than were predicted for the Scotian Basin. Sound propagation in June should be more similar to that modelled in May in Flemish Pass than that in August or February for the Scotian Basin. However, Figure 8c shows that a weak sound channel is present in the profile for EL 1145. This feature can be favourable to long-range propagation for some sound sources, depending on the source's depth and frequency content. In both EL, we expect the profiles for July to November to lead to slightly shorter distances to sound thresholds (for similar sound sources) than in June, since more downward-refracting profiles are expected at that time. Similarly, we expect profiles for December to April to lead to similar or longer distances than in June.

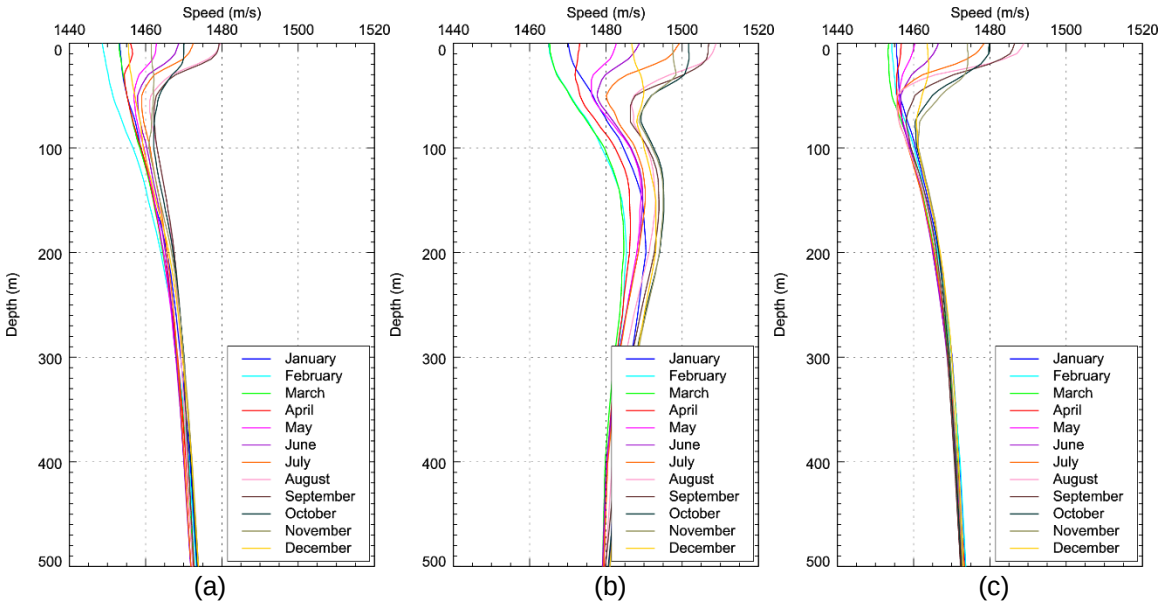

Figure 13. Mean monthly sound speed profiles for the (a) Program Area (West Orphan, in EL 1145), (b) Scotian Basin (Zykov 2016), and (c) Flemish Pass Project (Matthews et al. 2017). All profiles were derived from data obtained from *GDEM V 3.0* (Teague et al. 1990, Carnes 2009).

4.2.2. Transmission Loss

Transmission loss (TL) at Orphan Basin Sites in EL 1145 and EL 1149 was quantified using a parabolic equation (PE) numerical treatment (Section 3.1). The bathymetry (Section 3.1.2.1), geoacoustics (Section 3.1.2.2), and historical average June sound speed profiles (Section 3.1.2.3) were used as the environmental basis of this modelling. Broadband TL results representative of each Program activity were estimated based on the representative source level spectra and source depth, presented in Section 4.1. Two depths for the semi-submersible platform was analyzed: 18 and 23 m.

The results are presented as vertical cross-sections of the TL field, southwest (215° from UTM north) to northeast (045° from UTM north) of the sound source (Figures 14–18), and as overview maps of minimum broadband TL over depth for a 50 × 50 km area surrounding the modelling sites (Figures 19–23).

To quantify TL associated with each activity, the minimum-over-depth TL results were fitted to a general function of the form:

$$TL = N \times log_{10}(R) \quad (2)$$

to estimate *N*, the transmission loss coefficient, for ranges, *R*, up to 50 km from the sources. Tables 10 and 11 list the estimated transmission loss coefficients, as well as distances to minimum-over-depth TL isopleths in terms of maximum radius (R_{max}) and the 95th percentile radius ($R_{95\%}$), defined in Section 3.1.

The transmission loss coefficients giving in Tables 10 and 11 can be used as preliminary estimates of received levels away from each Program activity. For example, an SPL of 140.3 dB re 1 µPa is predicted at 10 km from the deep (23 m) semi-submersible in EL 1145:

$$196.7 – 14.1 \times \log_{10}(10\,000) = 140.3 \text{ dB re 1 µPa} \quad (3)$$

The resulting values are estimated maximum-over-depth broadband received levels. Note that the extent to which these activities could be perceived by, potentially disturb, or potentially injure marine life should consider other factors, such as the hearing sensitivity of species of concerns (e.g., applying frequency filtering based on M-weighting functions).

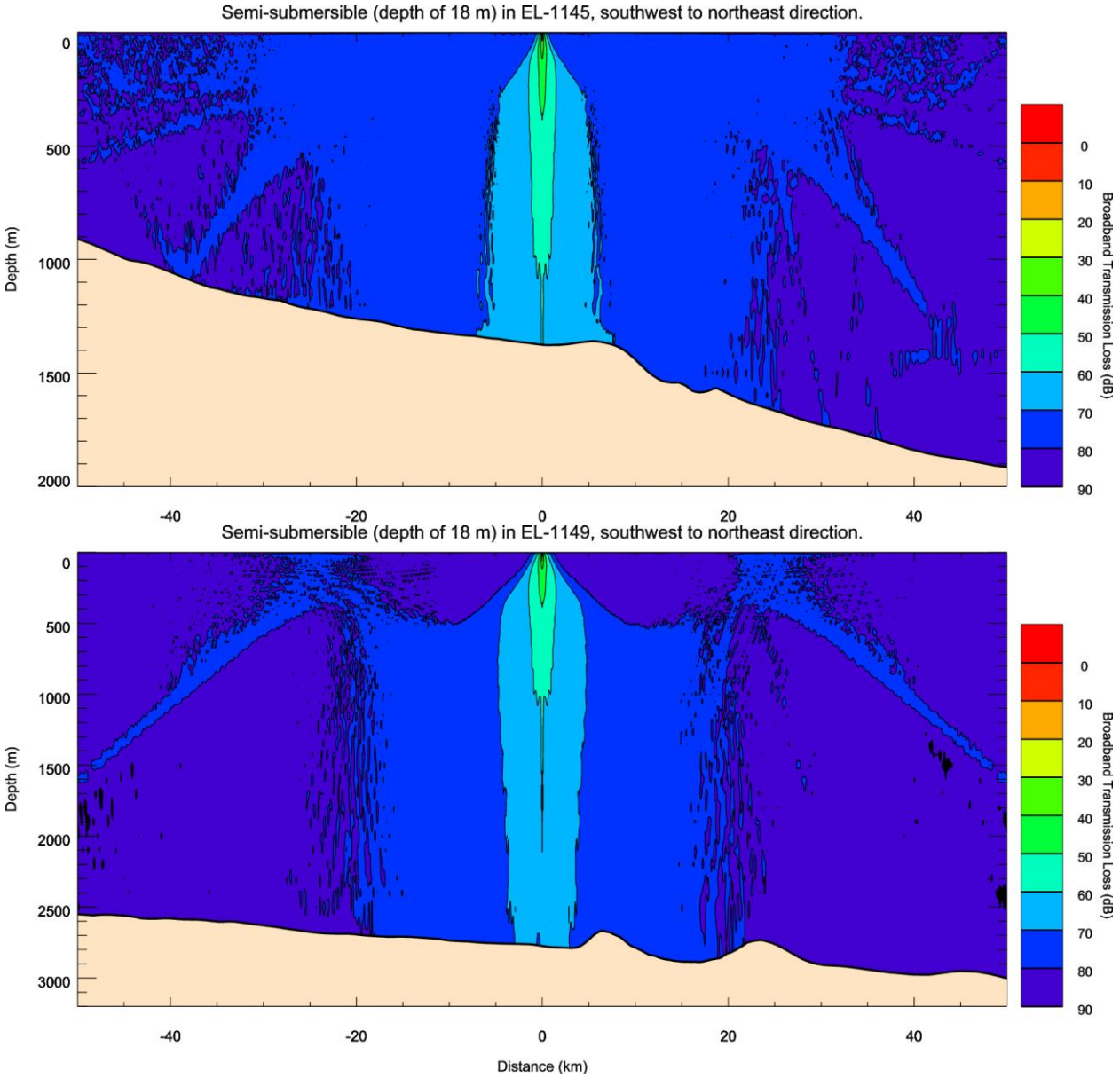

Figure 14. *Semi-submersible platform, 18 m depth*: Broadband transmission loss (dB) in June at the modelled sites in (top) EL 1145 and (bottom) EL 1149, as a function of range and depth, along a bearing of 215° to 045° from UTM north. TL was calculated over frequency bands from 10 to 1600 Hz.

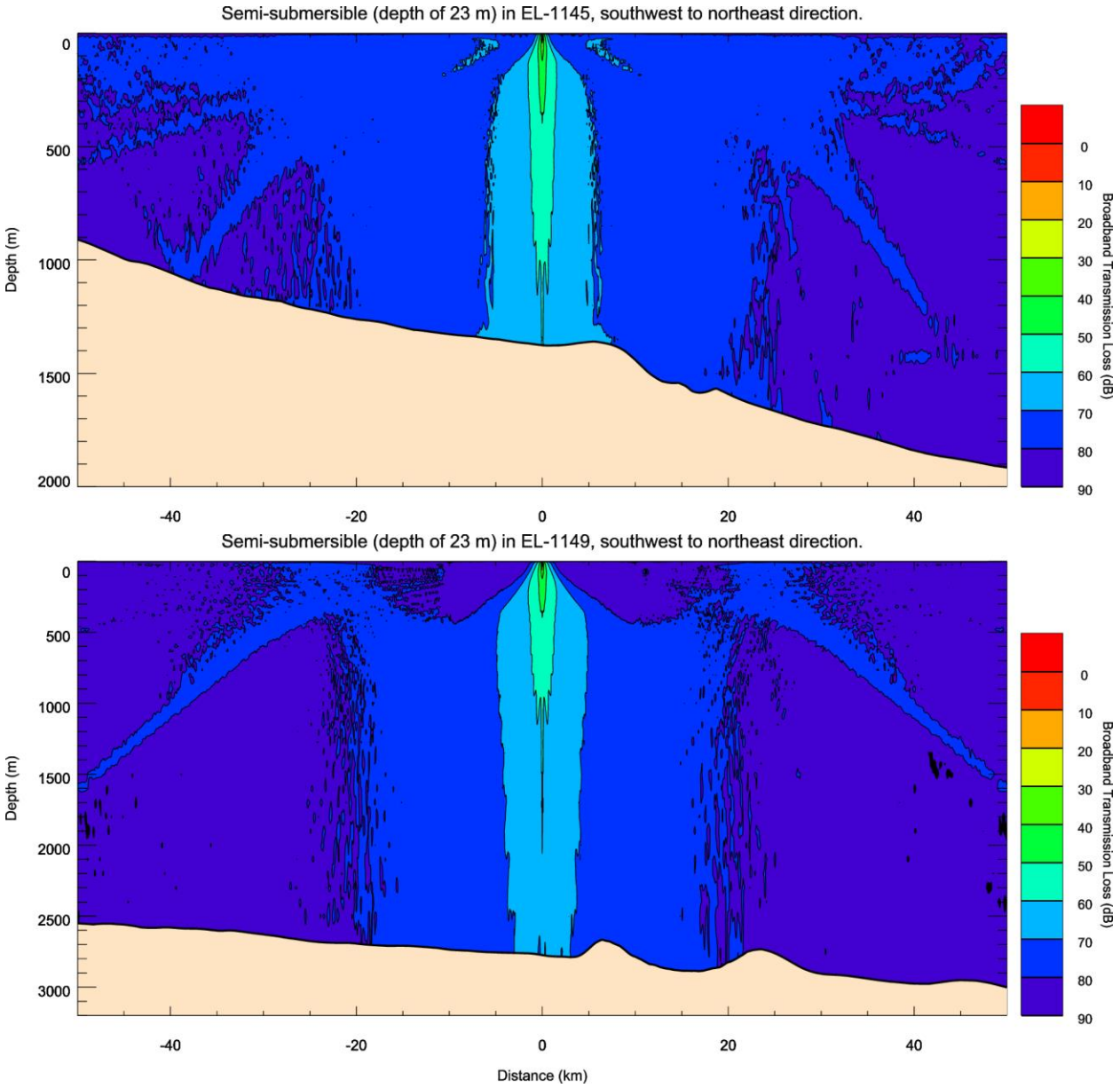

Figure 15. *Semi-submersible platform, 23 m depth*: Broadband transmission loss (dB) in June at the modelled sites in (top) EL 1145 and (bottom) EL 1149, as a function of range and depth, along a bearing of 215° to 045° from UTM north. TL was calculated over frequency bands from 10 to 1600 Hz.

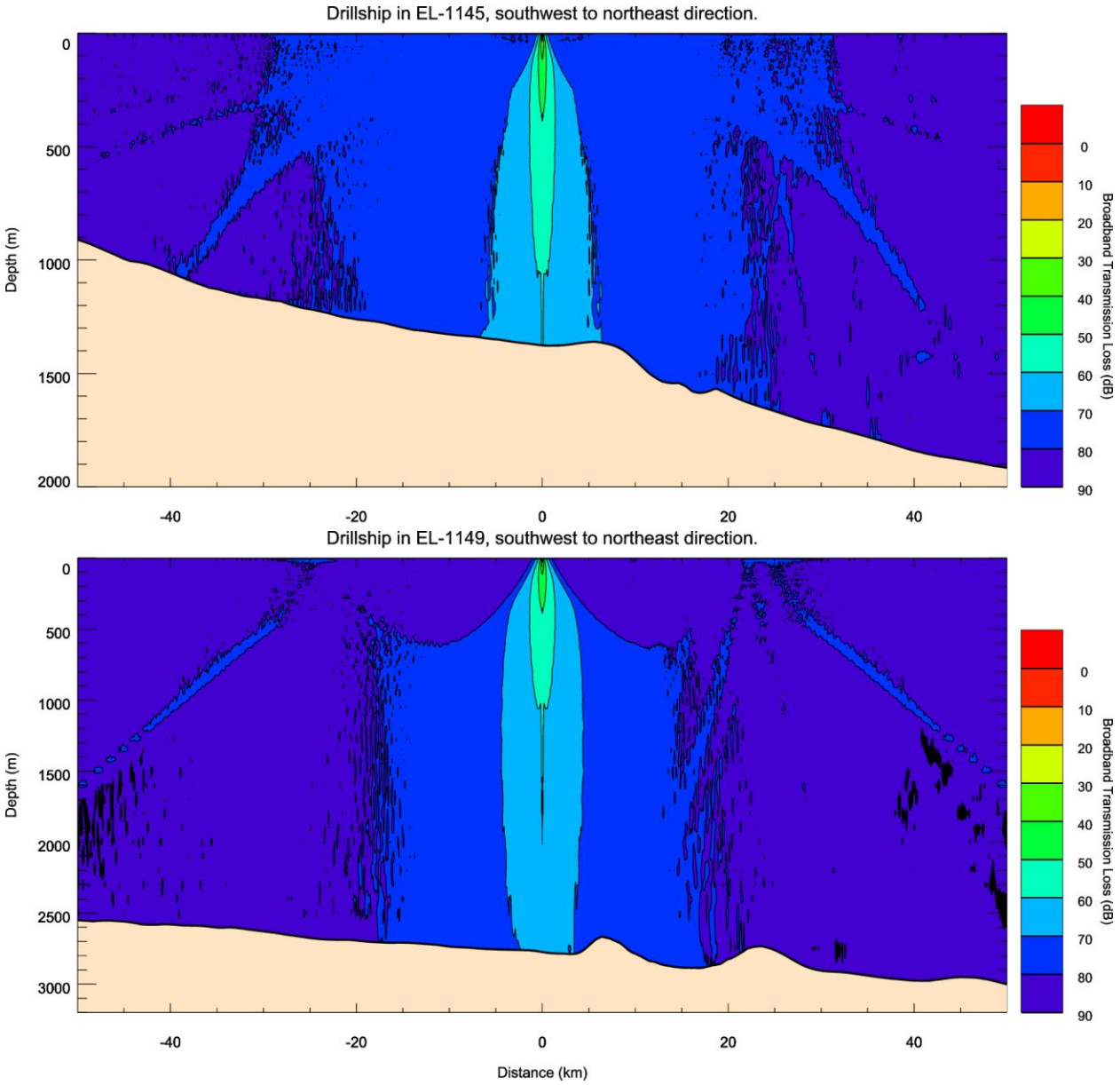

Figure 16. *Drillship, 10 m depth*: Broadband transmission loss (dB) in June at the modelled sites in (top) EL 1145 and (bottom) EL 1149, as a function of range and depth, along a bearing of 215° to 045° from UTM north. TL was calculated over frequency bands from 10 to 1600 Hz.

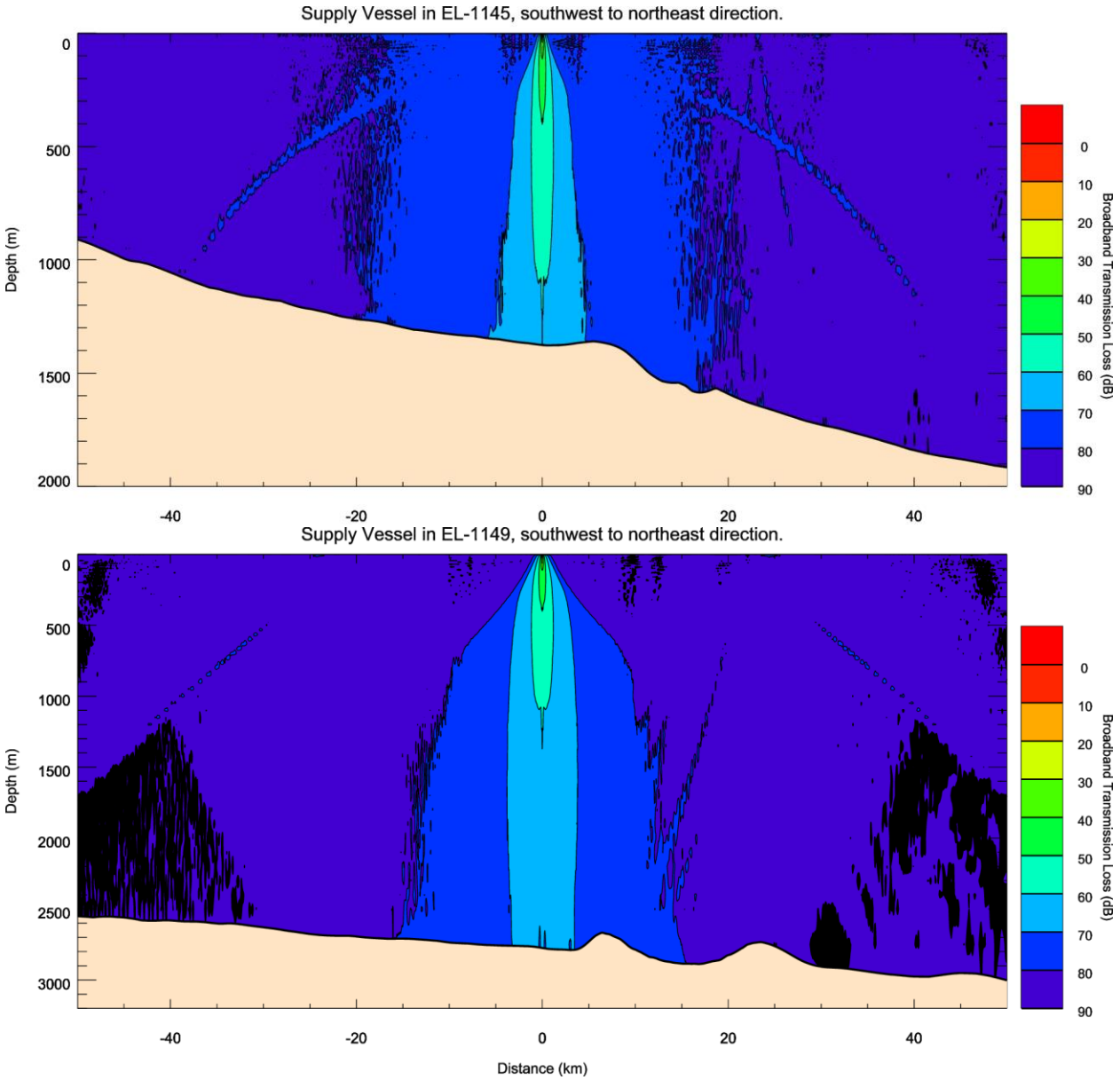

Figure 17. *Support vessel, 5 m depth*: Broadband transmission loss (dB) in June at the modelled sites in (top) EL 1145 and (bottom) EL 1149, as a function of range and depth, along a bearing of 215° to 045° from UTM north. TL was calculated over frequency bands from 10 to 1600 Hz.

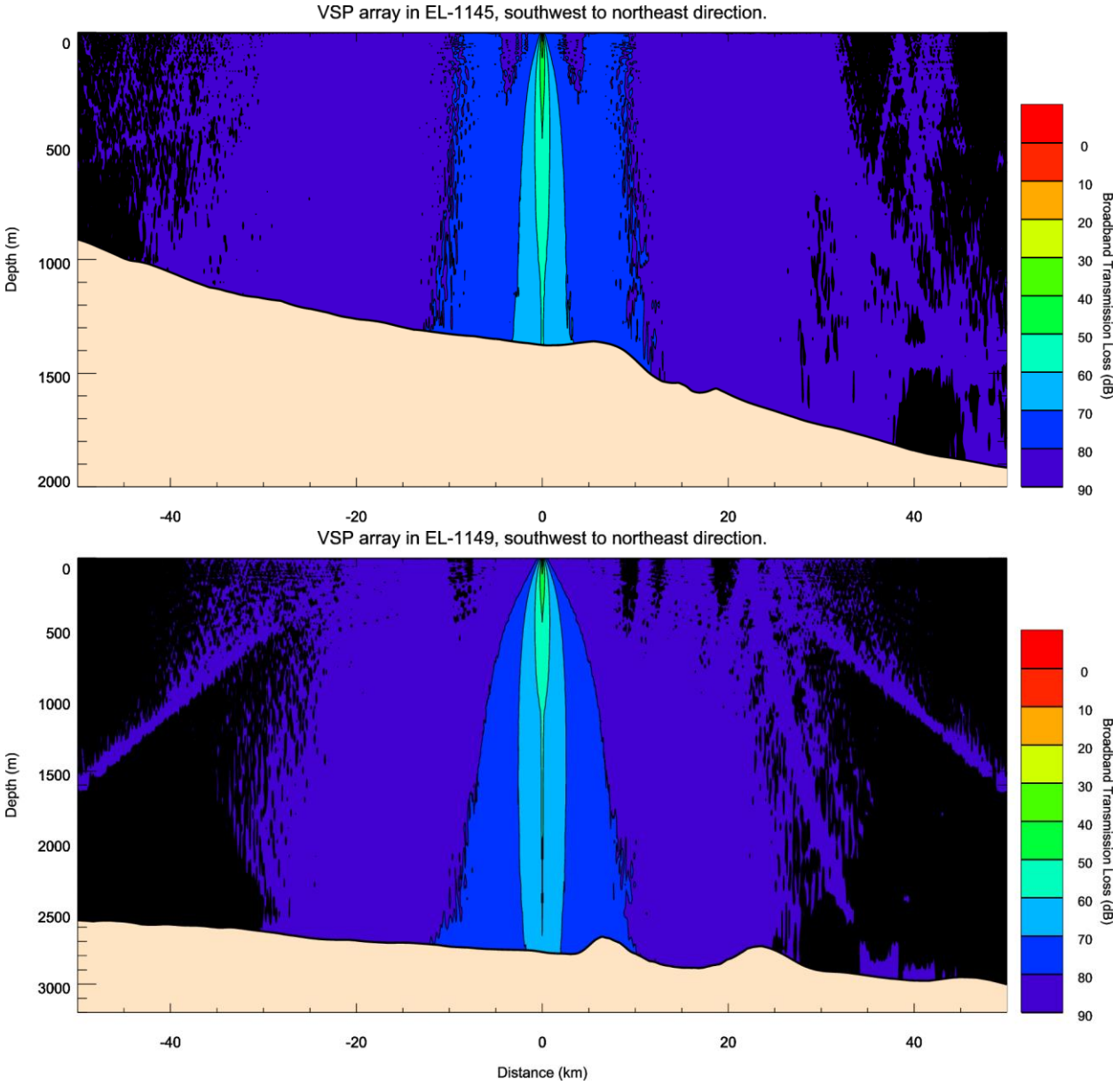

Figure 18. *VSP array, 5 m depth*: Broadband transmission loss (dB) in June at the modelled sites in (top) EL 1145 and (bottom) EL 1149, as a function of range and depth, along a bearing of 215° to 045° from UTM north. TL was calculated over frequency bands from 10 to 1600 Hz.The array heading was 000°, i.e., toward true north.

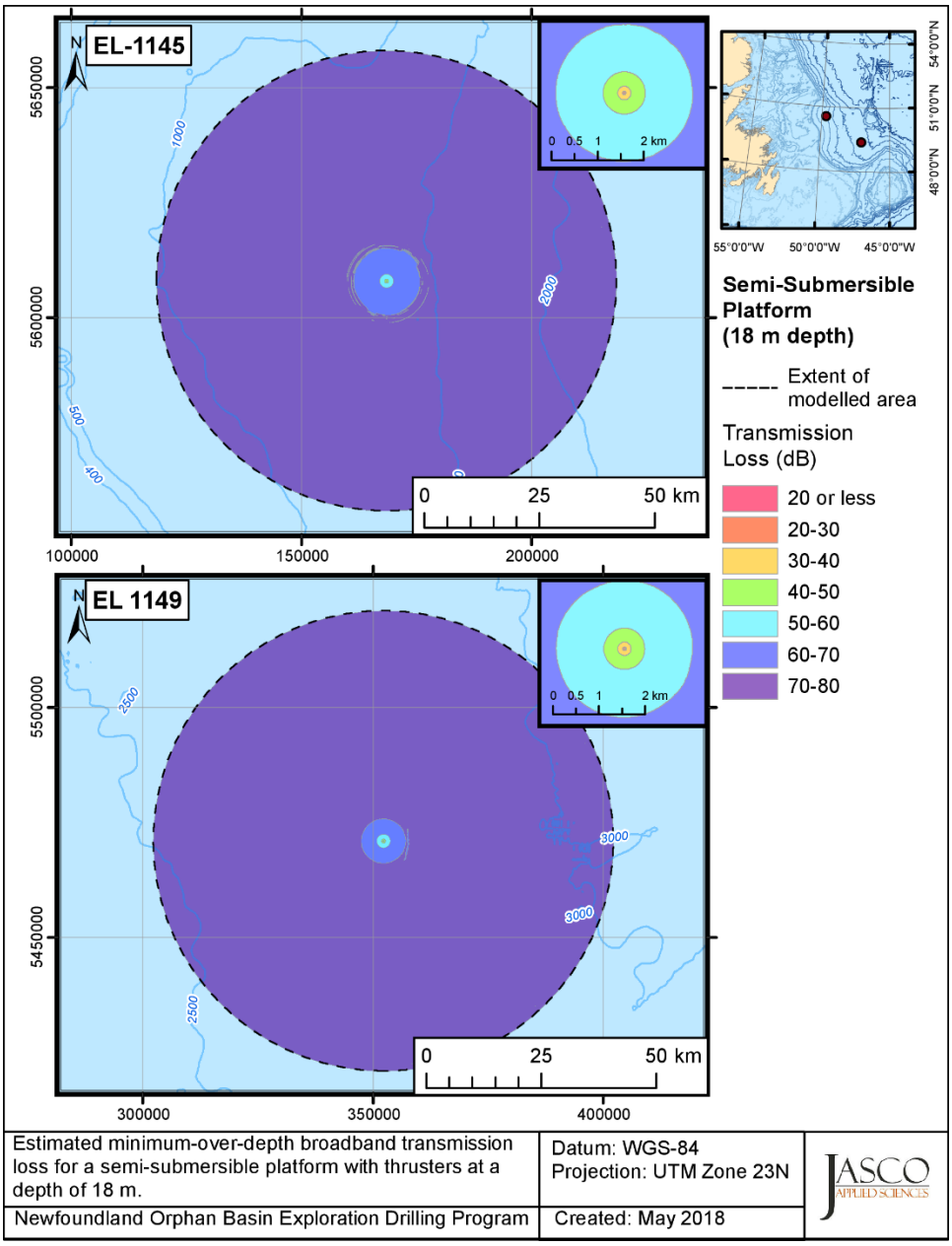

Figure 19. *Semi-submersible platform, 18 m depth*: Map of minimum-over-depth broadband transmission loss (dB) at the modelled site in (top) EL 1145 and (bottom) EL 1149, in June. TL was calculated over frequency bands from 10–1600 Hz.

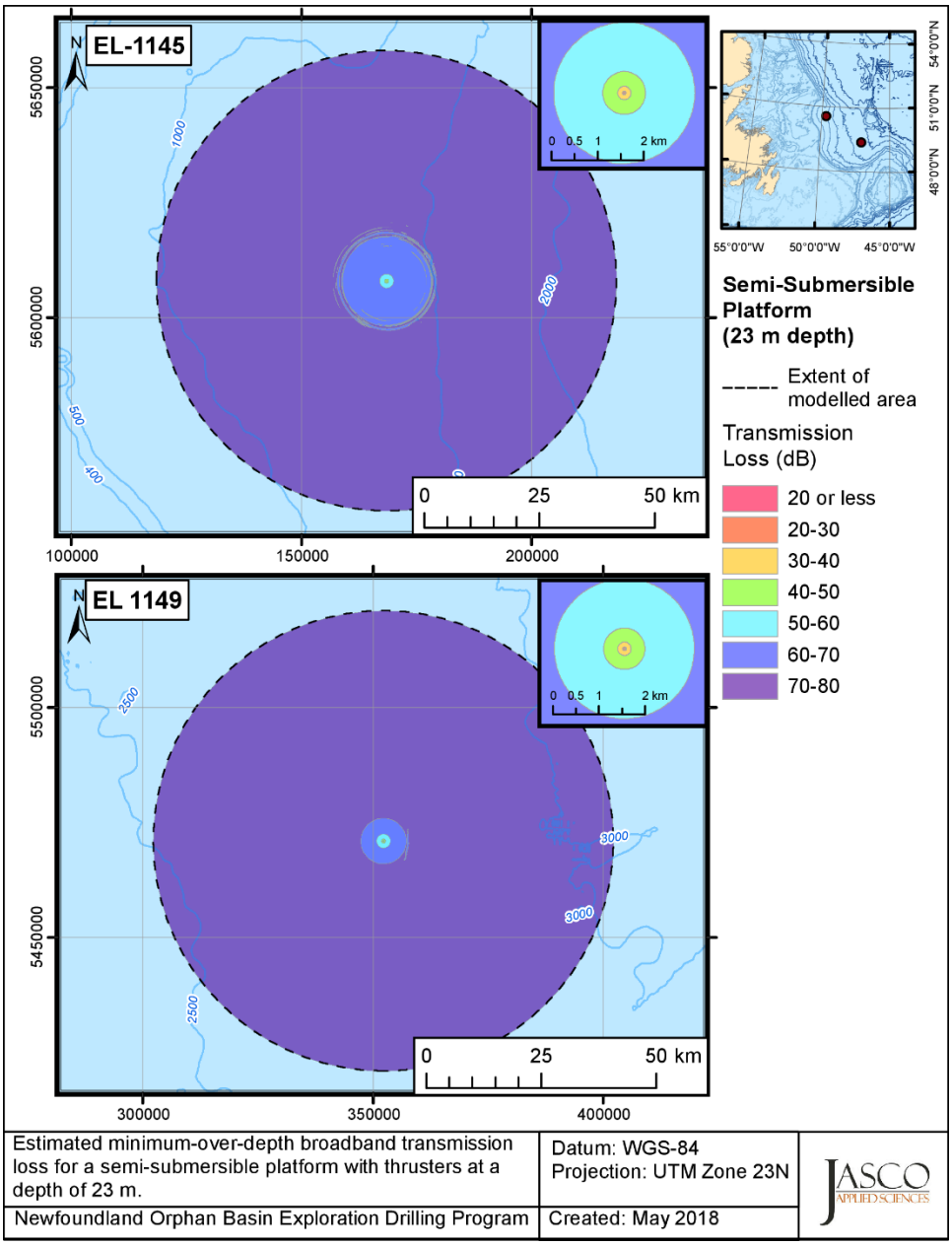

Figure 20. *Semi-submersible platform, 23 m depth*: Map of minimum-over-depth broadband transmission loss (dB) at the modelled site in (top) EL 1145 and (bottom) EL 1149, in June. TL was calculated over frequency bands from 10–1600 Hz.

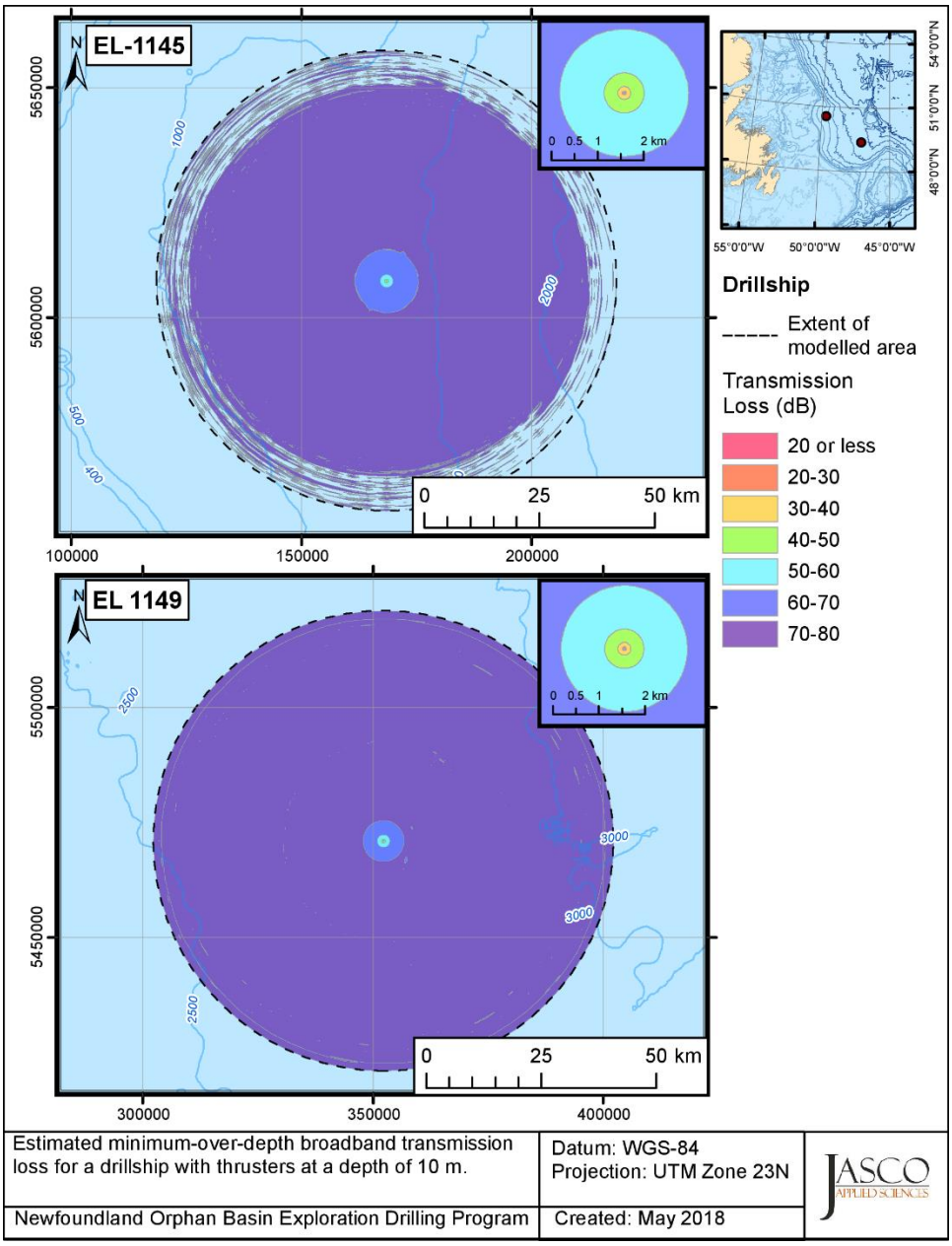

Figure 21. *Drillship, 10 m depth*: Map of minimum-over-depth broadband transmission loss (dB) at the modelled site in (top) EL 1145 and (bottom) EL 1149, in June. TL was calculated over frequency bands from 10–1600 Hz.

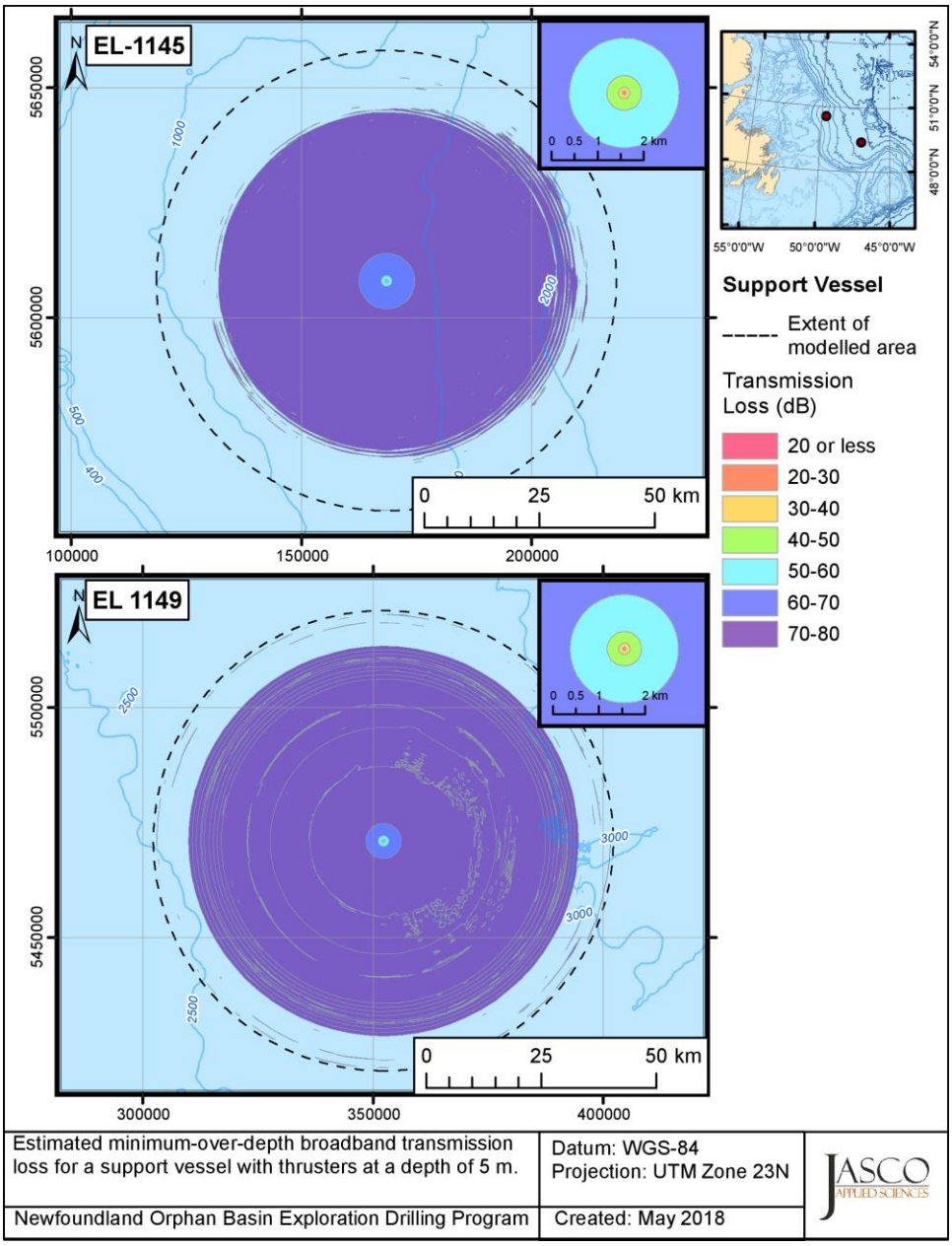

Figure 22. *Support vessel, 5 m depth*: Map of minimum-over-depth broadband transmission loss (dB) at the modelled site in (top) EL 1145 and (bottom) EL 1149, in June. TL was calculated over frequency bands from 10–1600 Hz.

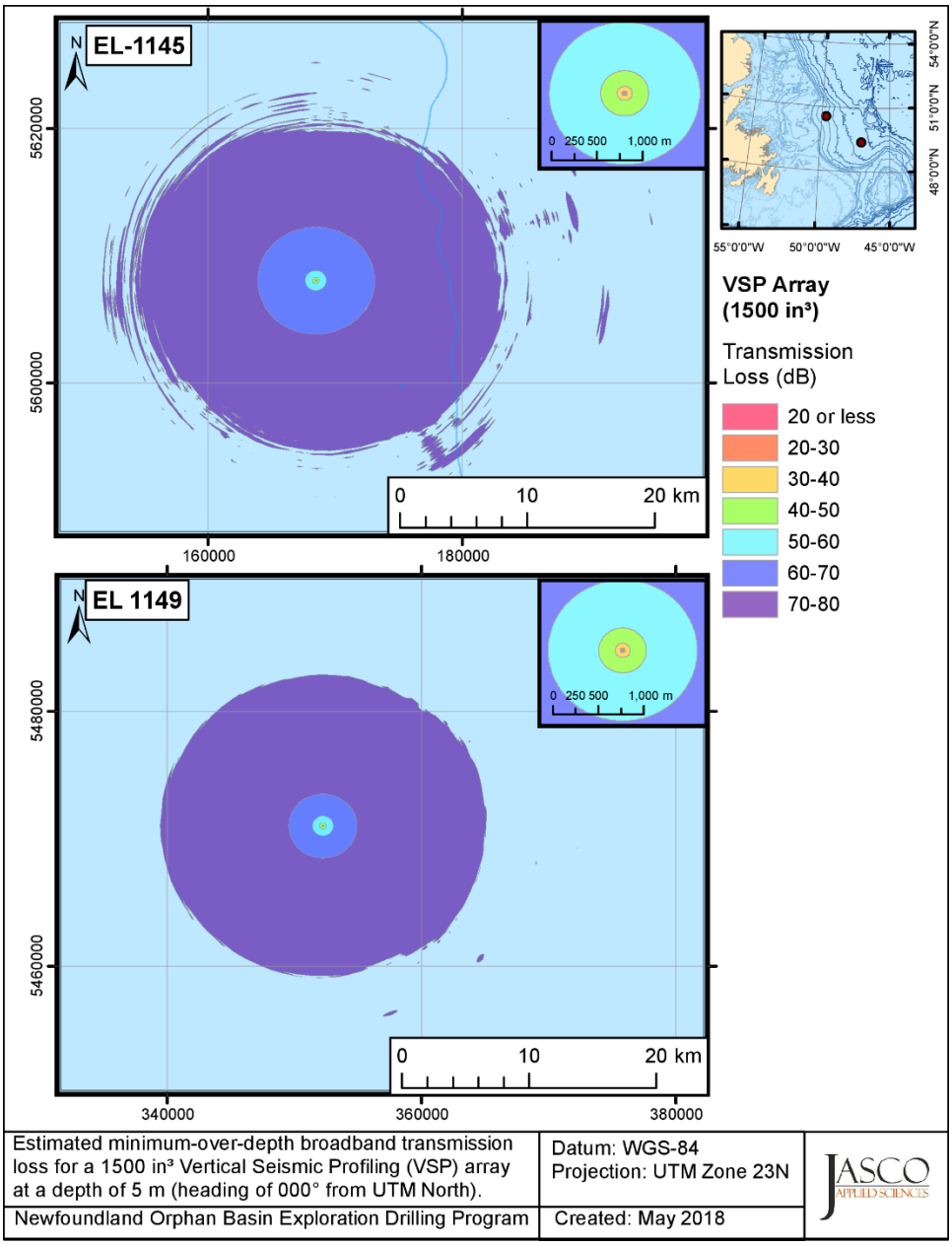

Figure 23. *VSP array, 5 m depth*: Map of minimum-over-depth broadband transmission loss (dB) at the modelled site in (top) EL 1145 and (bottom) EL 1149, in June. TL was calculated over frequency bands from 10–1600 Hz. The array heading was assumed to be toward UTM north.

Table 10. *Semi-submersible, drillship, and support vessel*: Maximum (R_{max}) and 95% ($R_{95\%}$) horizontal distances (in km) from the source to minimum-over-depth TL isopleths, associated with the Program activities.

TL (dB)	Semi-submersible, 18 m depth				Semi-submersible, 23 m depth				Drillship				Support vessel			
	EL 1145 TL ≅ 14.4×log10(R)		EL 1149 TL ≅ 17.7×log10(R)		EL 1145 TL ≅ 14.1×log10(R)		EL 1149 TL ≅ 17.4×log10(R)		EL 1145 TL ≅ 14.8×log10(R)		EL 1149 TL ≅ 17.9×log10(R)		EL 1145 TL ≅ 15.9×log10(R)		EL 1149 TL ≅ 18.7×log10(R)	
	R_{max}	$R_{95\%}$	R_{max}	$R_{95\%}$	R_{max}	$R_{95\%}$	R_{max}	$R_{95\%}$	R_{max}	$R_{95\%}$	R_{max}	$R_{95\%}$	R_{max}	$R_{95\%}$	R_{max}	$R_{95\%}$
20	< 0.02	< 0.02	< 0.02	< 0.02	< 0.02	< 0.02	< 0.02	< 0.02	< 0.02	< 0.02	< 0.02	< 0.02	< 0.02	< 0.02	< 0.02	< 0.02
30	0.03	0.03	0.03	0.03	0.03	0.03	0.03	0.03	0.04	0.04	0.04	0.04	0.03	0.03	0.03	0.03
40	0.14	0.14	0.14	0.14	0.14	0.14	0.14	0.14	0.13	0.13	0.13	0.13	0.12	0.12	0.12	0.12
50	0.46	0.45	0.45	0.44	0.47	0.45	0.45	0.44	0.43	0.42	0.43	0.42	0.38	0.37	0.37	0.36
60	1.50	1.45	1.50	1.45	1.55	1.50	1.53	1.48	1.41	1.36	1.38	1.34	1.19	1.16	1.18	1.15
70	9.22	7.30	6.24	4.76	12.77	10.49	6.21	4.88	7.50	6.70	7.45	4.35	6.16	5.88	3.84	3.72
80	>50.0	-	>50.0	-	>50.0	-	>50.0	-	>50.0	-	>50.0	-	49.86	37.75	49.45	41.41

Table 11. *VSP array*: Maximum (R_{max}) and 95% ($R_{95\%}$) horizontal distances (in km) from the source to minimum-over-depth TL isopleths, associated with the Program activities.

TL (dB)	VSP array			
	EL 1145 TL ≅ 16.7×log10(R)		EL 1149 TL ≅ 19.2×log10(R)	
	R_{max}	$R_{95\%}$	R_{max}	$R_{95\%}$
20	< 0.02	< 0.02	< 0.02	< 0.02
30	0.03	0.03	0.03	0.03
40	0.08	0.07	0.08	0.07
50	0.26	0.25	0.26	0.25
60	0.83	0.79	0.82	0.78
70	4.64	4.32	2.68	2.54
80	27.18	14.63	20.08	12.09

4.3. Ambient Sound in the Program Area

The ambient sound in the Program Area was estimated based on data from the two closest ESRF recording stations (see Figure 1). Long-term spectral averages along with median band-level time series figures (Figure 24) provide an overview of the time and frequency evolution in the soundscape. In 2015, ESRF Station 15 recorded seismic survey sounds until November 2015 and beginning again in June 2016. The winter period of 15 Nov 2015 to 1 Jun 2016 was representative of a normal ambient soundscape for this region (Figure 24). Dynamic positioning (DP) thrusters from the semi-submersible drilling platform West Hercules located 209 km from the recorder were faintly detectable. Fin whale mating choruses were a dominant sound source in the band of 18–25 Hz from November to March.

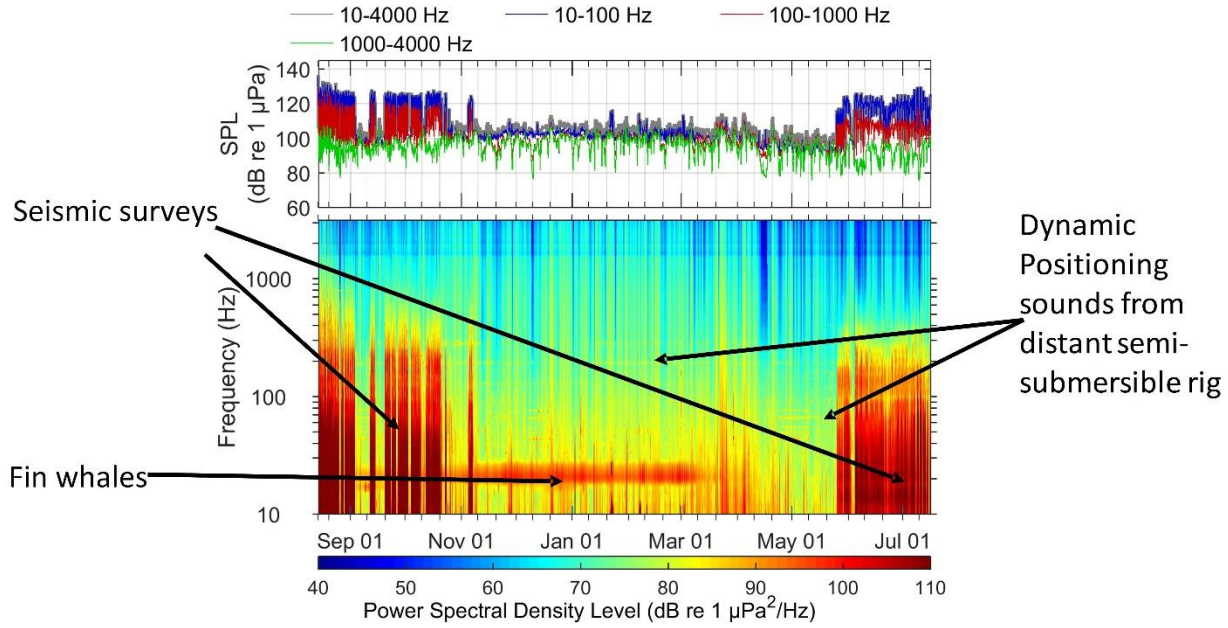

Figure 24. Annotated long-term spectrogram for Station 15, September 2015 to July 2016. The semi-submersible drill-rig West Aquarius was 209 km from the recorder.

Power spectral density and 1/3-octave-band distribution plots (Figure 25) can be directly compared to the Wenz plots (Figure 3). In 2015–2016, sound from seismic surveys increased the received sounds levels below 250 Hz for more than 25% of the recording period (Figure 25). Fin whale notes are clearly identifiable as a broad hump around 20 Hz. Constant but distant sound from dynamic positioning thrusters of the semi-submersible drill rig West Hercules (range 209 km) are visible as narrow peaks in the L_5 curve, but those sounds become obscured at times when higher level sounds are present. The sounds from the West Hercules did not elevate the total broadband sound levels. There were small nulls in the power spectrum density (PSD) throughout the recording at 1650 and 2000 Hz that were due to destructive interference from reflections off the AMAR Ultra Deep used at this deep location (Figure C-4). These artifacts are far less prominent in the AMAR data than data from most other recorders that have their hydrophones placed directly next to the recorder endcap.

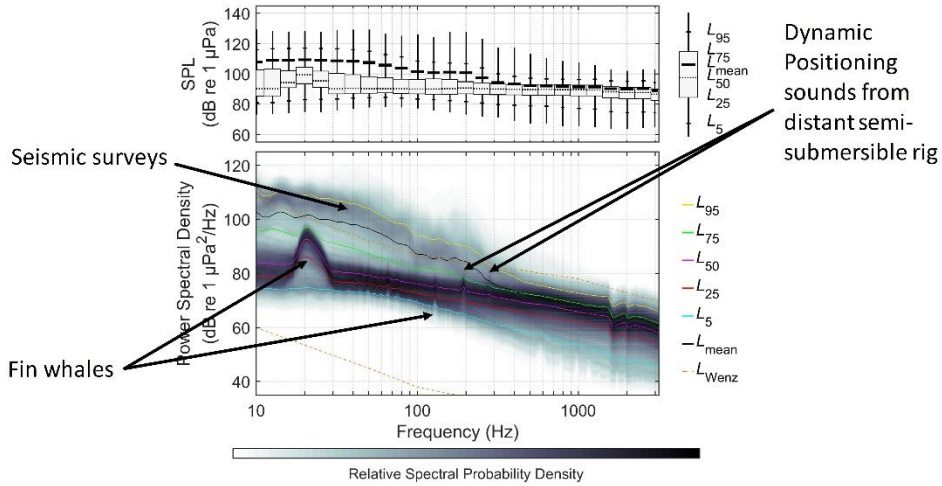

Figure 25. Summary of spectral content of ESRF Station 15. The top figure shows a box-and-whisker plot for the 1/3-octave-band SPLs, and bottom shows the power spectral density percentiles and probability density (grayscale) of 1-min PSD levels compared to the limits of prevailing levels (Wenz 1962). The signatures of seismic surveys, fin whales and distant dynamic positioning thrusters are annotated. The semi-submersible drill-rig West Aquarius was 209 km from the recorder.

The daily sound exposure level (SEL) integrates the total sound energy at a receiver location and is believed to be a good predictor of possible temporary threshold shifts in marine life hearing if it is high enough (NMFS 2016). Sound associated with seismic survey activity was the an easily detected contributor to the daily SEL in 2015–2017 (refer to Section 2.3 for information regarding how contribution to soundscape can be quantified). When seismic was present the daily SEL was 10–30 dB higher than daily SEL in the absence of seismic surveys (see Figures 28 and 31 in Sections 4.3.1 and 4.3.2). The daily SEL also increased in winter due to both fin whales and increased wind and wave activity.

4.3.1. Station 15

Station 15 was deployed off the northeastern coast Newfoundland at a depth of ~2000 m. The maximum and minimum broadband sound pressure level (SPL) measured in 2015–2016 were 137.6 and 87.9 dB re 1 µPa, respectively (Figure 26). The maximum and minimum broadband SPL measured in 2016–2017 were 144.3 and 91.1 dB re 1 µPa, respectively. In June to October, the soundscape at this station was mainly dominated by seismic survey activity, which raised the SPL below 300 Hz to exceed the expected prevailing levels (Figure 27) for the L_{95} percentile curve, or for 5% of the time. Seismic survey activity occurred from August to early November in 2015, from late May to October 2016, and from late June to July 2017 when the recorder was retrieved (Figure 28). The maximum sound levels were measured during periods of seismic survey activity. The range to the seismic surveys were different in 2015, 2016, and 2017, which resulted in much different daily SELs for each period (Figure 28).

Fin whale 20 Hz notes were detected as early as September 2015, but they were generally masked by seismic survey until the end of the survey in late October 2015. These notes were the main source of identifiable sound until mid-March 2016 (Figure 26). A similar pattern occurred in 2016–2017.

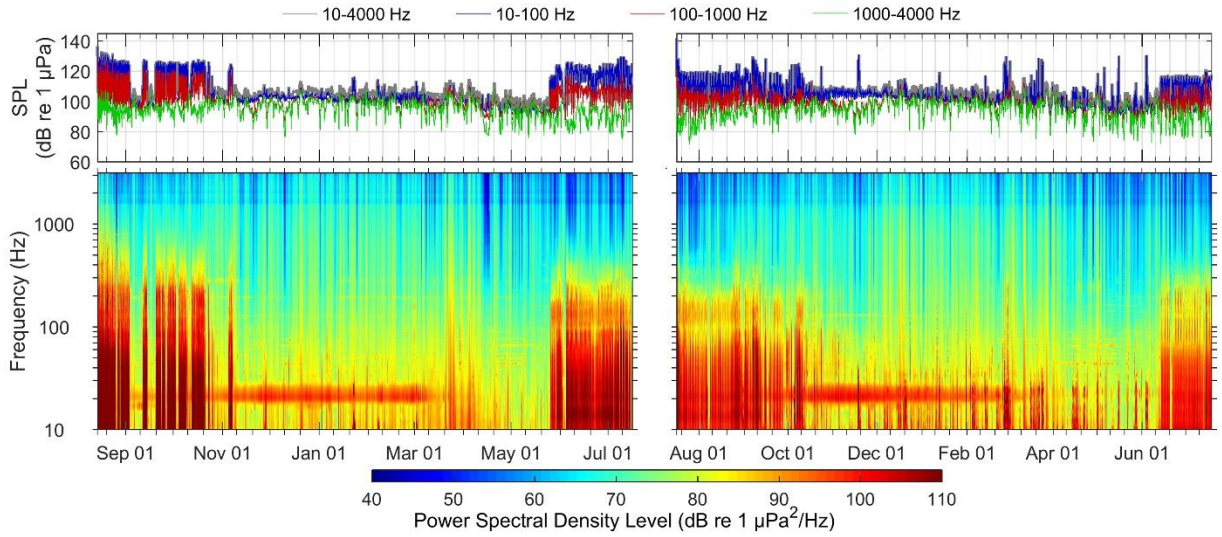

Figure 26. Station 15: (Top) In-band SPL and (bottom) spectrogram of underwater sound for (left) 2015 to 2016 and (right) 2016 to 2017.

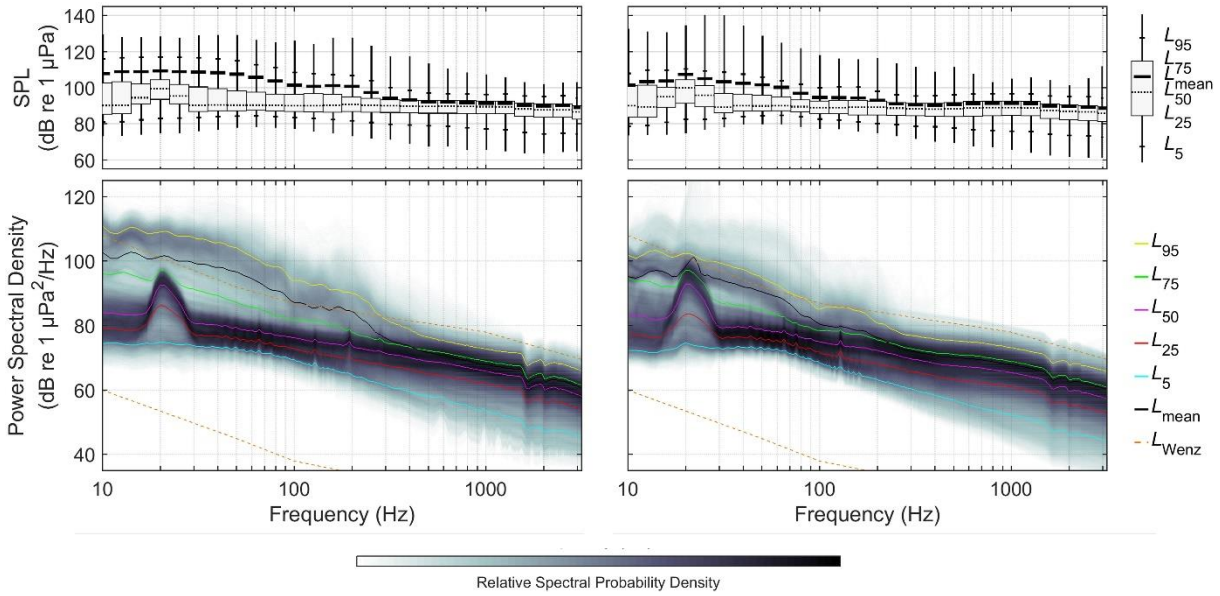

Figure 27. Station 15: (Top) Exceedance percentiles and mean of 1/3-octave-band SPL and (bottom) exceedance percentiles and probability density (grayscale) of 1-min PSD levels compared to the limits of prevailing levels (Wenz 1962) for (left) 2015 to 2016 and (right) 2016 to 2017.

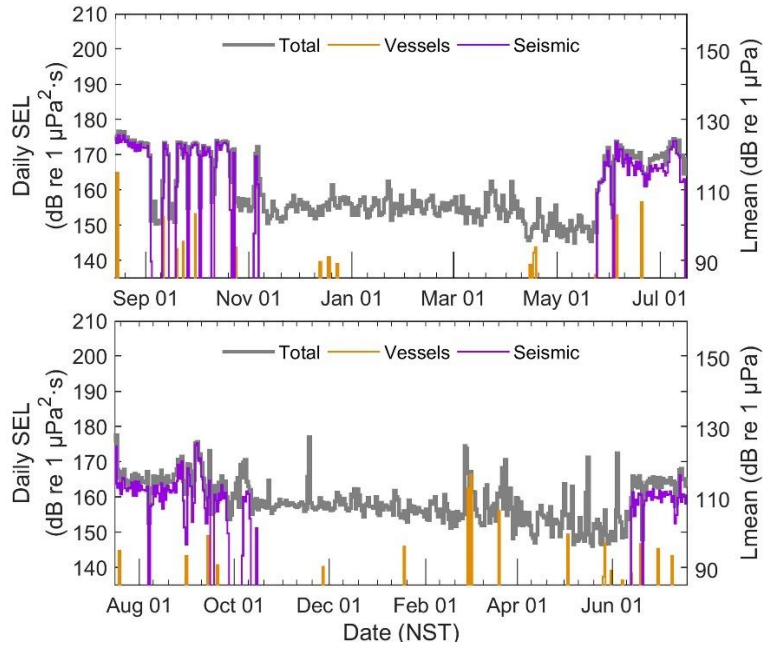

Figure 28. Station 15: Total (grey), vessel (orange), and seismic-associated (purple) daily SEL and equivalent continuous sound levels (L_{eq}) for (top) 2015 to 2016 and (bottom) 2016 to 2017.

4.3.2. Station 19

Station 19 was deployed off the northeastern coast of Newfoundland at slightly different locations in 2015–2016 and 2016–2017. In 2015–2016, it was deployed (1282 m depth) in the southwestern part of Orphan Basin to obtain baseline data ahead of anticipated oil and gas activity. In 2016–2017, the station was moved to the southeastern part of Orphan Basin to investigate mammal habitat use after repeated sightings of northern bottlenose whales in the area and due to increased oil and gas interest in the area. It was deployed at a depth of 1547 m.

The maximum and minimum broadband SPL measured in 2015–2016 were 139.5 and 90.6 dB re 1 µPa, respectively (Figure 29). The maximum and minimum broadband SPL measured in 2016–2017 were 157.6 and 95.5 dB re 1 µPa, respectively. The two main soundscape features at this station were seismic survey activity from July to October in both years (Figure 31), and fin whale calls. In 2015–2016, the recorder was relatively far from the seismic survey. Sound from the survey was clearly identifiable, but it did not often raise SPL above prevailing levels. In 2016–2017, the adjusted station location was closer to seismic survey sound, which frequently raised the SPL below 300 Hz to exceed the expected limits of prevailing levels (Figure 30). However, sound levels associated with environmental and mooring conditions at this location also regularly exceeded the limits of prevailing levels.

Fin whale 20 Hz notes were detected as early as September, but they were generally masked by seismic survey sounds until the end of the survey in late October 2015. These notes were the main source of identifiable sound until mid-March 2016 (Figure 29).

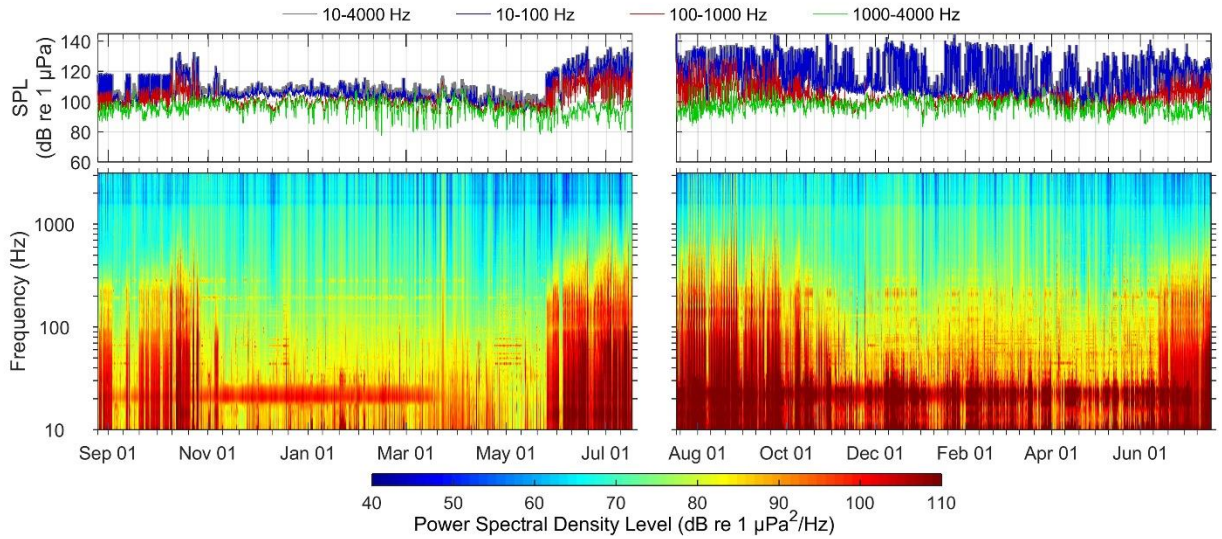

Figure 29. Station 19: (Top) In-band SPL and (bottom) spectrogram of underwater sound for (left) 2015 to 2016 and (right) 2016 to 2017.

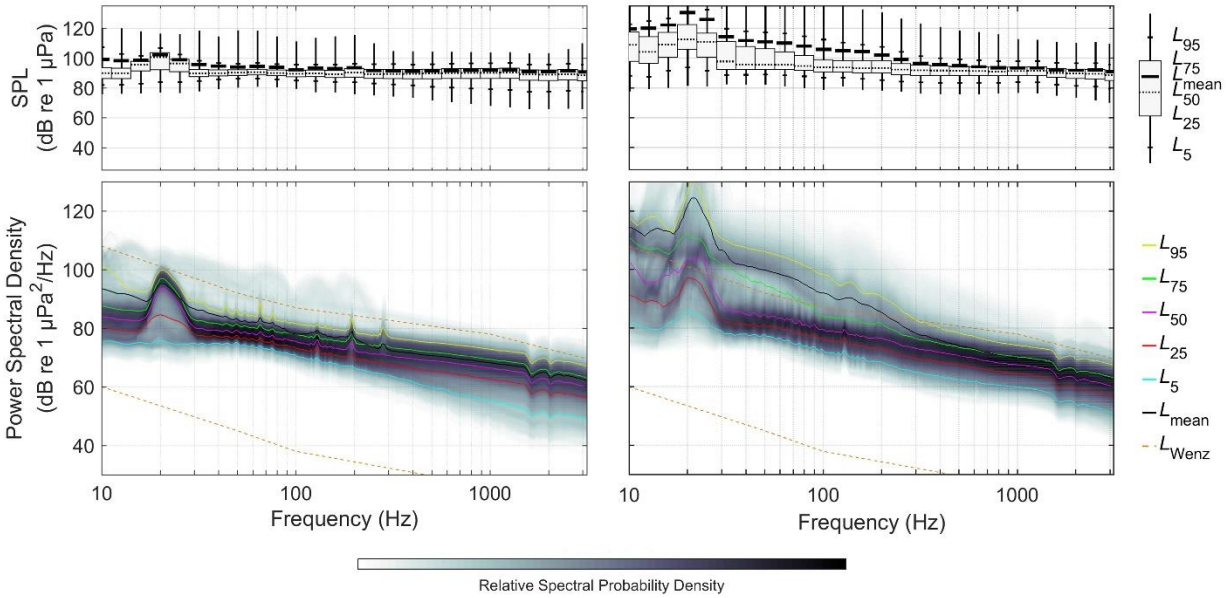

Figure 30. Station 19: (Top) Exceedance percentiles and mean of 1/3-octave-band SPL and (bottom) exceedance percentiles and probability density (grayscale) of 1-min PSD levels compared to the limits of prevailing levels (Wenz 1962) for (left) 2015 to 2016 and (right) 2016 to 2017.

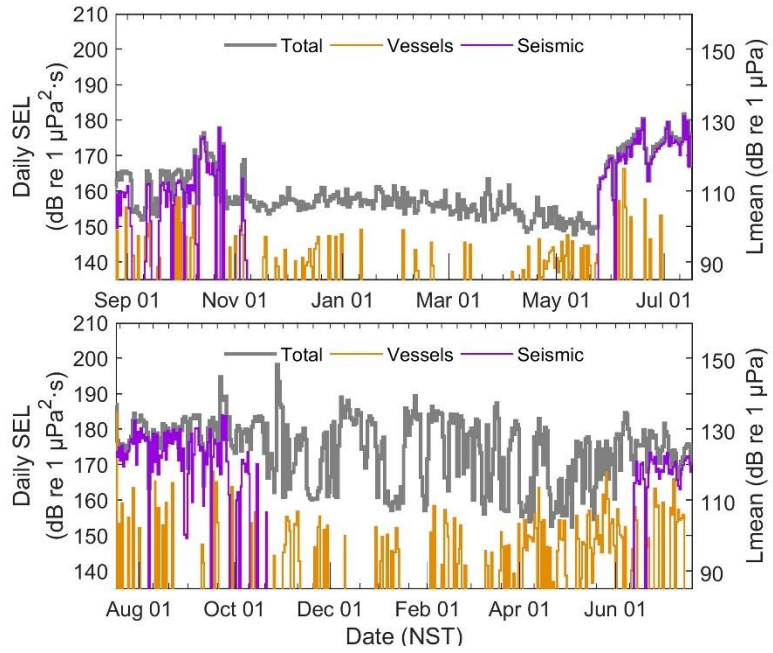

Figure 31. Station 19: Total (grey), vessel (orange), and seismic-associated (purple) daily SEL and equivalent continuous sound levels (L_{eq}) for (top) 2015 to 2016 and (bottom) 2016 to 2017.

4.3.3. Summary of Dominant Sound Sources Contributing to the Soundscape between 2015–2017

Based on measurements at the ESRF stations, there are three identifiable sources in the Orphan Basin Drilling Program Area that have long-term effects on the soundscape. We expect these sources to be present in the foreseeable future; the Program's sounds will add to these sources to create the cumulative soundscape in the area. These sources are:

1. Fin whales: Fin whales sing from October to March on the Grand Banks. They seem to favour the shallow waters on the Grand Banks compared to the deeper waters off the continental shelf. Their constant notes raise the total sound level in the 10–45 Hz band by 5–10 dB in winter across the Grand Banks and Scotian Shelf. Whales close to a recorder can temporarily increase the one-minute sound levels to 130 or 140 dB re 1 µPa. We can expect the same contribution by fin whales in future years. The Program's sounds will overlap in frequency with fin whale calls; however, the Program activities are mostly located off the continental shelf, where the whales are less present.
2. Shipping and oil and gas extraction platforms: Shipping, including supply vessels for the Program, are generally transient sources that are detectable at any one location over a period of several hours. Close to the Program sites and existing oil and gas extraction platforms, the sounds from vessels and dynamic positioning systems are continuously present. We can expect the same contribution from shipping and extraction platforms in near future. The Program's activities will mainly add to these sources in the area.
3. Seismic surveys: The seismic surveys detected at Stations 15 and 19 were over 100 km from the recorders and still a dominant sound source. The peak frequency of sound from seismic source arrays is near 50 Hz (Dragoset 1984), however the frequency range increases as the source vessel gets closer to a measurement location. The measurements reported here included energy up to 1 kHz. This sound source is variable in space and time depending on where the seismic source is located. It is expected that 2-D and 3-D seismic surveys will continue off Newfoundland for the foreseeable future each summer. The Program will conduct vertical seismic profiles (VSP) to image the well structures. This type of seismic activity is conducted over a much shorter period and with arrays at least half the volume of full-scale seismic surveys. Thus, VSP operations are expected contribute less than seismic surveys, but they could be an important contributor to the soundscape if the activities were to occur in winter, when seismic surveys are absent.
4. Ambient noise: Median sound levels increase 3–5 dB in winter due to higher wind speeds and storms. The peak frequency band for wind noise is 200–2000 Hz. See Hildebrand (2009) and Cato (2008) for overview of ocean ambient noise and man-made sound sources.

5. Discussion and Conclusion

In this study, JASCO reviewed sound source parameters representative of the Newfoundland Orphan Basin Exploration Drilling Program, compared the acoustic environment with related studies, and quantified transmission loss (TL). This information is compared to the parameters presented in two studies with similar sound source and environmental parameters: the Scotian Basin Exploration Drilling Project (Scotian Basin Project; Zykov 2016) and the Nexen Energy ULC Flemish Pass Exploration Drilling Project (Flemish Pass Project; Matthews et al. 2017). Modelled results in these studies help provide a preliminary assessment of sound propagation features in the Orphan Basin. JASCO also identified contributors to the ambient soundscape in the Program Area. These results help to anticipate the relative contribution of the Program activities to the soundscape.

The broadband source levels and the estimated source level spectra associated with the Program activities were based on modelling, analysis, and a literature review previously conducted by JASCO. The results in this report are appropriate for typical operational specifications for each activity. The accurate assessment of source levels for this Program will depend, however, on the particulars of the equipment and planned activities.

Because of the proximity of the sites, the acoustic environment of the Flemish Pass Project is most similar to that in Orphan Basin. The water depth in EL 1149, however, is closer to that seen in the Scotian Basin Project. Based on the similarity in acoustic environment, some sound propagation features in Orphan Basin can be deducted from these two comparable modelling projects. For example, the sound from the Program activities that reaches the continental shelf, west of the Program Area, will be rapidly attenuated between the 200 and 50 m isobaths. Other bathymetric features are expected to have a minimal influence on sound propagation. Seasonal variations in the sound speed profile will lead to variation in the sound propagation; longer distances to sound level isopleths are expected in winter than in summer.

The transmission loss (TL) coefficient calculated for the Program activities varies between 14.1 and 16.7 in EL 1145 and between 17.4 and 19.2 in EL 1149. Based on these coefficients, distances to sound levels isopleths are expected to be longer (due to less transmission loss) in EL 1145 than EL 1149. This is mainly due to the differences in water depth and sound speed profile between the two areas. This difference in TL can also be seen on the profiles shown in Figures 14–18.

Figures 32–34 compare TL as a function of distance from the Program's drillship, semi-submersible, and VSP operations, to TL curves using the coefficients calculated from SPL results for the Scotia Basin Project (between 16.2 and 18.2) and Flemish Pass Project (between 17.0 and 17.6). TL coefficients associated with supply vessels in the Program Area were also calculated (15.9 in EL 1145 and 18.7 in EL 1149). SPL results for these sources alone were not presented in the modelling studies for the Flemish Pass and Scotian Basin Projects; thus, direct comparison of TL for supply vessels could not be made.

For drillship and semi-submersible operations (Figures 32 and 33), coefficients vary between 16.2 and 18.2 for the Scotia Basin and between 17.0 and 17.6 in Flemish Pass. The corresponding TL coefficients in EL 1145 are lower (14.1–14.8). Thus, longer distances to sound level isopleths than those modelled in Flemish Pass and the Scotian Basin (in both, August and February) are expected in EL 1145. This is likely due to the seemingly weak sound channel present in the June sound speed profile in EL 1145 (Figure 8c). This channel is wider than the sound channel in the Scotian Basin in August; it may trap a wider range of frequencies, resulting in a lower TL coefficient. The TL coefficients for drillship and semi-submersible operations in EL 1149 (17.4–17.9) are similar to those in the other studies and would result in distances to sound level isopleths close to those in May in Flemish Pass and those in August in the Scotian Basin.

For the VSP operations (Figure 34), TL coefficients for the Scotia Basin vary between 17.6 and 17.8 and between 16.5 and 17.3 in Flemish Pass. The corresponding TL coefficient is similar in EL 1145 (16.7) and higher in EL 1149 (19.2). Therefore, distances to sound level isopleths in June in EL 1145 are expected to be similar to those than in May in Flemish Pass, and longer than modelled in the Scotian Basin (in both, August and February). Distances to sound level isopleths in June in EL 1149 are expected to be shorter than those in May in Flemish Pass, and those in the Scotian Basin (in both, August and February).

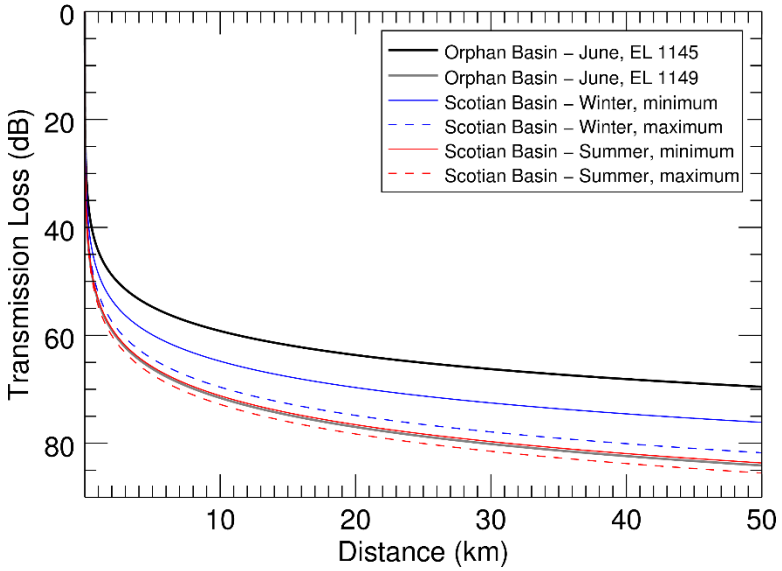

Figure 32. *Drillship*: Variation of transmission loss with distance from the modelled operation, based on estimated transmission loss coefficient (*N*) in the Orphan Basin (Program Area) and the Scotian Basin (Zykov 2016).

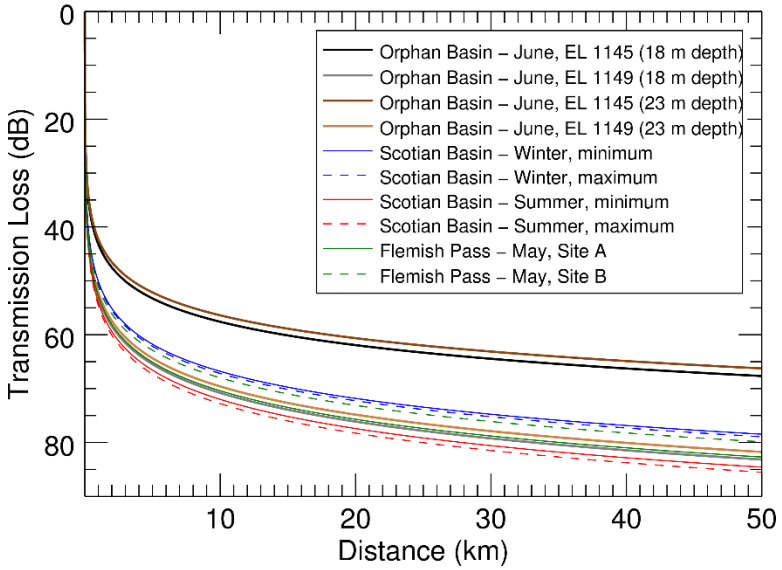

Figure 33. *Semi-submersible*: Variation of transmission loss with distance from the modelled operation, based on estimated transmission loss coefficient (*N*) in the Orphan Basin (Program Area), the Scotian Basin (Zykov 2016), and Flemish Pass (Matthews et al. 2017).

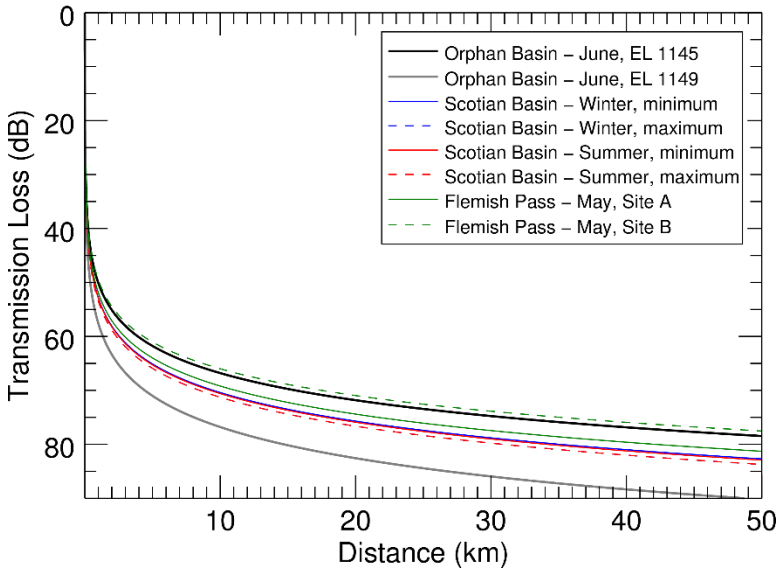

Figure 34. *Vertical Seismic Profiler (VSP) array*: Variation of transmission loss with distance from the modelled operation, based on estimated transmission loss coefficient (*N*) in the Orphan Basin (Program Area), the Scotian Basin (Zykov 2016), and Flemish Pass (Matthews et al. 2017).

The two-year-long data set collected in 2015–2017 provides information on the ambient soundscape in the Newfoundland Orphan Basin Exploration Drilling Program Area. In general, the ambient sound levels are higher in winter than summer due to fin whale calls, higher winds, and higher sea states. Within distances on the order of 10–40 km from oil and gas platforms, anthropogenic sounds are the dominant sources in the 45–2250 Hz band. The lower but non-negligible sound levels from oil and gas platforms can be measured at distances greater than 40 km. When present, seismic sources can increase the mean monthly sound pressure level by 20 dB or more over large areas.

The estimated broadband source levels associated with the Program activities (222.6 dB re 1 $\mu Pa^2 \cdot s$ m for the VSP array, 196.7 dB re 1 µPa m for MODU, and 188.6 dB re 1 µPa m for support vessels) are higher than the ambient levels measured in 2015–2017 (mean broadband SPL of 87.9–144.3 dB re 1 µPa at station 15 and 90.6–157.6 dB re 1 µPa at station 19). Therefore, these activities are expected to contribute to the soundscape in the Program Area during the course of the activities. VSP operations are expected to raise the ambient sound levels to a lesser extent than seismic surveys because of their shorter operational timeframe and lower source levels. The MODU and associated vessel traffic is like to contribute to the soundscape over a larger area, and for longer periods, than the VSP operations. The relative contribution to the ambient soundscape will depend on the specifications of the equipment and the planned activities, as well as the other simultaneous anthropogenic contributors in the region. For example, if multiple seismic surveys are present during MODU operations, the surveys would be larger contributors to the soundscape than the MODU.

Glossary

1/3-octave-band
Non-overlapping passbands that are one-third of an octave wide (where an octave is a doubling of frequency). Three adjacent 1/3-octave-bands comprise one octave. One-third-octave-bands become wider with increasing frequency. Also see octave.

absorption
The reduction of acoustic pressure amplitude due to acoustic particle motion energy converting to heat in the propagation medium.

ambient sound
All-encompassing sound at a given place, usually a composite of sound from many sources near and far (ANSI S1.1-1994 R2004), e.g., shipping vessels, seismic survey activity, precipitation, sea ice movement, wave action, and biological activity.

attenuation
The gradual loss of acoustic energy from absorption and scattering as sound propagates through a medium.

azimuth
A horizontal angle relative to a reference direction, which is often magnetic north or the direction of travel. In navigation it is also called bearing.

Background sound
Total of all sources of interference in a system used for the production, detection, measurement, or recording of a signal, independent of the presence of the signal (ANSI S1.1-1994 R2004). Ambient sound detected, measured, or recorded with a signal is part of the background sound.

bandwidth
The range of frequencies over which a sound occurs. Broadband refers to a source that produces sound over a broad range of frequencies (e.g., seismic airguns, vessels) whereas narrowband sources produce sounds over a narrow frequency range (e.g., sonar) (ANSI/ASA S1.13-2005 R2010).

box-and-whisker plot
A plot that illustrates the centre, spread, and overall range of data from a visual 5-number summary. The ends of the box are the upper and lower quartiles (25th and 75th percentiles). The horizontal line inside the box is the median (50th percentile). The whiskers and points extend outside the box to the highest and lowest observations, where the points correspond to outlier observations (i.e., observations that fall more than 1.5 × IQR beyond the upper and lower quartiles, where IQR is the interquartile range).

broadband sound level
The total sound pressure level measured over a specified frequency range. If the frequency range is unspecified, it refers to the entire measured frequency range.

broadside direction
Perpendicular to the travel direction of a source. Compare with endfire direction.

cavitation
A rapid formation and collapse of vapor cavities (i.e., bubbles or voids) in water, most often caused by a rapid change in pressure. Fast-spinning vessel propellers typically cause cavitation, which creates a lot of sound.

compressional wave
A mechanical vibration wave in which the direction of particle motion is parallel to the direction of propagation. Also called primary wave or P-wave.

continuous sound
A sound whose sound pressure level remains above ambient sound during the observation period (ANSI/ASA S1.13-2005 R2010). A sound that gradually varies in intensity with time, for example, sound from a marine vessel.

decibel (dB)
One-tenth of a bel. Unit of level when the base of the logarithm is the tenth root of ten, and the quantities concerned are proportional to power (ANSI S1.1-1994 R2004).

duty cycle
The time when sound is periodically recorded by an acoustic recording system.

endfire direction
Parallel to the travel direction of a source. See also broadside direction.

far field
The zone where, to an observer, sound originating from an array of sources (or a spatially-distributed source) appears t o radiate from a single point. The distance to the acoustic far-field increases with frequency.

fast Fourier transform (FFT)
A computationally efficiently algorithm for computing the discrete Fourier transform.

frequency
The rate of oscillation of a periodic function measured in cycles-per-unit-time. The reciprocal of the period. Unit: hertz (Hz). Symbol: *f*. 1 Hz is equal to 1 cycle per second.

geoacoustic
Relating to the acoustic properties of the seabed.

hertz (Hz)
A unit of frequency defined as one cycle per second.

hydrophone
An underwater sound pressure transducer. A passive electronic device for recording or listening to underwater sound.

impulsive sound
Sound that is typically brief and intermittent with rapid (within a few seconds) rise time and decay back to ambient levels (NOAA 2013, ANSI S12.7-1986 R2006). For example, seismic airguns and impact pile driving.

masking
Obscuring of sounds of interest by sounds at similar frequencies.

median
The 50th percentile of a statistical distribution.

non-impulsive sound
Sound that is broadband, narrowband or tonal, brief or prolonged, continuous or intermittent, and typically does not have a high peak pressure with rapid rise time (typically only small fluctuations in decibel level) that impulsive signals have (ANSI/ASA S3.20-1995 R2008). For example, marine vessels, aircraft, machinery, construction, and vibratory pile driving (NIOSH 1998, NOAA 2015).

octave
The interval between a sound and another sound with double or half the frequency. For example, one octave above 200 Hz is 400 Hz, and one octave below 200 Hz is 100 Hz.

parabolic equation method
A computationally-efficient solution to the acoustic wave equation that is used to model transmission loss. The parabolic equation approximation omits effects of back-scattered sound, simplifying the computation of transmission loss. The effect of back-scattered sound is negligible for most ocean-acoustic propagation problems.

percentile level, exceedance
The sound level exceeded n% of the time during a measurement.

point source
A source that radiates sound as if from a single point (ANSI S1.1-1994 R2004).

power spectrum density
The acoustic signal power per unit frequency as measured at a single frequency. Unit: $\mu Pa^2/Hz$, or $\mu Pa^2 \cdot s$.

power spectral density level
The decibel level ($10\log_{10}$) of the power spectrum density, usually presented in 1 Hz bins. Unit: dB re 1 $\mu Pa^2/Hz$.

pressure, acoustic
The deviation from the ambient hydrostatic pressure caused by a sound wave. Also called overpressure. Unit: pascal (Pa). Symbol: p.

pressure, hydrostatic
The pressure at any given depth in a static liquid that is the result of the weight of the liquid acting on a unit area at that depth, plus any pressure acting on the surface of the liquid. Unit: pascal (Pa).

received level
The sound level measured at a receiver.

rms
root-mean-square.

shear wave
A mechanical vibration wave in which the direction of particle motion is perpendicular to the direction of propagation. Also called secondary wave or S-wave. Shear waves propagate only in solid media, such as sediments or rock. Shear waves in the seabed can be converted to compressional waves in water at the water-seabed interface.

signature
Pressure signal generated by a source.

sound
A time-varying pressure disturbance generated by mechanical vibration waves travelling through a fluid medium such as air or water.

sound exposure
Time integral of squared, instantaneous frequency-weighted sound pressure over a stated time interval or event. Unit: pascal-squared second ($Pa^2 \cdot s$) (ANSI S1.1-1994 R2004).

sound exposure level (SEL)
A cumulative measure related to the sound energy in one or more pulses. Unit: dB re 1 $\mu Pa^2 \cdot s$. SEL is expressed over the summation period (e.g., per-pulse SEL [for airguns], single-strike SEL [for pile drivers], 24-hour SEL).

sound field
Region containing sound waves (ANSI S1.1-1994 R2004).

sound pressure level (SPL)
The decibel ratio of the time-mean-square sound pressure, in a stated frequency band, to the square of the reference sound pressure (ANSI S1.1-1994 R2004).

For sound in water, the reference sound pressure is one micropascal (p_0 = 1 µPa) and the unit for SPL is dB re 1 µPa:

$$\mathrm{SPL} = 10\log_{10}\left(p^2 / p_0^2\right) = 20\log_{10}\left(p / p_0\right)$$

Unless otherwise stated, SPL refers to the root-mean-square sound pressure level. See also 90% sound pressure level and fast-average sound pressure level. Non-rectangular time window functions may be applied during calculation of the rms value, in which case the SPL unit should identify the window type.

sound speed profile
The speed of sound in the water column as a function of depth below the water surface.

source level
The sound level measured in the far-field and scaled back to a standard reference distance of 1 metre from the acoustic centre of the source. Unit: dB re 1 µPa @ m (sound pressure level) or dB re 1 $\mu Pa^2 \cdot s$ m(sound exposure level).

spectrogram
A visual representation of acoustic amplitude compared with time and frequency.

spectrum
An acoustic signal represented in terms of its power (or energy) distribution compared with frequency.

surface duct
The upper portion of a water column within which the sound speed profile gradient causes sound to refract upward and therefore reflect off the surface resulting in relatively long-range sound propagation with little loss.

transmission loss (TL)
The decibel reduction in sound level between two stated points that results from sound spreading away from an acoustic source subject to the influence of the surrounding environment. Also called propagation loss.

wavelength
Distance over which a wave completes one oscillation cycle. Unit: meter (m). Symbol: λ.

Literature Cited

[CNLOPB] Canada-Newfoundland Offshore Petroleum Board. 2016. *2015-16 Annual report*. 18 pp. http://www.cnlopb.ca/pdfs/ar2016e.pdf?lbisphpreq=1.

[NIOSH] National Institute for Occupational Safety and Health. 1998. *Criteria for a recommended standard: Occupational noise exposure*. Document Number 98-126. U.S. Department of Health and Human Services, NIOSH, Cincinnati, Ohio. 122 pp.

[NMFS] National Marine Fisheries Service. 2016. *Technical Guidance for Assessing the Effects of Anthropogenic Sound on Marine Mammal Hearing: Underwater Acoustic Thresholds for Onset of Permanent and Temporary Threshold Shifts*. U.S. Department of Commerce, NOAA. NOAA Technical Memorandum NMFS-OPR-55. 178 pp. http://www.nmfs.noaa.gov/pr/acoustics/Acoustic%20Guidance%20Files/opr-55_acoustic_guidance_tech_memo.pdf.

[NOAA] National Oceanic and Atmospheric Administration. 2013. *Draft guidance for assessing the effects of anthropogenic sound on marine mammals: Acoustic threshold levels for onset of permanent and temporary threshold shifts*, December 2013, 76 pp. Silver Spring, Maryland: NMFS Office of Protected Resources. http://www.nmfs.noaa.gov/pr/acoustics/draft_acoustic_guidance_2013.pdf.

[NOAA] National Oceanic and Atmospheric Administration. 2015. *Draft guidance for assessing the effects of anthropogenic sound on marine mammal hearing: Underwater acoustic threshold levels for onset of permanent and temporary threshold shifts*, July 2015, 180 pp. Silver Spring, Maryland: NMFS Office of Protected Resources. http://www.nmfs.noaa.gov/pr/acoustics/draft%20acoustic%20guidance%20July%202015.pdf.

[NRC] National Research Council. 2003. *Ocean Noise and Marine Mammals*. National Research Council (U.S.), Ocean Studies Board, Committee on Potential Impacts of Ambient Noise in the Ocean on Marine Mammals. The National Academies Press, Washington, DC. http://www.nap.edu/openbook.php?record_id=10564.

Aerts, L., M. Blees, S. Blackwell, C. Greene, K. Kim, D. Hannay, and M. Austin. 2008. *Marine mammal monitoring and mitigation during BP Liberty OBC seismic survey in Foggy Island Bay, Beaufort Sea, July-August 2008: 90-day report*. Document Number LGL Report P1011-1. Report by LGL Alaska Research Associates Inc., LGL Ltd., Greeneridge Sciences Inc. and JASCO Applied Sciences for BP Exploration Alaska. 199 pp. http://www.nmfs.noaa.gov/pr/pdfs/permits/bp_liberty_monitoring.pdf.

Andrew, R.K., B.M. Howe, and J.A. Mercer. 2011. Long-time trends in ship traffic noise for four sites off the North American West Coast. *Journal of the Acoustical Society of America* 129(2): 642-651. https://doi.org/10.1121/1.3518770.

ANSI S12.7-1986. R2006. *American National Standard Methods for Measurements of Impulsive Noise*. American National Standards Institute, New York.

ANSI S1.1-1994. R2004. *American National Standard Acoustical Terminology*. American National Standards Institute, New York.

ANSI/ASA S1.13-2005. R2010. *American National Standard Measurement of Sound Pressure Levels in Air*. American National Standards Institute and Acoustical Society of America, New York.

ANSI/ASA S3.20-1995. R2008. *American National Standard Bioacoustical Terminology*. American National Standards Institute and Acoustical Society of America, New York.

Arveson, P.T. and D.J. Vendittis. 2000. Radiated noise characteristics of a modern cargo ship. *Journal of the Acoustical Society of America* 107(1): 118-129. https://doi.org/10.1121/1.428344.

Brown, N.A. 1977. Cavitation noise problems and solutions. *Proceedings International Symposium on Shipboard Acoustics*: 18.

Buckingham, M.J. 1992. Ocean-acoustic propagation models. *Journal d'Acoustique* 5: 223-287.

Buckingham, M.J. 2005. Compressional and shear wave properties of marine sediments: Comparisons between theory and data. *Journal of the Acoustical Society of America* 117(1): 137-152. http://dx.doi.org/10.1121/1.1810231.

Carnes, M.R. 2009. *Description and Evaluation of GDEM-V 3.0*. Document Number NRL Memorandum Report 7330-09-9165. US Naval Research Laboratory, Stennis Space Center, MS. 21 pp.

Cato, D.H. 2008. Ocean ambient noise: Its measurement and its significance to marine animals. *Proceedings of the Institute of Acoustics* 30(5): 1-9.

Collins, M.D. 1993. A split-step Padé solution for the parabolic equation method. *Journal of the Acoustical Society of America* 93(4): 1736-1742.

Collins, M.D., R.J. Cederberg, D.B. King, and S. Chin-Bing. 1996. Comparison of algorithms for solving parabolic wave equations. *Journal of the Acoustical Society of America* 100(1): 178-182.

Coppens, A.B. 1981. Simple equations for the speed of sound in Neptunian waters. *Journal of the Acoustical Society of America* 69(3): 862-863. http://dx.doi.org/10.1121/1.385486.

Deane, G.B. 2000. Long time-base observations of surf noise. *Journal of the Acoustical Society of America* 107(2): 758-770.

Divins, D.L. 2007. Total sediment thickness of the world's oceans & marginal seas. National Geophysical Data Centre, National Oceanic and Atmospheric Administration, US Department of Commerce. http://www.ngdc.noaa.gov/mgg/sedthick/sedthick.html.

Dragoset, W.H. 1984. A comprehensive method for evaluating the design of airguns and airgun arrays. *Proceedings, 16th Annual Offshore Technology Conference* Volume 3, May 7-9, 1984. OTC 4747, Houston, Houston. pp 75–84.

Etter, P.C. 1996. *Underwater Acoustic Modeling - Principles, Techniques, and Applications*. Second edition. E & FN Spon, London, UK. 344 pp.

Fisher, F.H. and V.P. Simmons. 1977. Sound absorption in sea water. *Journal of the Acoustical Society of America* 62(3): 558-564. http://link.aip.org/link/?JAS/62/558/1.

François, R.E. and G.R. Garrison. 1982a. Sound absorption based on ocean measurements: Part II: Boric acid contribution and equation for total absorption. *Journal of the Acoustical Society of America* 72(6): 1879-1890.

François, R.E. and G.R. Garrison. 1982b. Sound absorption based on ocean measurements: Part I: Pure water and magnesium sulfate contributions. *Journal of the Acoustical Society of America* 72(3): 896-907.

Funk, D., D. Hannay, D. Ireland, R. Rodrigues, and W. Koski (eds.). 2008. *Marine mammal monitoring and mitigation during open water seismic exploration by Shell Offshore Inc. in the Chukchi and Beaufort Seas, July–November 2007: 90-day report*. LGL Report P969-1. Prepared by LGL

Alaska Research Associates Inc., LGL Ltd., and JASCO Research Ltd. for Shell Offshore Inc., National Marine Fisheries Service (US), and US Fish and Wildlife Service. 218 pp.

Géli, L., J. Cochran, T. Lee, J. Francheteau, C. Labails, C. Fouchet, and D. Christie. 2007. Thermal regime of the Southeast Indian Ridge between 88°E and 140°E: Remarks on the subsidence of the ridge flanks. *J. Geophys. Res.* 112(B10): B10101.

Hannay, D. and R. Racca. 2005. *Acoustic Model Validation*. Document Number 0000-S-90-04-T-7006-00-E, Revision 02. Technical report for Sakhalin Energy Investment Company Ltd. by JASCO Research Ltd. 34 pp.

Hildebrand, J.A. 2009. Anthropogenic and natural sources of ambient noise in the ocean. *Marine Ecology Progress Series* 395: 5-20.

Huppertz, T.J. 2007. *Late Quaternary History of Flemich Pass, Southeast Canadian Continental Margin*. M.Sc. Thesis. Dalhousie University, Halifax, Nova Scotia. 137 pp.

Ireland, D.S., R. Rodrigues, D. Funk, W. Koski, and D. Hannay. 2009. *Marine mammal monitoring and mitigation during open water seismic exploration by Shell Offshore Inc. in the Chukchi and Beaufort Seas, July–October 2008: 90-Day Report*. Document Number LGL Report P1049-1. 277 pp.

Jensen, F.B., W.A. Kuperman, M.B. Porter, and H. Schmidt. 2011. *Computational Ocean Acoustics*. 2nd edition. AIP Series in Modern Acourics and Signal Processing. AIP Press - Springer, New York. 794 pp.

Landro, M. 1992. Modeling of GI gun signatures. *Geophysical Prospecting* 40: 721–747.

Larsen, S.B. and W. Ashby. 2015. *Successful completion of 2015 seismic acquisition season in offshore Newfoundland Labrador*. Houston. http://www.tgs.com/News/2015/Successful_completion_of_2015_seismic_acquisition_season_in_Offshore_Newfoundland_Labrador/.

Laws, M., L. Hatton, and M. Haartsen. 1990. Computer modeling of clustered airguns. *First Break* 8: 331–338.

Lurton, X. 2002. *An Introduction to Underwater Acoustics: Principles and Applications*. Springer, Chichester, U.K. 347 pp.

MacDonnell, J. 2017. *Shelburne Basin Venture Exploration Drilling Project: Sound Source Characterization, 2016 Field Measurements of the Stena IceMAX*. Document Number 01296. Version 3.0. Technical report by JASCO Applied Sciences for Shell Canada Limited. http://www.cnsopb.ns.ca/sites/default/files/pdfs/shelburne_ceaa_3.12.3_sound_source_characterization_final_april202017.pdf.

MacGillivray, A.O. 2006. *Acoustic Modelling Study of Seismic Airgun Noise in Queen Charlotte Basin*. MSc Thesis. University of Victoria, Victoria, BC. 98 pp.

Martin, B., K. Broker, M.-N.R. Matthews, J. MacDonnell, and L. Bailey. 2015. *Comparison of measured and modeled air-gun array sound levels in Baffin Bay, West Greenland. OceanNoise 2015*, 11-15 May, Barcelona, Spain.

Matthews, M.-N.R., Z. Alavizadeh, L. Horwich, and M. Zykov. 2017. *Underwater Sound Propagation Assessment: Nexen Energy ULC Flemish Pass Exploration Drilling Project (2018–2028)*.

Document Number 01514, Version 2.0. Technical report by JASCO Applied Sciences for AMEC Foster Wheeler.

Miksis-Olds, J.L. and S.M. Nichols. 2016. Is low frequency ocean sound increasing globally? *Journal of the Acoustical Society of America* 139(1): 501-511.

Nieukirk, S.L., K.M. Stafford, D.K. Mellinger, R.P. Dziak, and C.G. Fox. 2004. Low-frequency whale and seismic airgun sounds recorded in the mid-Atlantic Ocean. *Journal of the Acoustical Society of America* 115(4): 1832-1843.

O'Neill, C., D. Leary, and A. McCrodan. 2010. Sound Source Verification. (Chapter 3) *In* Blees, M.K., K.G. Hartin, D.S. Ireland, and D. Hannay (eds.). *Marine mammal monitoring and mitigation during open water seismic exploration by Statoil USA E&P Inc. in the Chukchi Sea, August-October 2010: 90-day report*. LGL Report P1119. Prepared by LGL Alaska Research Associates Inc., LGL Ltd., and JASCO Applied Sciences Ltd. for Statoil USA E&P Inc., National Marine Fisheries Service (US), and US Fish and Wildlife Service. pp 1-34.

Quijano, J., M.-N. Matthews, and B. Martin. 2017. *Eastern Newfoundland Drilling Noise Assessment: Qualitative Assessment of Radiated Sound Levels and Acoustic Propagation Conditions*. Document Number 01366. Technical report by JASCO Applied Sciences for Stantec Consulting Ltd.

Racca, R., A. Rutenko, K. Bröker, and M. Austin. 2012a. A line in the water - design and enactment of a closed loop, model based sound level boundary estimation strategy for mitigation of behavioural impacts from a seismic survey. *11th European Conference on Underwater Acoustics 2012*. Volume 34(3), Edinburgh, United Kingdom.

Racca, R., A. Rutenko, K. Bröker, and G. Gailey. 2012b. *Model based sound level estimation and in-field adjustment for real-time mitigation of behavioural impacts from a seismic survey and post-event evaluation of sound exposure for individual whales*. *Acoustics 2012 Fremantle: Acoustics, Development and the Environment*, Fremantle, Australia. http://www.acoustics.asn.au/conference_proceedings/AAS2012/papers/p92.pdf.

Racca, R.G. and J.A. Scrimger. 1986. *Underwater Acoustic Source Characteristics of Air and Water Guns*. Document Number DREP Tech. Rep. 06SB 97708-5-7055. Report by JASCO Research Ltd. for Defence Research Establishment Pacific (Canada), Victoria, BC.

Rodríguez, E., C.S. Morris, Y.J.E. Belz, E.C. Chapin, J.M. Martin, W. Daffer, and S. Hensley. 2005. *An Assessment of the SRTM Topographic Products*. Document Number JPL D-31639. Jet Propulsion Laboratory, Pasadena, CA.

Ross, D. 1976. *Mechanics of Underwater Noise*. Pergamon Press, New York.

Teague, W.J., M.J. Carron, and P.J. Hogan. 1990. A comparison between the Generalized Digital Environmental Model and Levitus climatologies. *Journal of Geophysical Research* 95(C5): 7167-7183.

Warner, G., C. Erbe, and D. Hannay. 2010. Underwater Sound Measurements. (Chapter 3) *In* Reiser, C.M., D.W. Funk, R. Rodrigues, and D. Hannay (eds.). *Marine Mammal Monitoring and Mitigation during Open Water Shallow Hazards and Site Clearance Surveys by Shell Offshore Inc. in the Alaskan Chukchi Sea, July-October 2009: 90-Day Report*. LGL Report P1112-1. Report by LGL Alaska Research Associates Inc. and JASCO Applied Sciences for Shell Offshore Inc., National Marine Fisheries Service (US), and US Fish and Wildlife Service. pp 1-54.

Wenz, G.M. 1962. Acoustic Ambient Noise in the Ocean: Spectra and Sources. *Journal of the Acoustical Society of America* 34(12): 1936-1956. https://doi.org/10.1121/1.1909155.

Zhang, Y. and C. Tindle. 1995. Improved equivalent fluid approximations for a low shear speed ocean bottom. *Journal of the Acoustical Society of America* 98(6): 3391-3396. https://doi.org/10.1121/1.413789.

Ziolkowski, A. 1970. A method for calculating the output pressure waveform from an air gun. *Geophysical Journal of the Royal Astronomical Society* 21(2): 137-161.

Zykov, M.M. 2016. *Modelling Underwater Sound Associated with Scotian Basin Exploration Drilling Project: Acoustic Modelling Report.* Document Number JASCO Document 01112, Version 2.0. Technical report by JASCO Applied Sciences for Stantec Consulting Ltd. http://www.ceaa.gc.ca/050/documents/p80109/116305E.pdf.

Appendix A. Acoustic Metrics

Underwater sound pressure amplitude is measured in decibels (dB) relative to a fixed reference pressure of p_0 = 1 µPa. Because the perceived loudness of sound, especially pulsed noise such as from seismic airguns, pile driving, and sonar, is not generally proportional to the instantaneous acoustic pressure, several sound level metrics are commonly used to evaluate noise and its effects on marine life. We provide specific definitions of relevant metrics used in the accompanying report. Where possible we follow the ANSI and ISO standard definitions and symbols for sound metrics, but these standards are not always consistent.

Zero-to-peak sound pressure level, or peak pressure level (PK) ($L_{p,pk}$; dB re 1 µPa), is the maximum instantaneous sound pressure level in a stated frequency band attained by an acoustic pressure signal, $p(t)$:

$$L_{p,pk} = 20 \log_{10} \left[\frac{\max\left(\left| p(t) \right|\right)}{p_0} \right] . \qquad \text{(A-1)}$$

$L_{p,pk}$ is often included as a criterion for assessing whether a sound is potentially injurious; however, because it does not account for the duration of a noise event, it is generally a poor indicator of perceived loudness.

Sound pressure level (SPL) (L_p; dB re 1 µPa) is the root-mean-square (rms) pressure level in a stated frequency band over a specified time window (T, s) containing the acoustic event of interest. It is important to note that SPL always refers to an rms pressure level and therefore not instantaneous pressure:

$$L_p = 10 \log_{10} \left(\frac{1}{T} \int_T g(t)\, p^2(t) dt \Big/ p_0^2 \right) , \qquad \text{(A-2)}$$

where $g(t)$ is an optional time weighting function. The SPL represents a nominal effective continuous sound over the duration of an acoustic event, such as the emission of one acoustic pulse, a marine mammal vocalization, the passage of a vessel, or over a fixed duration. Because the window length, T, is the divisor, events with similar sound exposure level (SEL) but more spread out in time have a lower SPL.

In in-air studies of impulsive noise, the time weighting function $g(t)$ is often a decaying exponential that emphasizes more recent pressure signals to mimic the leaky integration of the mammalian hearing system. For example, human-based fast time weighting applies an exponential function with time constant 125 ms. Other approaches for evaluating L_p of impulsive signals include setting g(t) to a boxcar (constant amplitude) function and T to the "90% time window" (T_{90}; the period over which cumulative square pressure function passes between 5% and 95% of its full per-pulse value) or to a constant value (e.g., T_{fix} = 125 ms).

Sound exposure level (SEL, dB re 1 µPa²·s) is a measure related to the acoustic energy contained in one or more acoustic events (N). The SEL for a single event is computed from the time-integral of the squared pressure over the full event duration (T):

$$L_E = 10 \log_{10} \left(\int_T p^2(t) dt \Big/ T_0 p_0^2 \right) , \qquad \text{(A-3)}$$

where T_0 is a reference time interval of 1 s. The SEL continues to increase with time when non-zero pressure signals are present. It therefore can be construed as a dose-type measurement, so the integration time used must be carefully considered in terms of relevance for impact to the exposed recipients.

SEL can be calculated over periods with multiple acoustic events or over a fixed duration. For a fixed duration, the square pressure is integrated over the duration of interest. For multiple events, the SEL can be computed by summing (in linear units) the SEL of the *N* individual events:

$$L_{E,N} = 10\log_{10}\left(\sum_{i=1}^{N} 10^{\frac{L_{E,i}}{10}}\right) . \quad \text{(A-4)}$$

Because the SPL and SEL are both computed from the integral of square pressure, these metrics are related by the following expression, which depends only on the duration of the time window *T*:

$$L_p = L_E - 10\log_{10}(T) . \quad \text{(A-5)}$$

Appendix B. Acoustic Models

B.1. JASCO's Airgun Array Source Model (AASM)

The source levels and directivity of the airgun array were predicted with JASCO's Airgun Array Source Model (AASM; MacGillivray 2006). AASM includes both a low-frequency and a high-frequency module for predicting different components of the airgun array spectrum. The low frequency module is based on the physics of oscillation and radiation of airgun bubbles, as originally described by Ziolkowski (1970), that solves the set of parallel differential equations that govern bubble oscillations. Physical effects accounted for in the simulation include pressure interactions between airguns, port throttling, bubble damping, and generator-injector (GI) gun behaviour discussed by Dragoset (1984), Laws et al. (1990), and Landro (1992). A global optimization algorithm tunes free parameters in the model to a large library of airgun source signatures. These airgun data are measurements of the signatures of Bolt 600/B guns ranging in volume from 5 to 185 in^3 (Racca and Scrimger 1986).

AASM produces a set of notional signatures for each array element based on:

- Array layout;
- Volume, tow depth, and firing pressure of each airgun; and
- Interactions between different airguns in the array.

These notional signatures are the pressure waveforms of the individual airguns at a standard reference distance of 1 m; they account for the interactions with the other airguns in the array. The signatures are summed with the appropriate phase delays to obtain the far-field source signature of the entire array in all directions. This far-field array signature is filtered into 1/3-octave-bands to compute the source levels of the array as a function of frequency band and azimuthal angle in the horizontal plane (at the source depth), after which it is considered to be a directional point source in the far field.

A seismic array consists of many sources and the point-source assumption is invalid in the near field where the array elements add incoherently. The maximum extent of the near field of an array (R_{nf}) is:

$$R_{\mathrm{nf}} < \frac{l^2}{4\lambda} \tag{B-1}$$

where λ is the sound wavelength and l is the longest dimension of the array (Lurton 2002, §5.2.4). For example, an airgun array length of l = 16 m yields a near-field range of 85 m at 2 kHz and 17 m at 100 Hz. Beyond this R_{nf} range, the array is assumed to radiate like a directional point source and is treated as such for propagation modelling.

The interactions between individual elements of the array create directionality in the overall acoustic emission. Generally, this directionality is prominent mainly at frequencies in the mid-range between tens of hertz to several hundred hertz. At lower frequencies, with acoustic wavelengths much larger than the inter-airgun separation distances, the directionality is small. At higher frequencies, the pattern of lobes is too finely spaced to be resolved and the effective directivity is less.

B.2. Sound Propagation Model

B.2.1. Transmission loss

The propagation of sound through the environment was modelled by predicting the acoustic transmission loss—a measure, in decibels, of the decrease in sound level between a source and a receiver some distance away. Geometric spreading of acoustic waves is the predominant way by which transmission loss occurs. Transmission loss also happens when the sound is absorbed and scattered by the seawater, and absorbed scattered, and reflected at the water surface and within the seabed. Transmission loss depends on the acoustic properties of the ocean and seabed; its value changes with frequency.

If the acoustic source level (SL), expressed in dB re 1 µPa m or dB re 1 $\mu Pa^2 \cdot s$ m, and transmission loss (TL), in units of dB, are known at a given frequency, then the received level (RL) at a receiver location can be calculated in dB re 1 µPa by:

$$RL = SL - TL \, . \tag{B-2}$$

The concept of transmission loss is intrinsically tied to the spectral makeup of the source signal, since different frequencies will be variously attenuated by propagation through the medium due to differences in propagation path, interaction with the bottom, and other factors (as mentioned in Section 2.1). It may be useful in some cases, for the sole purpose of comparing two acoustic propagation environments with no knowledge of the signal being emitted through them, to assume a source signal with flat spectrum (all frequencies having the same amplitude between stated upper and lower limits), commonly known as a "white noise". In those cases, broadband transmission loss can be computed as merely the sum of the losses in individual frequency bands. Such a quantity, however, does not enable the subsequent computation of transmission loss for any signal with a different spectral makeup. A broadband transmission loss, in other words, is only applicable computationally to signals having the exact same spectral profile (whether flat or otherwise) as the one used to compute it. To provide a transmission loss descriptor that can be applied computationally to a source signal of arbitrary spectrum, the loss in individual frequency bands must be computed and reported separately.

B.2.2. JASCO's Marine Operations Noise Model (MONM)

Underwater sound transmission loss (TL) was predicted with JASCO's Marine Operations Noise Model (MONM). The model computes acoustic propagation at low frequency (below 2 kHz for the present study) via a wide-angle parabolic equation solution to the acoustic wave equation (Collins 1993) based on a version of the U.S. Naval Research Laboratory's Range-dependent Acoustic Model (RAM), which has been modified to account for a solid seabed (Zhang and Tindle 1995). The parabolic equation method has been extensively benchmarked and is widely employed in the underwater acoustics community (Collins et al. 1996). This version of MONM accounts for sound attenuation due to energy absorption through ion relaxation and viscosity of water in addition to acoustic attenuation due to reflection at the medium boundaries and internal layers (Fisher and Simmons 1977). The former type of sound attenuation is significant for frequencies higher than 5 kHz and cannot be neglected without noticeably affecting the model results. MONM's predictions have been validated against experimental data from several underwater acoustic measurement programs conducted by JASCO (Hannay and Racca 2005, Aerts et al. 2008, Funk et al. 2008, Ireland et al. 2009, O'Neill et al. 2010, Warner et al. 2010, Racca et al. 2012a, Racca et al. 2012b, Martin et al. 2015).

MONM accounts for the additional reflection loss at the seabed, which results from partial conversion of incident compressional waves to shear waves at the seabed and sub-bottom interfaces, and it includes wave attenuations in all layers. MONM incorporates the following site-specific environmental properties: a bathymetric grid of the modelled area, underwater sound speed as a function of depth, and a geoacoustic profile based on the overall stratified composition of the seafloor.

MONM computes acoustic fields in three dimensions by modelling transmission loss within two-dimensional (2-D) vertical planes aligned along radials covering a 360° swath from the source, an

approach commonly referred to as N×2-D. These vertical radial planes are separated by an angular step size of $\Delta\theta$, yielding N = 360°/$\Delta\theta$ number of planes (Figure B-1).

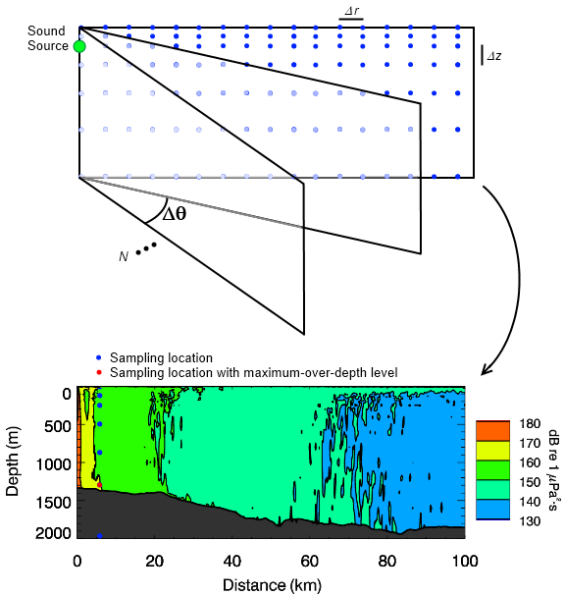

Figure B-1. The N×2-D and maximum-over-depth modelling approach used by MONM.

MONM treats frequency dependence by computing acoustic transmission loss at the centre frequencies of 1/3-octave-bands. Sufficiently many 1/3-octave-bands, starting at 10 Hz, are modelled to include the majority of acoustic energy emitted by the source. At each centre frequency, the transmission loss is modelled within each of the N vertical planes as a function of depth and range from the source.

Broadband transmission loss can be calculated by weighting the 1/3-octave-band band transmission loss values according to the source spectrum in each band. Composite broadband transmission loss levels are then computed by summing the weighted 1/3-octave-band levels.

The TL field within each vertical radial plane is sampled at various ranges from the source, generally with a fixed radial step size. At each sampling range along the surface, the sound field is sampled at various depths, with the step size between samples increasing with depth below the surface. The step sizes are chosen to provide increased coverage near the depth of the source and at depths of interest in terms of the sound speed profile. TL at a sampling location is taken as the minimum value that occurs over all samples within the water column, i.e., the minimum loss over depth.

Appendix C. Data Collection for the 2015–2017 ESRF Study

C.1. Deployment Locations and Mooring Designs

C.1.1. 2015–2016

AMARs were deployed at 20 locations (Figure C-1) between 3 Aug 2015 and 23 Jul 2016 (Table C-1).

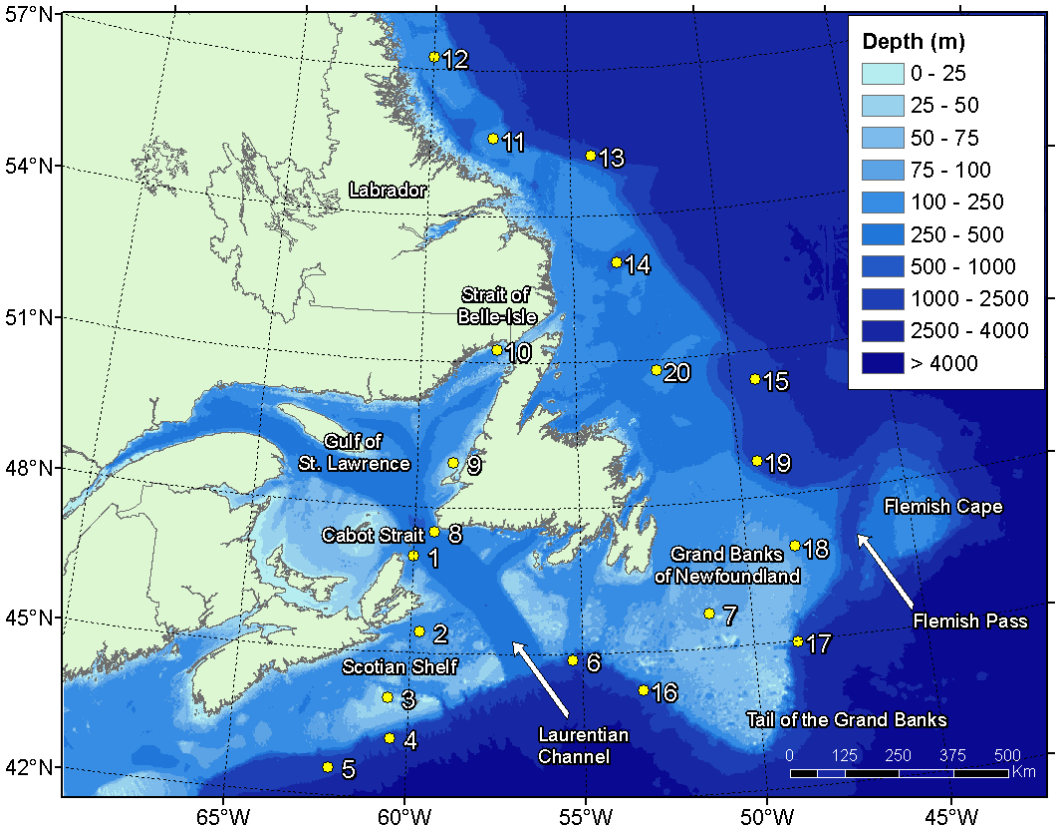

Figure C-1. AMAR deployment locations off the Canadian East coast from 3 Aug 2015 to 23 Jul 2016.

Table C-1. Operation period, location, and depth of the AMARs deployed for the ESRF study.

Station	Latitude	Longitude	Depth (m)	Deployment	Retrieval	Duration (days)
1	46.99134	−60.02403	186	17 Aug 2015	8 Jul 2016	327
2	45.42599	−59.76398	126	18 Aug 2015	21 Jul 2016	339
4	43.21702	−60.49943	1830	19 Aug 2015	22 Jul 2016	339
5	42.54760	−62.17624	2002	19 Aug 2015	23 Jul 2016	340
6	44.85309	−55.27108	1802	22 Aug 2015	20 Jul 2016	334
7	45.70082	−51.23315	78	23 Aug 2015	19 Jul 2016	332
8	47.49307	−59.41325	428	16 Aug 2015	8 Jul 2016	328
9	48.92733	−58.87786	44	16 Aug 2015	26 Apr 2016	255
10	51.26912	−57.53759	121	3 Aug 2015	5 Jul 2016	338
11	55.60300	−57.75040	158	9 Aug 2015	13 Jul 2016	340
12	57.25273	−60.00175	143	10 Aug 2015	13 Jul 2016	339
13	55.22797	−54.19047	1750	8 Aug 2015	11 Jul 2016	339
14	53.01567	−53.46022	582	4 Aug 2015	14 Jul 2016	346
15	50.41327	−49.19638	2000	14 Aug 2015	16 Jul 2016	338
16	44.19230	−53.27441	1602	23 Aug 2015	20 Jul 2016	333
17	44.97141	−48.73373	1282	24 Aug 2015	18 Jul 2016	330
18	46.90877	−48.50418	111	25 Aug 2015	18 Jul 2016	329
19	48.72873	−49.38087	1282	25 Aug 2015	17 Jul 2016	328
20	50.75232	−52.33602	237	13 Aug 2015	15 Jul 2016	338

Four mooring configurations were used because the water depth varied from shallow to very deep across the deployment locations. Stations 3, 7, and 9 were deployed at depth less than 80 m. The AMARs at these three stations were mounted on bottom plates, which prevented motion due to currents (Figure C-2). All other stations were deployed using three variants of suspended mooring designs and recorder housing to account for the effects of increasing depth (Figures C-3, 4, and 5). In all deep mooring designs, the AMAR was suspended about 25 m above the seafloor.

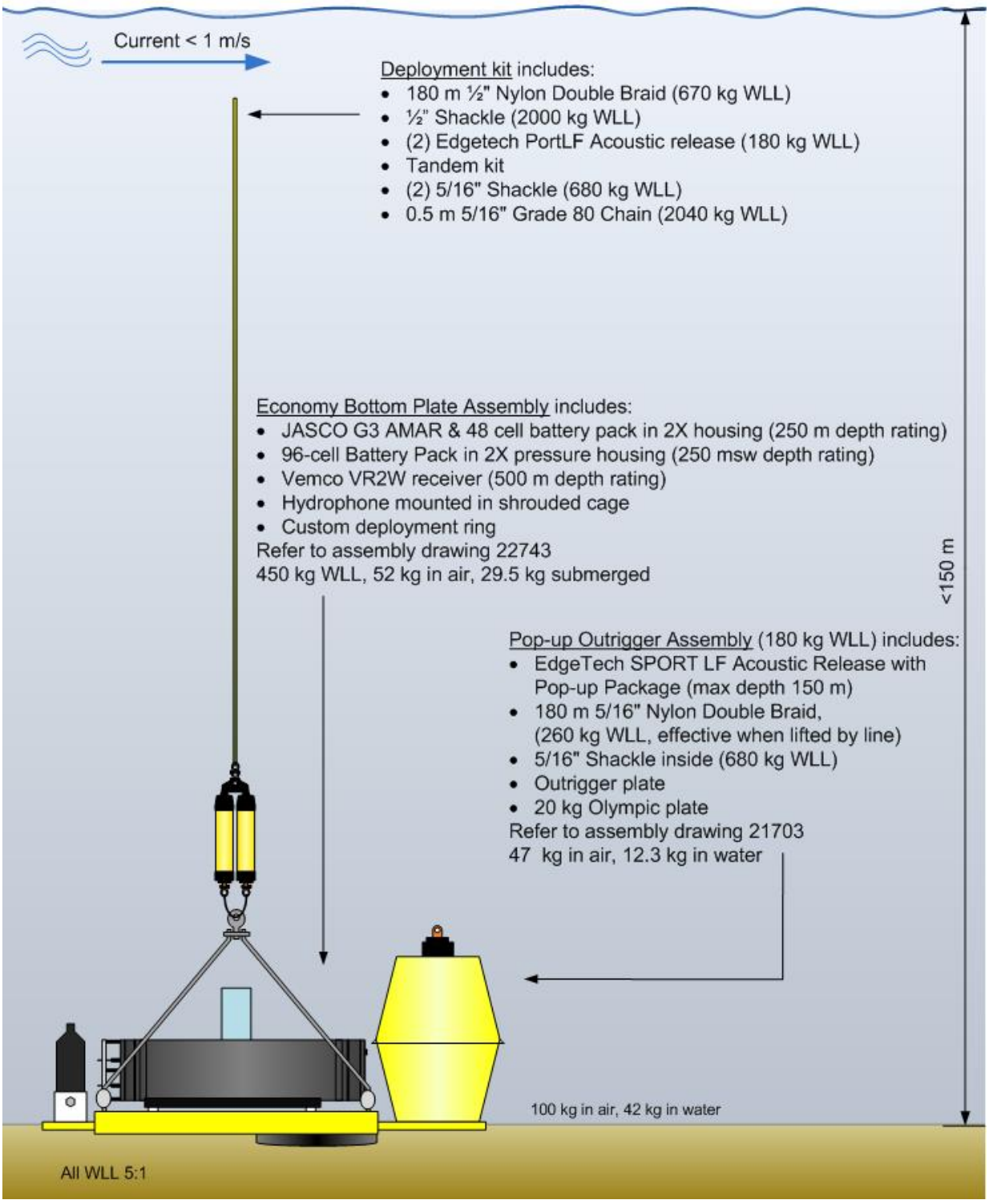

Figure C-2. Shallow mooring design with one PVC-housing AMAR attached to a bottom plate with a pop-up release and a fish logger. This configuration was used at Station 3, 7, and 9.

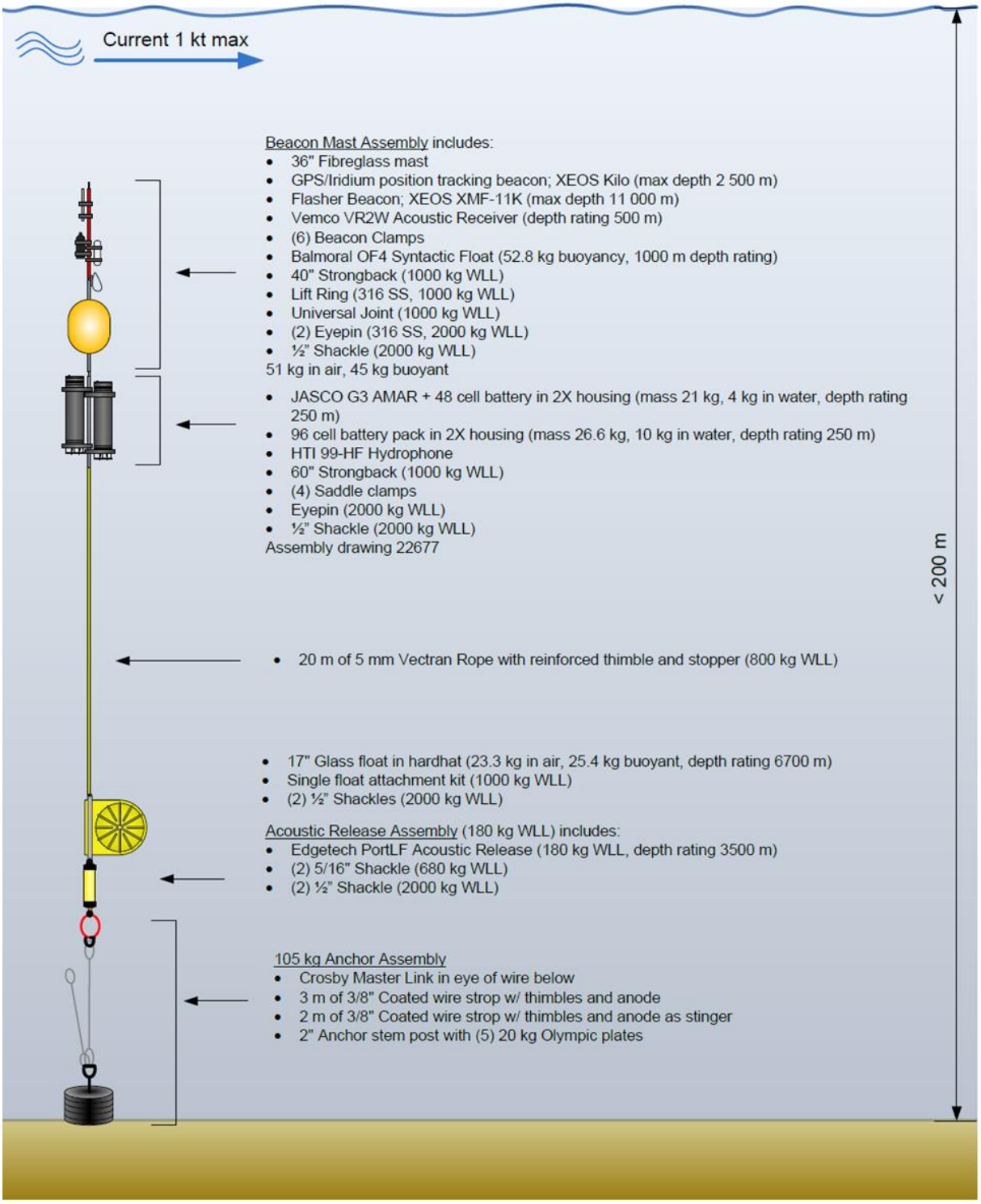

Figure C-3. Shallow mooring design with a PVC-housing AMAR and battery pack attached to an anchor. This configuration was used at used at Station 1, 2, 10, 11, 12, 18, and 20.

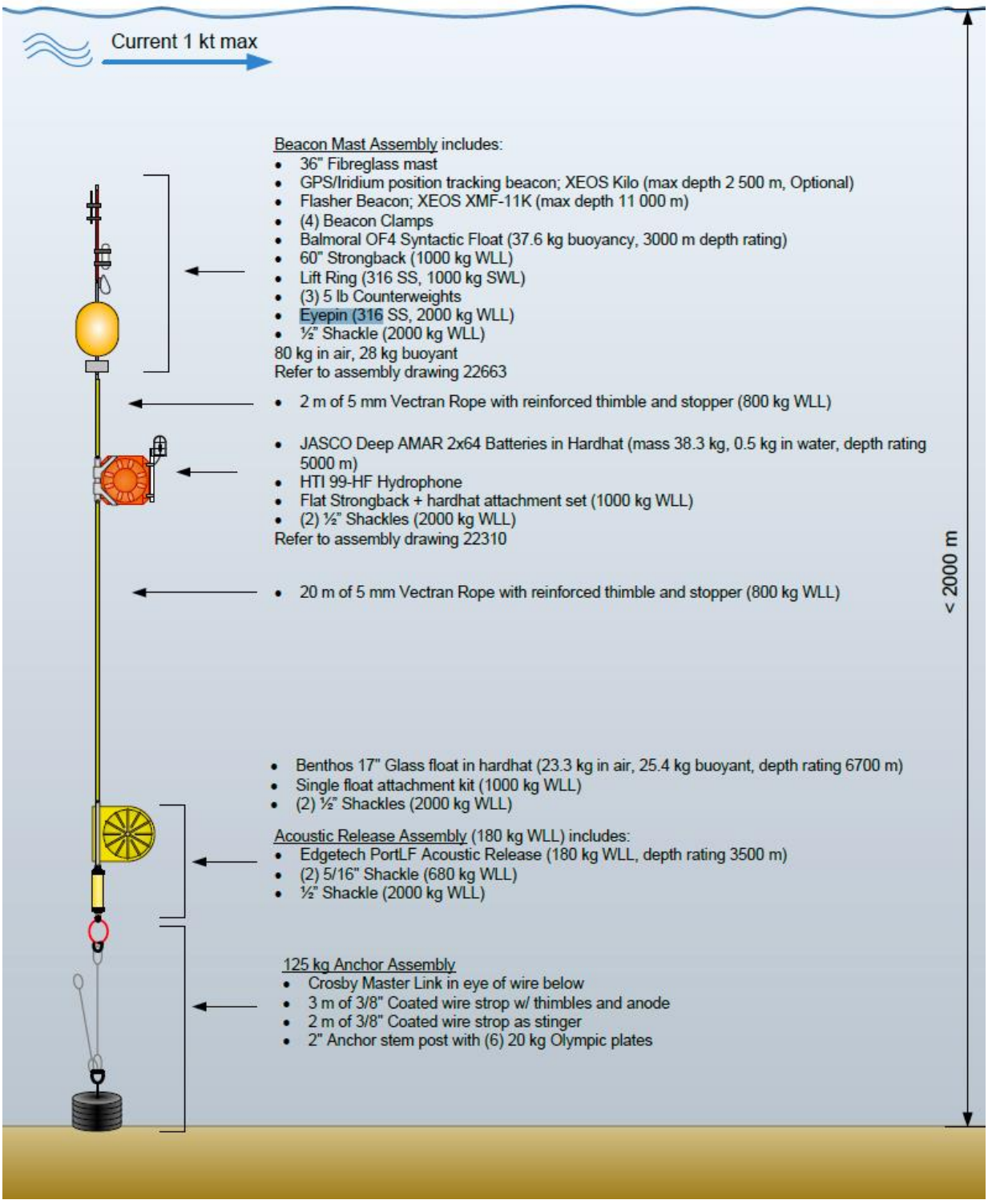

Figure C-4. Deep mooring design with one AMAR ultra-deep (UD) attached to an anchor. This configuration was used at Station 4, 5, 6, 13, 14, 15, 16, 17, and 19.

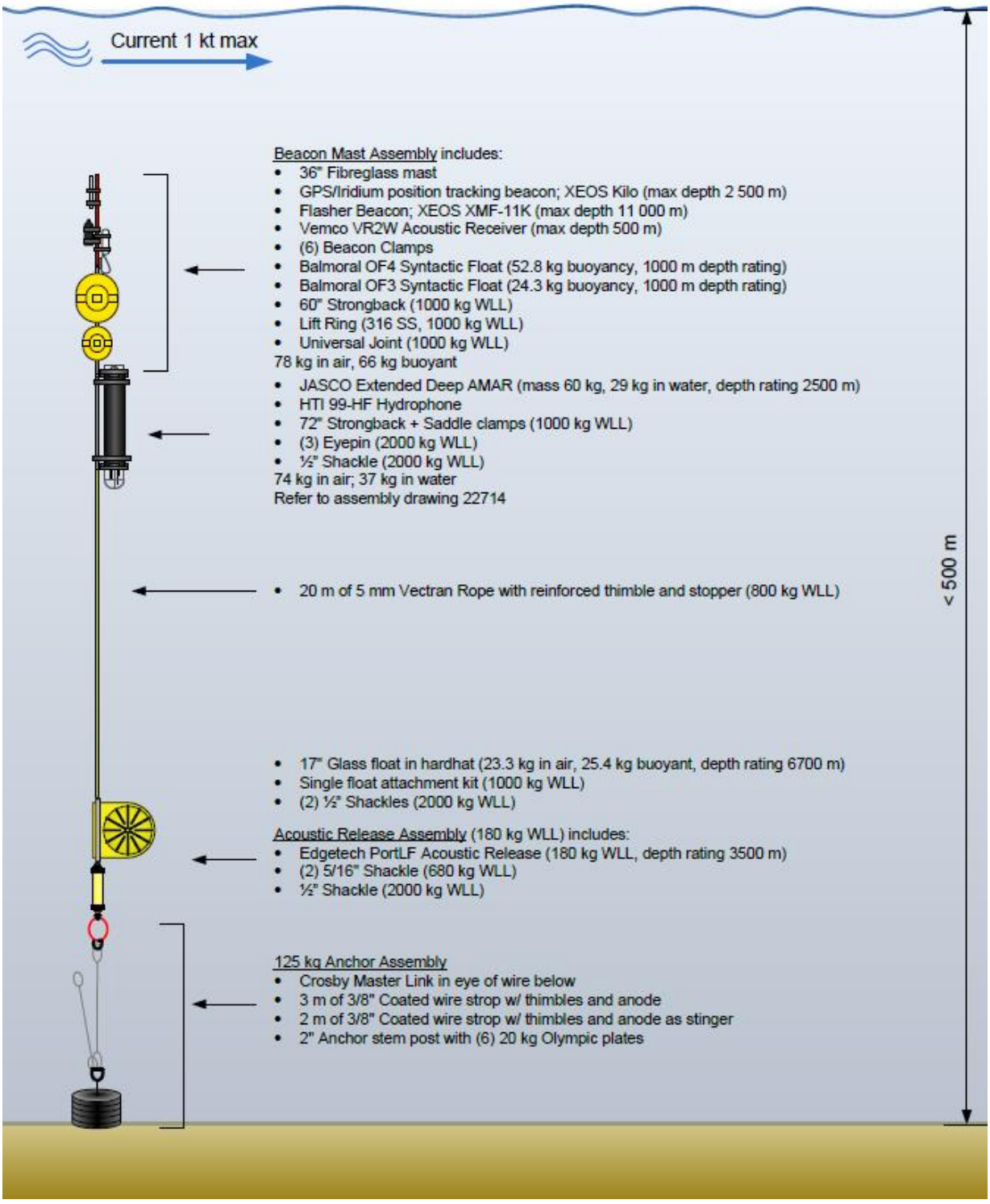

Figure C-5. Deep mooring design with one aluminum-housing AMAR attached to an anchor. This configuration was used at Station 8.

C.1.2. 2016–2017

Table C-2 and Figure C-6 present the deployment locations.

Table C-2. Deployment locations of each recorder with corresponding mooring designs.

Station ID	Location	Lat (N)	Long (W)	Depth (m)	Mooring design
1	Cape Breton	46° 59.218	060° 01.251	175	151
2	Louisburg Line	45° 25.892	059° 46.351	120	151
3	Sable	44° 08.973	060° 35.76	72	147
4	SW Sable	43° 12.96	060° 30.1	1558	146
5	Deep SW Nova	42° 32.86	062° 10.616	1831	146
6	Mouth Laurentian Ch.	44° 51.126	055° 16.244	1790	146
7	Central Grand Banks	45° 42.127	051° 13.715	76	147
8	North Slope Cabot Strait	47° 29.581	059° 24.743	420	150
9	West NFLD	48° 55.644	058° 52.643	43	147
10	Belle Isle	51° 16.615	057° 32.094	110	151
11	Makkovik Bank	55° 36.303	057° 44.927	150	151
12	Nain Bank	57° 14.911	060° 00.474	142	151
13	Labrador Offshore	55° 13.673	054° 11.407	1700	146
14	S Hamilton Bank	53° 01.244	053° 27.63	551	146
15	W Orphan Knoll	50° 24.667	049° 11.755	1993	146
16	Desbarres Canyon	44° 11.564	053° 16.486	1608	146
17	Lily Canyon	44° 58.066	048° 44.015	1273	146
18	Hibernia	46° 54.708	048° 30.069	214	151
19	Sackville Spur	48° 22.812	046° 31.526	1547	146
20	Funk Island Bank	50° 45.514	052° 19.819	236	151

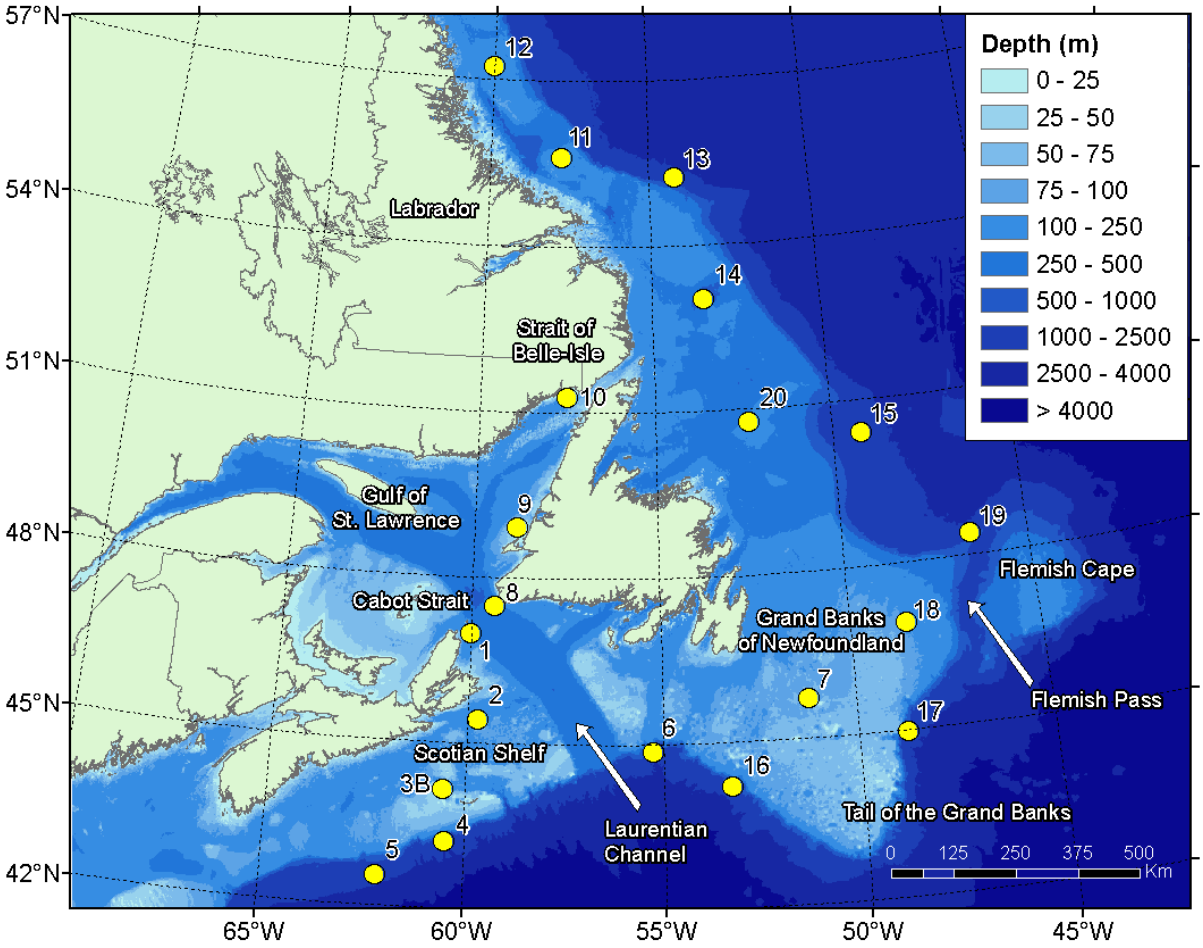

Figure C-6. Summer 2017 mooring locations and proposed cruise plan. Departure is from Dartmouth Cove, NS. Stations shown in red are less than 230 m deep. Stations shown in green >550 m deep.

C.2. Acoustic Recorders

Underwater sound was recorded with Autonomous Multichannel Acoustic Recorders (AMARs, JASCO) (Figure C-7). The recorder configuration used for 2015–2016 and 2016–2017 were similar.

In 2015–2016, each AMAR was fitted with an HTI-99 omnidirectional hydrophone (HTI, Inc., −165 ± 3 dB re 1 V/µPa sensitivity). The AMAR hydrophones were protected by a hydrophone cage, which was covered with a cloth shroud to minimize noise artifacts due to water flow. The AMARs operated on a duty cycle. They recorded at 8000 samples per second (for a recording bandwidth of 10 Hz to 4 kHz) during 11 min 18 s and at 250,000 samples per second (for a recording bandwidth of 10 Hz to 125 kHz) during 1 min 4 s, for a total cycle of 20 min. The low-frequency recording channel had 24-bit resolution with a spectral noise floor of 31 dB re 1 µPa^2/Hz and a nominal ceiling of 171 dB re 1 µPa. The high-frequency recording channel had 16-bit resolution with a spectral noise floor of 32 dB re 1 µPa^2/Hz and a nominal ceiling of 171 dB re 1 µPa. Acoustic data were stored on 1792 GB of internal solid-state flash memory.

In 2016–2017, each AMAR was fitted with an GTI M36-V35-100 omnidirectional hydrophone (GeoSpectrum, Inc., −165 ± 3 dB re 1 V/µPa sensitivity). The AMAR hydrophones were protected by a hydrophone cage, which was covered with a cloth shroud to minimize noise artifacts due to water flow. The AMARs operated on a duty cycle. They recorded at 8000 samples per second (for a recording bandwidth of 10 Hz to 4 kHz) during 11 min 18 s and at 250,000 samples per second (for a recording bandwidth of 10 Hz to 125 kHz) during 1 min 4 s, for a total cycle of 20 min. The low-frequency recording channel had 24-bit resolution with a spectral noise floor of 34 dB re 1 µPa^2/Hz and a nominal ceiling of 164 dB re 1 µPa. The high-frequency recording channel had 16-bit resolution with a spectral noise floor of 33 dB re 1 µPa^2/Hz and a nominal ceiling of 164 dB re 1 µPa. Acoustic data were stored on 1792 GB of internal solid-state flash memory.

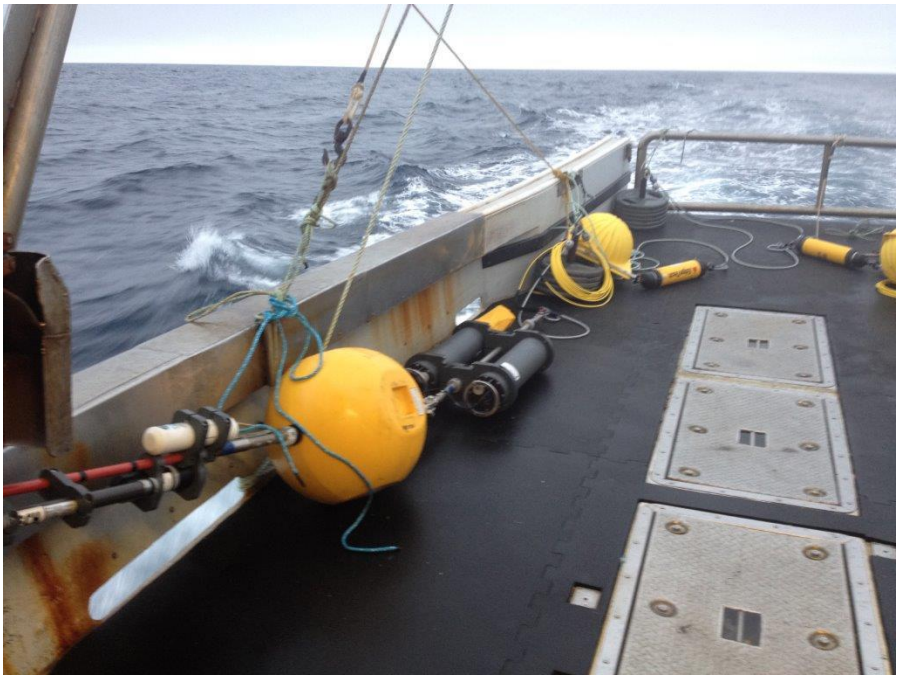

Figure C-7. Mooring set up prior to deployment.

C.3. Recorder Calibrations

A 42AC pistonphone calibrator (G.R.A.S. Sound & Vibration A/S; Figure C-8) was used to verify the sensitivity of the whole recording apparatus—the hydrophone, pre-amplifier, and AMAR. The pressure response of the recording system was verified by placing the pistonphone and its adapter over the hydrophone while the pistonphone produced a known pressure signal on the hydrophone element (a 250 Hz sinusoid at 152.2 dB re 1 µPa). The system sensitivity was measured independently of the software that performed the data analysis. This independently calibrated the analysis software. Calibrations were performed in JASCO's facility before the recorders were shipped. The reading was verified for consistency before data analysis was performed.

Figure C-8. Split view of a G.R.A.S. 42AC pistonphone calibrator with an M15B hydrophone.

C.4. Total Ocean Noise and Time Series Analysis

For the ESRF study, ambient noise levels at the recording stations were examined to document the local baseline underwater sound conditions. Ambient noise levels are presented as:

- Statistical distribution of SPL in each 1/3-octave-band. The boxes of the statistical distributions indicate the first (L_{25}), second (L_{50}), and third (L_{75}) quartiles. The whiskers indicate the maximum and minimum range of the data. The solid line indicates the mean SPL, or L_{mean}, in each 1/3-octave.
- Spectral density level percentiles: Histograms of each frequency bin per 1 min of data. The L_{eq}, L_5, L_{25}, L_{50}, L_{75}, and L_{95} percentiles are plotted. The L_5 percentile curve is the frequency-dependent level exceeded by 5% of the 1 min averages. Equivalently, 95% of the 1 min spectral levels are above the 95th percentile curve.
- Broadband and approximate-decade-band SPL over time for these frequency bands: 10 Hz to 8 kHz, 10–100 Hz, 100 Hz to 1 kHz, and 1–63 kHz.
- Spectrograms: Ambient noise at each station was analyzed by Hamming-windowed fast Fourier transforms (FFTs), with 1 Hz resolution and 50% window overlap. The 120 FFTs performed with these settings are averaged to yield 1 min average spectra.
- Daily sound exposure levels (SEL): Computed for the total received sound energy and the detected shipping energy. The SEL is the linear sum of the 1 min SEL. For shipping, the 1 min SEL values are the linear 1 min squared SPL values multiplied by the duration, 60 s. For seismic survey pulses, the 1 min SEL is the linear sum of the per-pulse SEL.

The 50th percentile (median of 1 min spectral averages) can be compared to the well-known Wenz ambient noise curves (Figure 3), which show the variability of ambient spectral levels off the east coast of Canada as a function of frequency of measurements for a range of weather, vessel traffic, and geologic conditions. The Wenz curve levels are generalized and are used for approximate comparisons only (see Section 2.2).

C.4.1. Vessel Noise Detection

Vessels are detected in two steps:

1. Constant, narrowband tones produced by a vessel's propulsion system and other rotating machinery (Arveson and Vendittis 2000) are detected. These sounds are also referred to as tonals. We detect the tonals as lines in a 0.125 Hz resolution spectrogram of the data.
2. The root-mean-square sound pressure levels (SPL) are assessed for each minute in the 40–315 Hz frequency band, which commonly contains most sound energy produced by mid-sized to large vessels. Background estimates of the shipping band SPL and broadband SPL are then compared to their median values over the 12 h window, centred on the current time.

Vessel detections are defined by three criteria:

- The SPL in the shipping band is at least 3 dB above the median.
- At least 5 shipping tonals (0.125 Hz bandwidth) are present.
- The SPL in the shipping band is within 8 dB of the broadband SPL (Figure C-9).

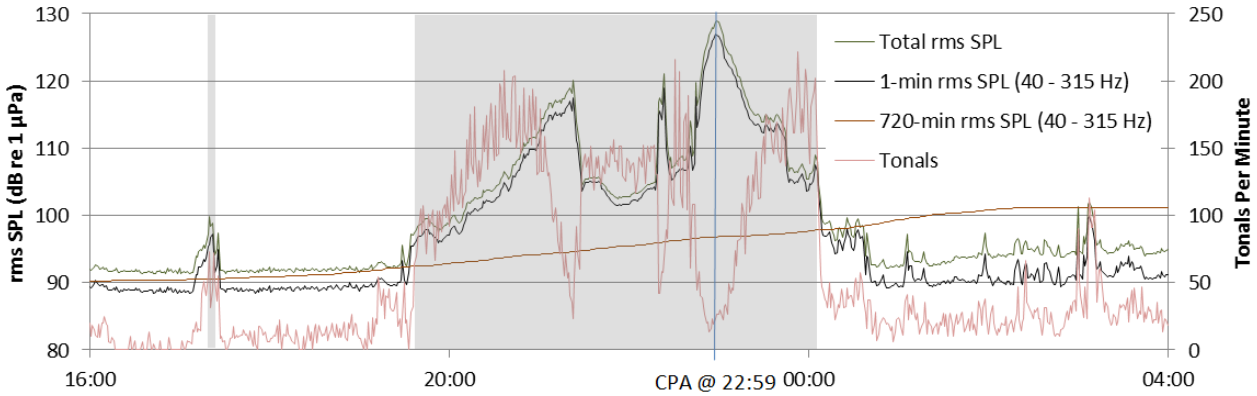

Figure C-9. Example of broadband and 40–315 Hz band SPL, as well as the number of tonals detected per minute as a ship approached a recorder, stopped, and then departed. The shaded area is the period of shipping detection. Fewer tonals are detected at the ship's closest point of approach (CPA) at 22:59 because of masking by broadband cavitation noise and due to Doppler shift that affects the tone frequencies.

C.4.2. Seismic Survey Event Detection

Seismic pulse sequences are detected using correlated spectrogram contours. We calculate spectrograms using a 300 s long window with 4 Hz frequency resolution and a 0.05 s time resolution (Reisz window). All frequency bins are normalized by their medians over window the 300 s window. The detection threshold is three times the median value at each frequency. Contours are created by joining the time-frequency bins above threshold in the 7–1000 Hz band using a 5 × 5 bin kernel. Contours 0.2–6 s in duration with a bandwidth of at least 60 Hz are retained for further analysis.

An "event" time series is created by summing the normalized value of the frequency bins in each time step that contained detected contours. The event time series is auto-correlated to look for repeated events. The correlated data space is normalized by its median and a detection threshold of 3 is applied. Peaks larger than their two nearest neighbours are identified and the peaks list is searched for entries with a set repetition interval. The allowed spacing between the minimum and maximum time peaks is 4.8 to 65 s, which captures the normal range of seismic pulse periods. Where at least six regularly spaced peaks occur, the original event time series is searched for all peaks that match the repetition period within a tolerance of 0.25 s. The duration of the 90% SPL window of each peak is determined from the originally sampled time series, and pulses more than 3 s long are rejected.